NTNU – Trondheim
Norwegian University of
Science and Technology

AVO Analysis of Turbidite Reservoir Rocks in the Alvheim Field

Katharina Banschbach Eggen

Earth Sciences and Petroleum Engineering
Submission date: June 2012
Supervisor: Per Åge Avseth, IPT

Norwegian University of Science and Technology
Department of Petroleum Engineering and Applied Geophysics

Preface

This master's thesis is written during the last semester of my study at the Norwegian University of Science and Technology (NTNU) as a part of the specialization within Petroleum Geophysics, TPG4930, for the Department of Petroleum Engineering and Applied Geophysics.

I would like to direct a great thank you to my supervisor at NTNU, Adjunct Professor Per Avseth for all the help he has given me throughout the work with this thesis. I would also like to thank Professor Martin Landrø and Associate Professor Egil Tjåland at NTNU for answering all my questions when my supervisor was not available. I would not have been able to finish this thesis without their help and guidance.

I would like to thank my parents for proofreading and all the encouraging words during times when I never saw the light at the end of the tunnel. I would also like to thank my boyfriend for his understanding for all the late nights and missed dinners due to long nights at the university. And last but not least, I would like to thank all my fellow students for their companionship and lunch breaks making these past five years the best years of my life.

Trondheim, June 04, 2012

_____

Katharina B. Eggen

Sammendrag

Alvheim feltet består av et turbiditt reservoar. Dette betyr at på grunn av den komplekse avsetningshistorien vil det være et vanskelig reservoar å forutsi både litologi og fluid innhold i. I den foregående prosjektoppgaven (Eggen 2012) ble det gjennomført AVO analyser på tolv modellerte scenarioer som ble antatt at de kunne være til stede i et turbiditt reservoar. Disse modellerte scenarioene ble sammenlignet med analysene som ble gjennomført i denne masteroppgaven for å se om det var mulig å bruke de modellerte scenarioene til å forutsi hvilke svar som kunne forventes av analysene på de reelle dataene.

Et ”post-stack” datasett som bestod av en Nær og en Fjern stack som viste hele Alvheim feltet, inkludert de tre hydrokarbonfunnene som er gjort, og et ”pre-stack” datasett bestående av data tatt fra rundt oljefunnet, kalt Kneler, var tilgjengelige som informasjonskilder for denne masteroppgaven. I tillegg fantes det også brønnlogger fra brønn 25/4-7. I denne oppgaven er det fokusert på oljereservoaret Kneler, og på de seismiske gatherene fra ”pre-stack” dataene var det mulig å identifisere toppen av reservoaret ved hjelp av en ganske tydelig AVO effekt. Det ble gjennomført flere analyser av denne AVO effekten og resultatene ble sammenlignet med resultatene fra prosjektoppgaven. I tillegg til å gjøre AVO analyse på dataene var det interessant å se om det var mulig å se hvordan reservoaret endret seg i en retning bort fra brønnlokasjonen. For å øke signal til støy forholdet på seismikken ble det laget supergather rundt brønnlokasjonen og en avstand bort fra brønnen for å se om det var mulig å observere endringer på seismikken.

AVO analysen ble gjennomført på topp reservoar, hvor reservoaret befinner seg i Heimdal Member som ligger i Listaformasjonen. Det ble laget AVO kryssplott fra begge datasettene hvor området rundt Kneler ble valgt for hånd på ”post-stack” dataene for at det analyserte området skulle passe med området som ble plottet fra ”pre-stack” dataene. Ut ifra denne analysen var det mulig å se at det var kryssplottet som ble laget av ”post-stack” dataene som viste det største avviket fra bakgrunnstrenden, og at denne anomalien kunne bli klassifisert som en klasse III AVO anomali. I tillegg til å gjennomføre denne analysen ble det også gjennomført en AVO gradientanalyse av AVO effekten på et ”pre-stack”-gather og på et syntetisk gather laget ved hjelp av en normal Ricker-bølge og hastighetene fra brønn 25/4-7. Begge AVO-kurvene fra denne analysen hadde et negativt krysningspunkt og en negativ gradient noe som også klassifiserte dem som en klasse III AVO anomali. Det var kjent på forhånd at den øvre delen av reservoaret bestod av en ukonsolidert lagvis seksjon bestående av sand- og skiferlag, og ut i fra dette var det forventet at svarene ville stemme med resultatene fra det modellerte scenarioet for ukonsolidert lagdelt sand og skifer. Det viste seg at dette ikke stemte helt og at resultatene fra

analysene av de reelle dataene passet bedre med analysene som ble gjennomført for den modellerte ukonsoliderte massive sandsteinen.

Selv om svarene fra analysene som ble gjennomført i denne masteroppgaven ikke stemmer fullstendig overens med de forventede resultatene fra prosjektoppgaven er det mulig å si at analysene fra de reelle dataene gir korrekte svar. Forskjellen ved sammenligningen av resultatene kommer av at analysene i denne oppgaven er gjennomført på toppen av en ukonsolidert lagdelt seksjon bestående av sand- og skiferlag hvor det øverste laget er et rent sandlag. Dette betyr at den faktiske analysen viser det samme svaret for både de reelle dataene og de modellerte dataene, men at det er antagelsene når analysene ble gjort som skaper usikkerheter.

Ut ifra disse resultatene er det mulig å se at det skal ikke bli tatt for gitt at resultatene fra de reelle dataene nødvendigvis passer overens med resultatene fra de modellerte dataene. Spesielt ikke dersom det er muligheter for at det finnes usikkerheter som er relatert til antagelsene som de modellerte dataene er basert på.

Abstract

The Alvheim reservoir is a turbidite reservoir, which means that the complex deposition makes it a difficult reservoir to perform predictions regarding reservoir content on. In the preceding project work (Eggen 2012) AVO analyses were performed on the twelve modelled scenarios that can be present in a turbidite reservoir. These modelled scenarios were to be compared with the analyses performed on the real data in this master's thesis to see if the modelled scenarios can help to predict what answers to expect from the analyses performed on the real data.

One post-stack data set consisting of Near and Far stacks covering the whole Alvheim field including all three hydrocarbon discoveries, and one pre-stack data set focusing on the oil discovery named Kneler were available for this thesis in addition to well logs from well 25/4-7. Naturally, it was the Kneler oil discovery that was focused on, and on the gathers from the pre-stack data the top reservoir could be identified by a clear AVO effect. Different AVO analyses were performed on this AVO effect and the results were compared with the results obtained from the project work. In addition to performing AVO analyses on the data it was interesting to see if it was possible to see how the reservoir changed when moving away from the well location on the seismic data. To increase the signal to noise ratio, super gathers around the well location were created in addition to super gathers at some distance away from the well to see if there were changes that were noticeable on the seismic.

The AVO analysis was performed on the top oil sand (top reservoir) in the Heimdal Member located in the Lista Formation. An AVO crossplot was created from both data sets, where the area around the Kneler discovery was picked by hand on the post-stack data set to match the area that was plotted from the pre-stack data. The crossplot created from the post-stack data showed the best deviation from the background trend out of the two, and the anomaly could be classified as a class III AVO anomaly. It was also performed an AVO gradient analysis on the AVO effect on a pre-stack seismic gather and on a synthetic seismic gather created with a normal Ricker wavelet and velocities taken from well 25/4-7. Both AVO curves from these analyses had a negative intercept and a negative gradient, which also could classify them as a class III AVO anomaly. It was known in advance that the upper part of the reservoir consisted of unconsolidated interbedded sand-shale and it was expected that the results would match the results obtained from the modelled scenario of the unconsolidated interbedded sand-shale. However, this was not completely the case and the results from the analyses of the real data turned out to match the analyses for the modelled unconsolidated massive sandstone.

Even if the analyses from this master's thesis do not match the expected analyses performed in the preceding project work, they can be said to be correct. The error in comparison is due to the fact that the analyses in this master's thesis are performed on the top of a section of unconsolidated interbedded sand-shale, but the top layer is actually a layer of unconsolidated massive sandstone. This means that when making assumptions it should not be taken for granted that the real data will match the modelled data, especially not if there are uncertainties related to the assumptions the modelling is based on.

Contents

Figures

Introduction

Due to the complex sand distribution that follows the deposition from turbidity currents, it is very difficult to be able to say anything about the content of a turbidite reservoir. Turbidite reservoirs consist of both clean channel sands and dirty levee deposits. It is the clean channel sands that may act as reservoirs, but since the deposition is unsystematic, knowing the exact location and extent of the sand bodies is almost impossible.

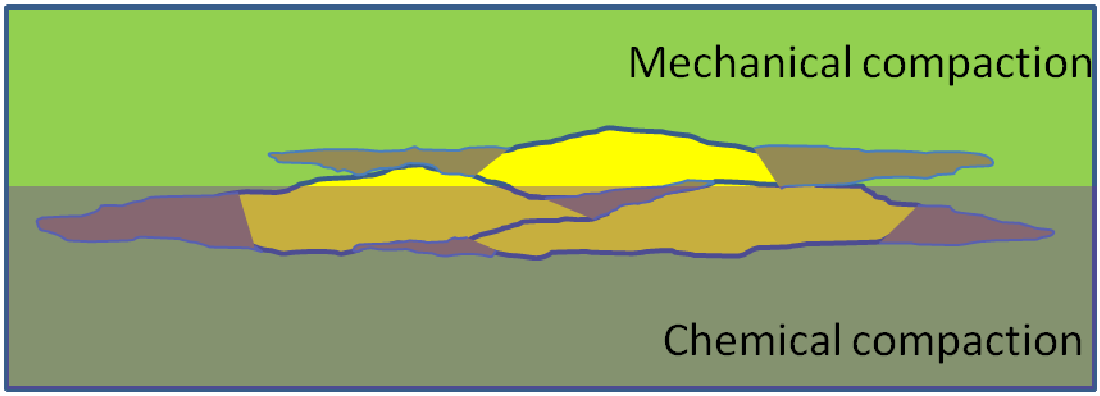

Figure I: Schematic figure of the Alvheim reservoir (Avseth, Handed figures 2011).

In the figure above the clean channel sands are represented by the yellow colour while the levee deposits are the ones represented by the brown colour. The levee deposits may be composed of either interbedded sand-shale units or massive sand units with higher shale content. Since the deposition from turbidity currents is chaotic, the levee deposits can be accumulated parallel to the clean sand channel, which normally is the case, or they may form on top of old channel sands. This gives that these reservoirs may be complex systems of clean and dirty sands interchangeably. Due to the arrangement of the different lithologies it is difficult to know anything about how the sandy channel reservoirs behave in the subsurface.

For this master's thesis, real seismic data from the Alvheim field in the Norwegian part of the North Sea has been used. The Alvheim field is one of these turbidite fields with complex reservoir structure due to the deposition from turbidity currents. The complexity of the reservoir is caused by both different lithofacies and lobe switching within the reservoir. The lobe switching is caused by avulsion where there has been almost a vertical stacking of delta lobes. This stack of delta lobes will then represent both depositional and ecological changes (Hudson 2005). The complexity of the reservoir makes it very difficult to say anything about where the good reservoir sands are located and where there is a possibility of finding hydrocarbon reservoirs. From well reports it is known that the Alvheim field contains three hydrocarbon discoveries; one oil discovery and two gas discoveries. The reservoirs in the Alvheim field are located at around 2 km depth. This is the depth where quartz cementation is

expected to happen in the North Sea (Avseth, Dræge, et al. 2008). With beginning quartz cementation at the reservoirs depth, the Alvheim reservoir is located in the transition zone between mechanical and chemical compaction (Figure I). This results in the fact that there are not only lateral facies variations in the reservoir, but also vertical changes related to the diagenesis. The presence of both oil and gas and the diagenesis changes in addition to the already mentioned facies changes makes the task of discovering viable sands for hydrocarbon storage even more difficult. But, even if the diagenetic changes may create challenges regarding the prediction of good reservoir sands, this initial cementation in the reservoir is important for the elastic properties and for the possibility of being able to observe the reservoir fluids on seismic. The diagenesis effect does also have a large influence on the fluid sensitivity. According to the Gassmann theory it is mainly the stiffness that controls the fluid sensitivity and not so much the porosity. This gives that the unconsolidated sandstones will have a larger fluid sensitivity than the cemented sandstones. From this it can be seen that there are both advantages and disadvantages with the beginning cementation at the reservoir depth. When performing the task of discovering good reservoir sands, a good seismic understanding is essential and an AVO analysis can be very helpful when performing reservoir characterization of the Alvheim field.

The challenge by performing AVO analysis on these data is that even if the quality of the seismic data is good, and there are observable anomalies on the data, it is very difficult to say whatever content in the reservoir that causes these anomalies; what kind of fluid they contain, if it is oil or gas. Even if the fact is that one of the anomalies has been drilled, and that it has been found that it contains hydrocarbons, it does not have to mean that the other, similar anomalies contain the same type of hydrocarbons or any hydrocarbons at all. So, knowing the content of one anomaly does not have to mean that the content of all of them are known.

The work done in this master's thesis follows the work done by Avseth et al. (2008) where there was performed an AVO analysis on the Alvheim reservoir. This analysis was much centered on the two wells from the reservoir, well 25/4-7 named Kneler and well 24/6-2 named Kameleon, and one set of partial stacked seismic. In this thesis two sets of seismic data will be used and it will be focused more on one of the hydrocarbon discoveries, the Kneler oil discovery. Will the two data sets give the same result, and how do the lithologies and reservoir content change when moving away from the well are questions that will be attempted to be answered.

This master's thesis is written as a continuation of the project work finished January 2012 (Eggen 2012). The AVO analysis performed on modelled data from the Alvheim field in the project work has in this master's thesis been compared with the results from an AVO analysis performed on the real data from the Alvheim field. The purpose of doing this comparison was to see if the modelled data can represent a good substitute for the real data and give the same result.

1. Geological background[1]

1.1 Paleocene

The Alvheim reservoir is located in tertiary sediments; representing Paleocene age (65.5 – 2.6 Ma) sedimentary rocks. The Paleocene sediments are distributed throughout the whole North Sea and they represent one of the most productive hydrocarbon plays. The sediments from the Paleocene that are present in the central to northern North Sea are variable in depth, and they can vary from the sea bed to over 3000 meters. Regarding the whole area, the sediments can reach a maximum thickness of 1000 m. The Paleocene is the most sand-prone part in the Paleogene, and the strata in the North Sea consist mainly of silisiclastic sediments in addition to smaller amounts of other sediments such as volcaniclastic rocks, coal and tuff (Ahmadi, et al. 2003).

During the Paleocene there was an evolvement of the basin where the architecture went from basin-centered to basin-margin deposition. This happened as all the Atlantic and European tectonic events influenced the depositional systems. During the late Paleocene there was some regional uplift that was caused by the development of the Iceland plume, also called the North Atlantic hot spot. In addition to the stresses caused by the regional uplift, there were stresses along the line of the future north-east Atlantic Ocean. These stresses led to some major volcanic activity which is, in this area, represented by tuffs. Erosion of the uplifted areas led to input of silisiclastic sediments instead of the preceding calcareous deposition. The tectonic events were followed by rapid subsidence of the North Sea Basin. The subsidence in the North Sea Basin was centred above the main Mesozoic rift system and was followed by tilting of the flanks in the Viking and Central graben where the Horda Platform was tilted up towards the east and the East Shetland Platform was tilted up towards the west. The basins formed and overlying the Mesozoic graben were increasingly filled with deep-water turbidites interbedded with hemipelagic mudstone units (Ahmadi, et al. 2003).

The top of the Paleocene interval can be recognized almost across all of the Central and Northern North Sea by the ash-fall deposits of the Balder formation. This tuff-layer is also an excellent seismic reflector and has been used to define the top of the Paleocene.

[1] The fundamental literature used as reference for this chapter is the Millennium Atlas. In addition to this main reference some other literature has also been used as references, however not to the same extent.

1.2 Stratigraphy

In the Paleocene and earliest Eocene there is a record of several cycles of second-order regression and transgression. Regardless of in which order these cycles appear they are characterized by the input of sand into the basin during the regressions and the constraint of deposition during the transgressions. Above the already mentioned cycles there are two higher-order transgressive and regressive cycles, which again are superimposed by another eight high-order transgressive and regressive cycles. These last cycles correspond to units of formation or member status. Throughout the layers deposited in the Paleocene, there occur minor amounts of shallow-water deposits, such as the Dornoch and Fiskebank Formations. These shallow-water deposits include shallow-marine, coastal, deltaic and shelf systems that are typically regressive. They are also sandstone rich and may have associated coals (Ahmadi, et al. 2003).

The dominant processes for transport of sand from the shelf into the basin were well developed, restricted and unrestricted sediment gravity flows evolved from either a point or a line source. Common depositional elements of restricted systems include erosional and depositional channels, overbank and levee deposits and channelled lobes. In both restricted and unrestricted systems, the sea-floor topography controls both the sand deposition and sand preservation. Sedimentation processes within restricted and unrestricted systems include high- and low-density sediment gravity flows, slurries, slumps and debris flows. It is normally in overbank deposits, such as levees and crevasse splays, in distal terminal lobes and in distal submarine aprons that the low-density gravity flows can be observed. On the other hand, the high-density sediment gravity flow deposits normally occur in confined channels, proximal terminal lobes and submarine aprons. Such deposits display planar-laminated sandstones, massive, unstructured sandstones and massive sandstones with load and dish structures. Siltstones and shales are present in many areas between the individual sandstone systems (Ahmadi, et al. 2003).

Figure 1. 1 shows the lithostratigraphic column for the area of interest. The lithostratigraphic column is taken from the available well, 25/4-7, however not all of the observable lithologies are of importance. The Nordland Group consists of four formations and is mainly dominated by marine claystones. The observable Utsira Formation is quite sandy and consists of both marine sandstones and claystones that probably represent shallow marine shelf sandstones. The Hordaland Group consists of five different formations, but only the Grid Formation is observable in this well. This Formation consists of sandstones which have interbeds of claystone and siltstone which most likely have been deposited in an open marine environment. The most interesting Group is the Rogaland Group since this is where the reservoir of interest is located. The dominant lithologies are sandstones that are interbedded with shales. This is most in the western part of the northern and central North Sea while further east the sandstones form lobes that pass laterally into shales. Towards the top of the

group the lithology becomes more tuffaceous when moving into the Balder Formation (FactPages - Norwegian Petroleum Directorate n.d.).

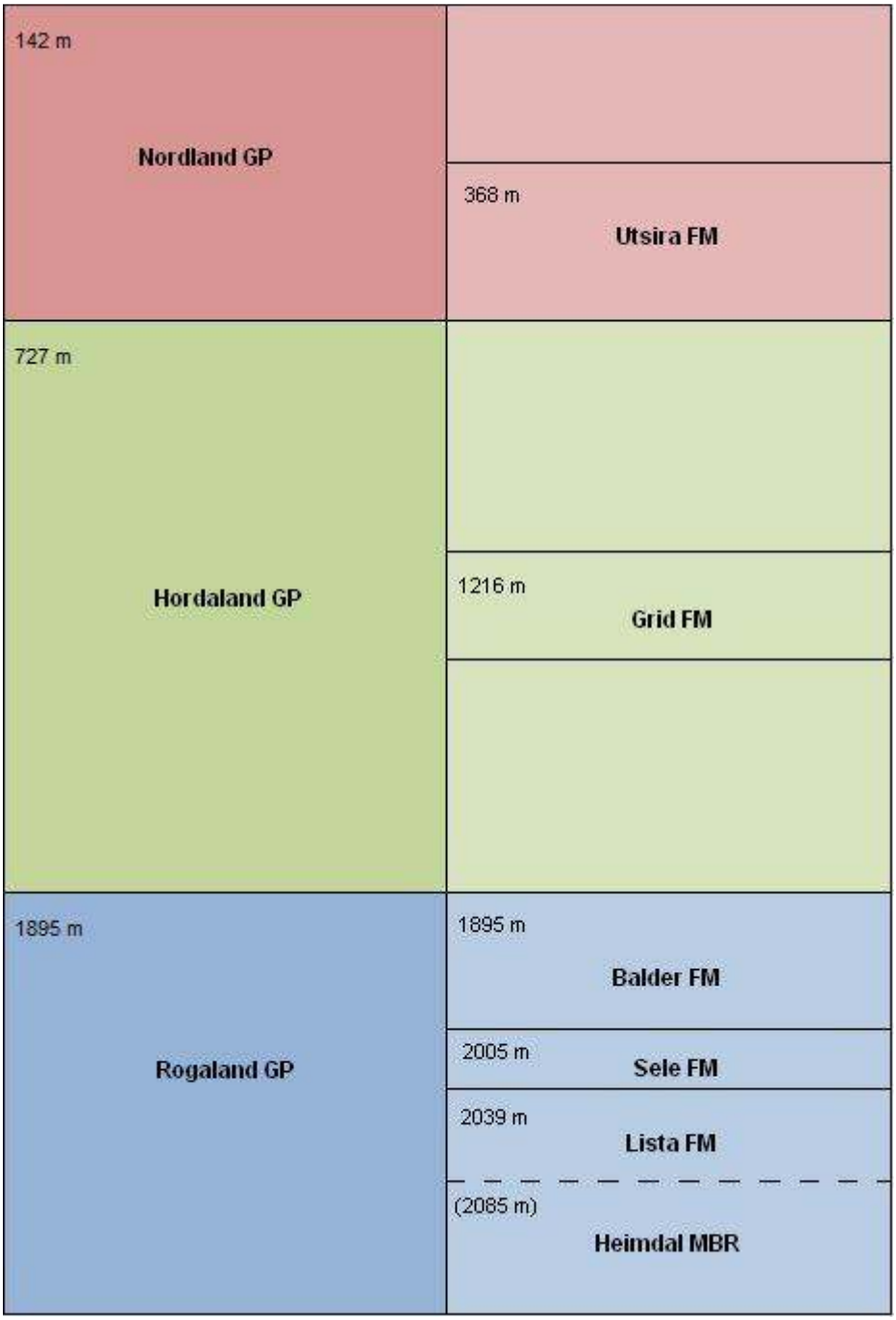

Figure 1. 1: Lithostratigraphic column from well 25/4-7.
Showing the lithologies observed in the well drilled through the Kneler oil discovery. The Alvheim reservoir is located in the Heimdal Member which recently changed status from being a separate Formation to a Member in the Lista Formation.

Figure 1. 2 shows a regional seismic line, taken from the Millennium Atlas (Ahmadi, et al. 2003). This line is located slightly further south than where the Alvheim field is located, but it still gives a good picture of how the Paleocene interval is distributed.

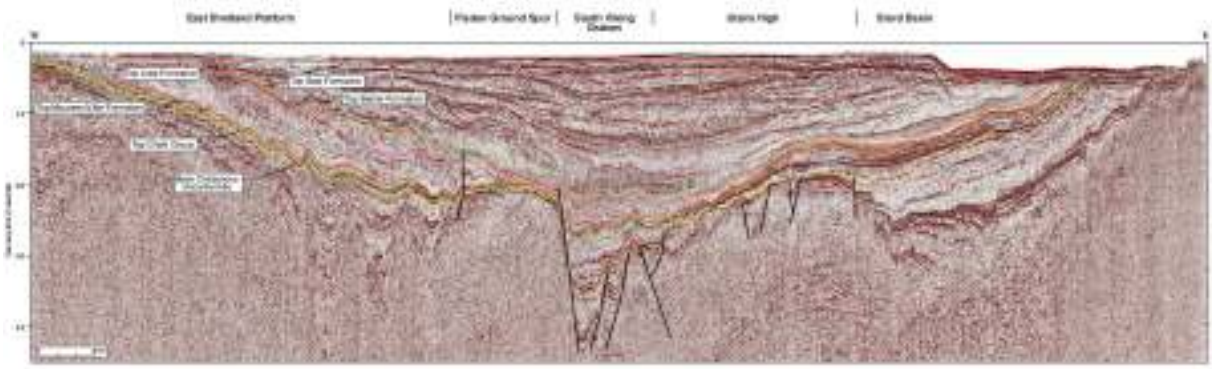

Figure 1. 2: Regional seismic profile showing the Paleocene interval (Ahmadi, et al. 2003). Located slightly further south than the Alvheim field, but gives a good picture of how the Paleocene lithologies are distributed in the area. A larger version of the section is shown in Figure A in the Appendix.

1.2.1 The Balder Formation

The Balder Formation is transgressive and consists mainly of multicoloured, laminated shales with coals, tuffs, and occasional thin limestones interbedded with local sandstones that might be massive. The Balder Formation was deposited in a generally deep marine, anoxic environment, mainly as hemipelagic sediments with frequent income of tuffaceous rain caused by ash falls from volcanic activity (Balder Formation n.d.). Most likely there were more than only one volcanic source for the extensive tuffaceous components of the sediments, but they seem mainly to have been connected to volcanic eruptions that were linked to the onset of break-up of Greenland and the European continents. In some cases the Balder Formation was deposited from gravitational streams i.e. causing turbidites.

The Balder Formation can be divided into two units. The separation of the two units is based on wire log readings, and the lower unit has a higher velocity and lower gamma readings than the upper unit. The lower unit provides therefore a strong datum for correlation. The upper unit is represented by poorly consolidated mudstone and contains the Odin Member sandstone. The lower unit is generally more tuffaceous than the upper unit and is often referred to as the Balder Tuff and is characterized by subaqueous airfall tuffs. The lower unit helps providing for seals for the reservoirs in the area. The Balder Tuff is deposited with shales both above and below, and this makes the Balder Tuff to form a very good seismic marker horizon due to the difference in acoustic impedance between the shales and the tuff.

1.2.2 The Sele Formation

The Sele Formation is quite thin in relation to the over- and underlying formations. It consists mainly of tuffaceous clay-rich shales and siltstones. The Sele shale is a pelagic shale, i.e. it is formed by precipitation from ooze in the water column. The

shales are finely laminated and carbonaceous with some interbeds of laminated sandstones, but they are more clay rich than the shale in the underlying Lista Formation. Where the Sele Formation is located directly over the Lista Formation, it is possible to see that the boundaries are defined by an upwards increase in gamma ray readings and at the same time a decrease in velocity (FactPages - Norwegian Petroleum Directorate n.d.). In this area where well 25/4-7 is penetrating the reservoir there is no sandy formation underlying the Sele Formation, and the boundary will therefore be very difficult to see.

1.2.3 The Lista Formation

An interesting section of the Paleocene is the Lista Formation. The Lista Formation is of latest Selandian to Thanetian age. It consists mainly of noncalcareous, blocky, grey mudstones interbedded with sandy, high-density, gravity-flow or debris-flow deposits and minor volcaniclastic rocks. The Lista shale contains more silt than the Sele shale and is a hemipelagic shale, i.e. they are mostly deposited from distal parts of turbiditic currents. Comparing the shale in the Lista Formation with the shale in the Sele Formation it can be found that there is a tendency that the clays in the Lista Formation contains more illite while the clays in the Sele Formation contains more smectite (Avseth, Jørstad, et al. 2009).

The Lista Formation is the second most sand-prone depositional system in the Paleocene after the Maureen Formation. The Lista Formation includes the Mey Sandstone Member of the central North Sea, the laterally equivalent Heimdal Sandstone Member of the northern North Sea and the Siri Sandstone Member in the Danish sector. This gives that nineteen Paleocene fields have their reservoirs located in Lista Formation sandstones. The hemipelagic shales deposited during higher-frequency transgressions and the local Balmoral tuffite unit provide seals for these reservoir sandstones. The Heimdal Sandstone Member is normally interbedded with claystones, siltstones and minor limestones or sandy limestones (Ahmadi, et al. 2003), and this is where the Alvheim reservoir is located; in the Heimdal Member.

1.2.4 The Heimdal Member

The Heimdal Member changed status a couple of years ago, and went from being the Heimdal Formation to the Heimdal Member, a part of the Lista Formation. The Heimdal Member is dominated by thick sandstone units interbedded with grey and black shales and limestones. The amount of carbonate increases towards the base of the formation. The sands are deposited as deep-marine fan deposits which now in this area are located at depths of approximately 2 km. The Heimdal Member is often completely unconsolidated with good porosity and permeability, but since it is located at the depth where the initial quartz cementation starts, it can also be cemented with

quartz cement (Avseth, Jørstad, et al. 2009). The reservoirs in the Alvheim field are located in the sandstones in the Heimdal Member and are thus one of the many fields in Paleocene sediments.

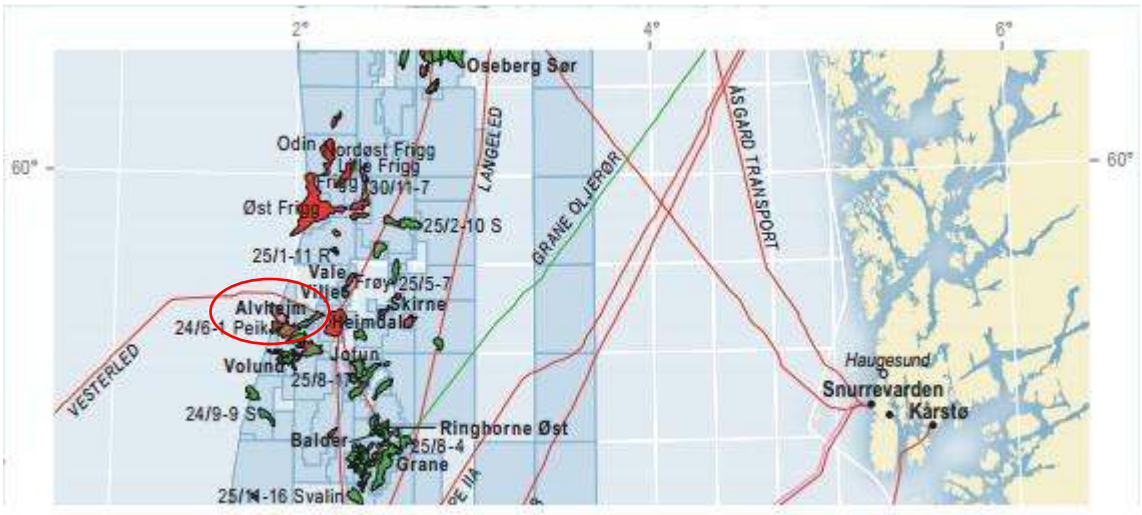

Figure 1. 3: Location of the Alvheim field (Petroleumsverksemnd 2011).
This map shows where the Alvheim field is located, marked by the red ellipse, relative to the other fields in the North Sea and the Norwegian coastline.

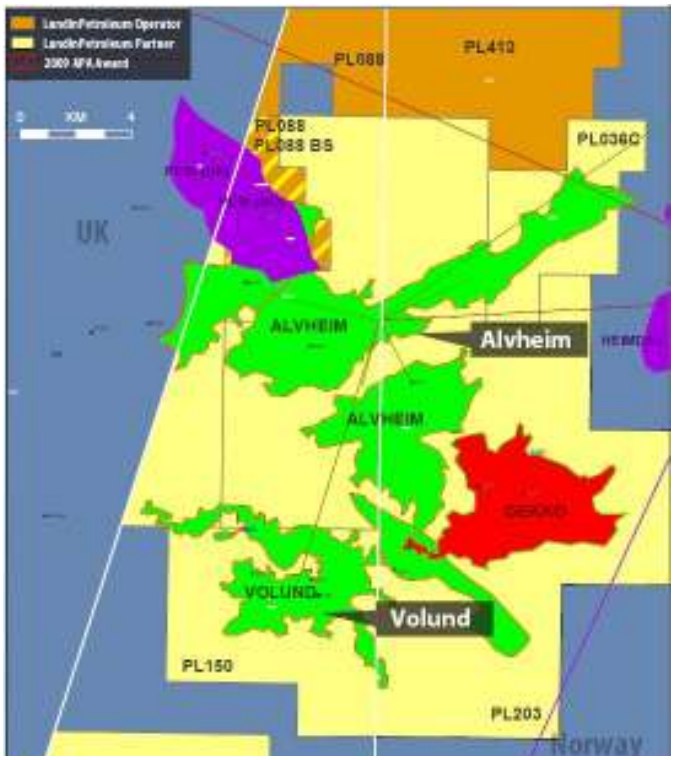

Figure 1. 4: Alvheim field (Norway: Lundin Petroleum commences oil production from the Volund field, offshore Norway n.d.).
The Alvheim field stretches over a quite large area. The Kneler oil discovery which is the discovery focused on in this thesis is located in the part situated North West of Gekko.

1.3 Petroleum Geology

Both oil and gas discoveries have been found in the Alvheim field. In the preceding work and in this thesis it has mainly been focused on two of the discoveries in this Alvheim field; the Kameleon gas and oil discovery and the Kneler oil discovery. For reservoirs of the Paleocene age, channelling within deep-water turbidites is widespread. In some places the combination of channels can lead to a sheet-like morphology with approximately uniform reservoir properties across an extensive area (Ahmadi, et al. 2003).

What is typical for Paleocene sandstones is that they have good connectivity within the separate sand lobes which helps forming excellent reservoirs, but there is often poor connectivity between the different lobes. The reservoirs have very good reservoir properties with good permeability and porosities up to 33 %. The reason for the high quality reservoirs is the maturity of the sandstones, both mineralogical and textural. Another important factor is that the depth-related diagenesis is relatively small in the Paleocene sediments. Due to the fact that there is very poor connectivity between the separate lobes there are no regional fluid contacts in the Alvheim field. This may result in differences in oil-water contacts (OWC) from one lobe to another; some lobes may be filled with gas while others are filled with oil. This appearance of complex filling of fluids in the reservoirs can be related to different migration times and different migration routes for both the oil and gas. Simultaneously as the hydrocarbons migrated, an east-west tectonic tilting took place both after deposition and between the oil and gas fillings (Avseth, Interview 2012).

2. Background theory

2.1 AVO Analysis

2.1.1 Theory

AVO analysis is the analysis of how the seismic amplitudes vary as a function of offset (distance between source and receiver). It is possible to relate the seismic amplitudes to the reflection angle at a single interface by the Zoeppritz equations. Here the reflection coefficient is described as a function of reflection angle. The Zoeppritz equations are complicated equations, and for calculation purposes approximations are often used. One of the often used approximations is the one by Shuey (1985). In this approximation it is possible to use the velocities, P-wave (V_P) and S-wave (V_S), and the density (ρ), to calculate the reflection coefficient for normal incidence (R(0)) and the AVO gradient (G), given in eq. (2.1) and (2.2).

$$R(0) = \frac{1}{2}\left(\frac{\Delta V_P}{V_P} + \frac{\Delta \rho}{\rho}\right) \tag{2.1}$$

$$G = \frac{1}{2}\frac{\Delta V_P}{V_P} - 2\frac{V_S^2}{V_P^2}\left(\frac{\Delta \rho}{\rho} + 2\frac{\Delta V_S}{V_S}\right) \tag{2.2}$$

Here ΔV_P, ΔV_S and $\Delta \rho$ are the differences in the seismic parameters between the upper and lower layer. V_P, V_S and ρ are the mean values of the upper and lower layer. For the calculation of the reflection coefficient as a function of reflection angle, Shuey's approximation (1985) is given as:

$$R(\theta) \approx R(0) + G\sin^2\theta + F(tan^2\theta - sin^2\theta) \tag{2.3}$$

Here F dominates the far offsets, near critical angle. Since the angles available for AVO analysis have to be less than approximately 30-40°, there is another approximation from Shuey (1985) that can be used where only the two first terms in the equation are considered:

$$R(\theta) \approx R(0) + G\sin^2\theta \tag{2.4}$$

This equation is valid for angles less than 30°. R(0) is the reflection coefficient for normal incidence, while G is the AVO gradient which is a measure of the amplitude variation as a function of offset.

2.1.2 Tuning effects

Tuning is an interference of waves that can happen if there are events or reflectors that are too closely spaced to be observed as separate events or reflectors on the seismic. If the spacing between two reflectors is less than one quarter of the wavelength, these two reflectors will show up as one single reflector with high amplitude (Schlumberger Oilfield Glossary n.d.).

Tuning will also have an effect on the AVO response. Juhlin and Young (1993) were able to show that the AVO response of thin layers imbedded in a homogeneous rock will be considerably different than the AVO response for a simple interface of the same lithology (Avseth, Mukerji and Mavko 2005). The AVO response for a thin bed could be approximated by modelling it as an interference phenomenon between plane P-waves from a thin layer, but this could only be done for weak contrasts in elastic properties across the layer boundaries.

It is possible to calculate the amplitude variation with angle (AVA), which for what Lin and Phair (1993) suggested the following equation:

$$R_t(\theta) = \omega_0 \Delta T(0) \cos\theta \cdot R(\theta) \qquad (2.5)$$

In this equation ω_0 is the wavelets dominant frequency, $\Delta T(0)$ is the two-way travel time at normal incidence from the top to the base of the thin layer, and $R(\theta)$ is the reflection coefficient from the top of this interface.

2.1.3 Crossplot

The AVO attributes can be interpreted by creating crossplots of AVO gradient versus intercept. The crossplot is divided into four quadrants, where the results can be divided into different AVO classes dependent on where they plot in the crossplot.

Rutherford and Williams (1989) defined three AVO classes for gas sands; class I, II and III shown in Figure 2. 1. The two remaining classes were added later, class IV (Castagna and Smith, 1994) and class IIp (Ross and Kinman, 1995). Class I represents hard sands saturated with hydrocarbons. Class II represents sands with a weaker intercept saturated with hydrocarbons. Class IIp will cause a polarity change with offset due to the fact that they have a weak but positive intercept and a negative gradient. Class III represents soft sands with high fluid sensitivity saturated with hydrocarbons. These are the “classical” AVO anomalies. In addition to these, there is class IV which represents soft sands capped by stiff cap-rock shales that have a V_P/V_S ratio that is slightly higher than in the underlying sands.

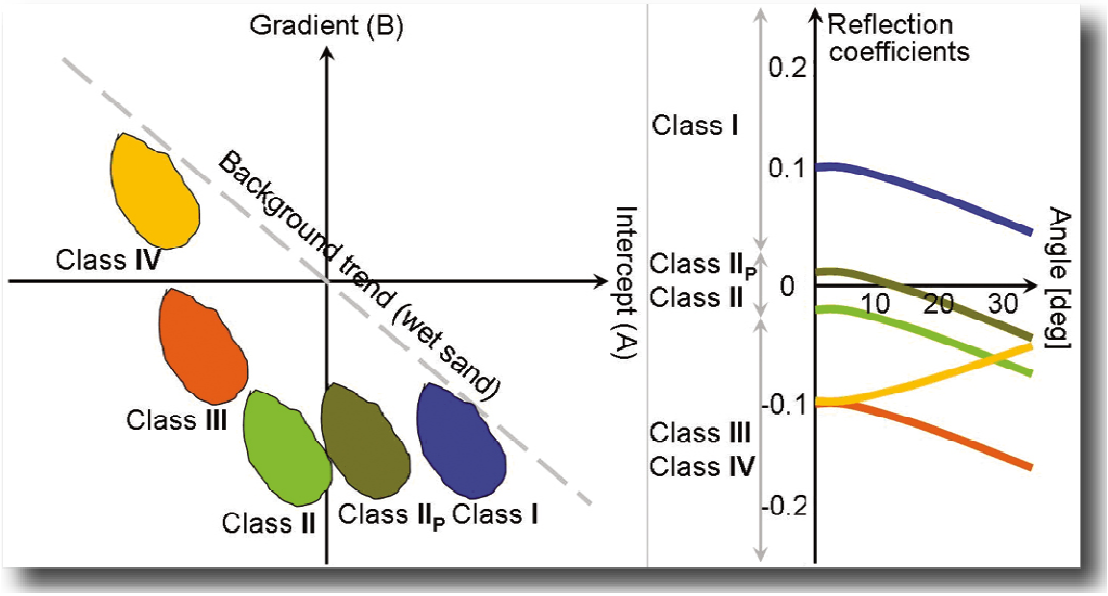

Figure 2. 1: AVO classification scheme (AVO Analysis n.d.)

Even if the different AVO classes are defined for gas sands, Avseth et al. (2005) suggest that the classification of the AVO classes only should be used as descriptive terms for observed AVO anomalies. If the lithologies contain gas or not should not affect the interpretation of the different AVO classes. The dotted line through the centre of the crossplot shows the background trend which is the theoretical average of rock property trend for brine filled rocks (Simm, White and Uden 2000).

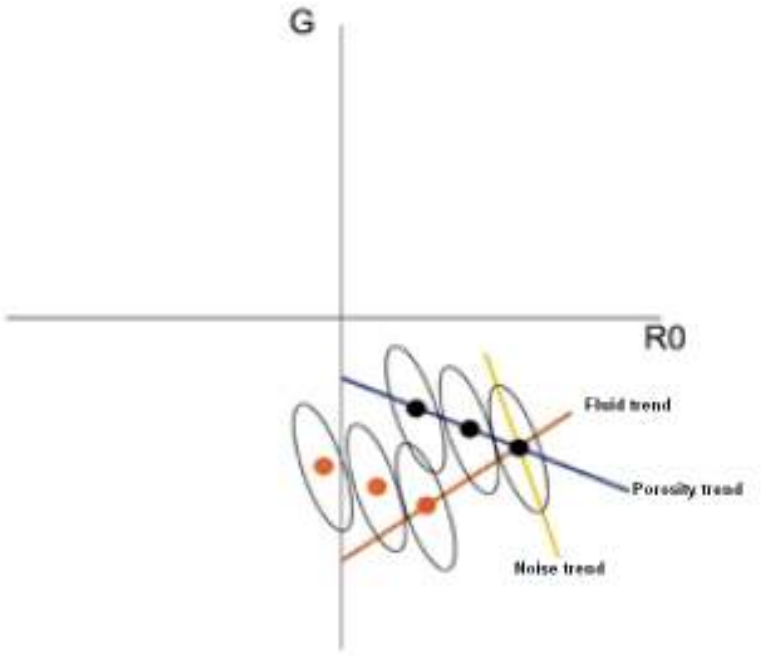

Figure 2. 2: AVO crossplot showing different trends (Simm, White and Uden 2000).
The yellow line shows the noise trend, the blue line shows the porosity trend while the orange line shows the fluid trend for saturated rocks.

Figure 2. 2 shows some of the different trends that can be observed on an AVO crossplot. The yellow line represents random noise associated with a single reflector on multiple gathers. The blue line represents the porosity trend, where the point furthest to the left has the highest porosity and the point furthest to the right has the lowest porosity. When the porosity is increased, both the gradient and the intercept decrease. When the lithology is changing due to the increasing shale content, the gradient and intercept will both decrease, and this trend will be somewhat steeper than the porosity trend. The orange line represents the fluid trend, also called the gas effect. The spread between the points for the hydrocarbon filled data points and the brine filled data points depend on the effect the hydrocarbon has on the V_P/V_S-ratio of the sand. The effect of the hydrocarbon will not create a very clear trend, but it will create a larger cluster of data which is located to the left of the data points from the brine-filled sand (Simm, White and Uden 2000).

By using Shuey's two-term approximation (1985) to the Zoeppritz equation shown in eq. 2.4, it is possible to find a linear relationship between the AVO gradient and the Far-Near stack data. For this to be possible it has to be assumed that the Far stack is around 30°. This is possible since the Far stack normally will be representative for angles that are somewhat lower than 30°. At the same time it has to be assumed that the Near stack is at 0°, which also is possible since the Near stack will be representative for angles that are somewhat higher than 0°. When these two assumptions are fulfilled it is possible to derive an approximate relationship between the AVO gradient and the Far-Near data (Avseth, Dræge, et al. 2008):

$$Far - Near = R(30) - R(0) = Gsin^2(30) = G \cdot 0{,}25 \qquad (2.6)$$

This means that a crossplot of the Near and Far-Near stack data will give the same information as a crossplot between the AVO gradient and the intercept even if the amplitudes of the Near and Far-Near stack data are unadjusted. The thing that is most important is that the Near stack and the Far stack are balanced correctly. To check if the two stacks are balanced correctly, a crossplot of Far versus Near stack can be made.

The Far stack minus the Near stack has, in addition to being a rough estimate of the AVO gradient, been found to be a very good attribute from which to detect class II AVO anomalies.

When working with AVO signatures or AVO curves it is important to have some knowledge of the geology and expected lithology before it makes any sense to interpret the fluid content. In Figure 2. 3 a schematic AVO curve is shown for cemented sandstone saturated with brine and capped by shale. Several different scenarios may have somewhat similar AVO curves. E.g. cemented sandstone saturated with hydrocarbons can have a more or less similar AVO signature as

unconsolidated sandstone saturated with brine due to the fact that the curves follow both the cementation and hydrocarbon trend.

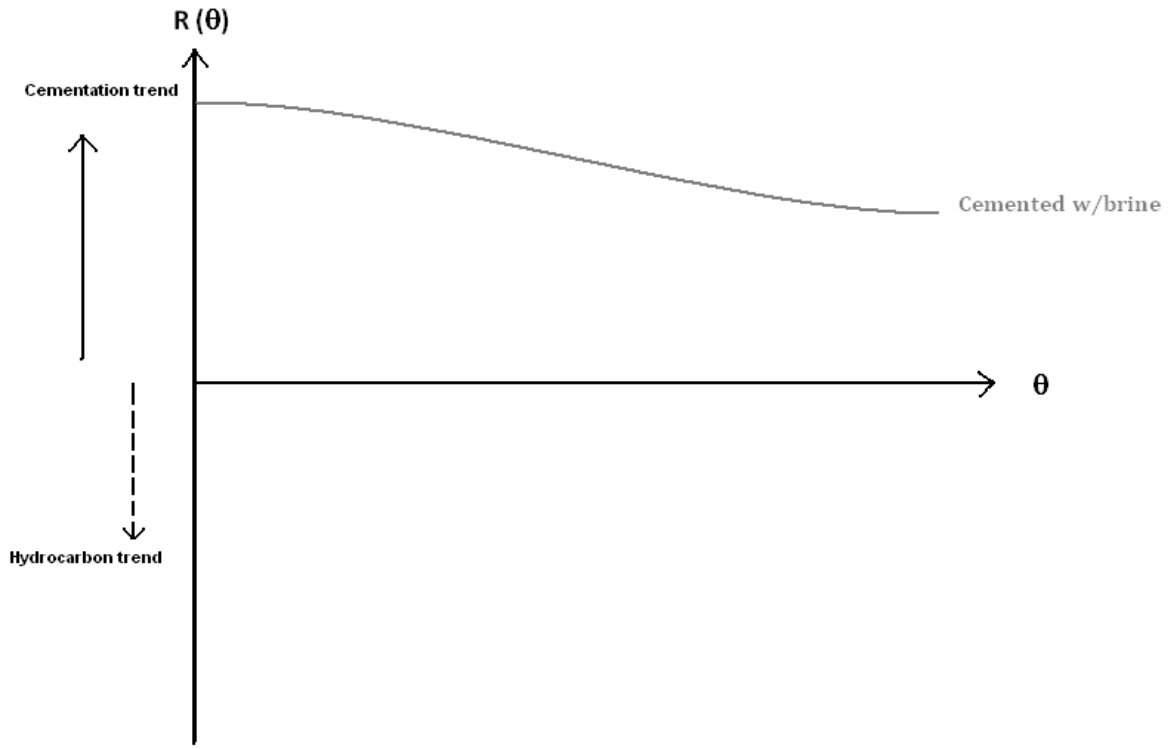

Figure 2. 3: Schematic AVO curve for cemented sandstone saturated with brine capped by shale.

2.2 Computer software

To be able to perform all the analyses and comparisons that were needed for this thesis, two different softwares have been used. The explained theory is only the theory that has been used in the project work which this thesis is based upon or which has been used in explanations. The analyses and the equations used by the computer softwares alone have not been explained since this is nothing that has been performed by hand.

The definitions given beneath for the used softwares are no introductions to these softwares but merely a definition for the programs and what they can be used for.

2.2.1 MATLAB

MATLAB is a programming software that can be used for algorithm development, data analysis, visualization, and numerical computation. It can be used to solve technical problems faster than what a traditional programming language can do (MATLAB; The Language of Technical Computing 1994-2012). In this thesis it has mostly been used to display some of the seismic data in different ways, to create crossplots and to show results from analyses.

2.2.2 Hampson-Russell

Hampson-Russell is a geophysical software specializing in AVO analysis, Seismic Inversion, Reservoir Characterisation and Near-Surface Refraction Analysis. For this thesis it was the part for AVO analyses that was important. The data used in Hampson-Russell were well data and pre-stack seismic data, and the software was used to work on the seismic itself, to perform AVO analyses and to create synthetic seismic data based on information from the well.

3. Previous work

Prior to working with this thesis it was important to become familiar with the area of the Alvheim reservoir and to get an understanding of AVO. This was done in a project work finished January 2012 (Eggen, 2012). In this preceding project work the available data consisted of two wells from the Alvheim area. The one well, 24/6-2, penetrates the one gas discovery, Kameleon, and the other well, 25/4-7, penetrates the oil discovery, Kneler. The second well, penetrating the oil discovery, has been used in this following master's thesis as a source for information. What is interesting is that the Alvheim field consists of a turbidite system and hence one or two wells will not give sufficient information about the whole area to state the lithologies or the content in the present reservoirs located outside the drilled wells.

Due to the fact that the Alvheim reservoir is a turbidite reservoir there were at least two different lithologies that could be said to be present in the reservoir before analysing the logs, massive sandstone and interbedded sand-shale. Since these lithologies can be both cemented and unconsolidated and that they in reservoir relation can contain a variety of three different fluids in all, there are a total of twelve different scenarios that can be present in the reservoir, but not all of them are represented in the wells. Evaluation of the available well log data could show that three of the twelve scenarios actually are present in the reservoir. Well 24/6-2 could show the presence of cemented massive sandstone saturated with gas, while well 25/4-7 showed the presence of unconsolidated interbedded sand-shale saturated with oil and cemented massive sandstone saturated with oil. For these three scenarios the seismic properties were available from the log reports, but since the seismic properties from all the scenarios were needed, a two-layer model was assumed and rock physics modelling was used to extrapolate to the unknown scenarios. When all the seismic properties were available, AVO analysis was performed to see what kind of responses these scenarios would give. The resulting responses could also be said to resemble the responses that could be expected from real data from the area.

Figure 3. 1 shows a crossplot of all the scenarios that can be present in the Alvheim reservoir. The results have been divided into cemented and unconsolidated massive sandstone and cemented and unconsolidated interbedded sand-shale. All these four lithologies can contain the three fluid types, brine, oil and gas, which are shown with separate colours; blue for brine, red for oil and green for gas. In addition to this crossplot, AVO curves were created. The results from the crossplot can together with the AVO curves help dividing the scenarios into the different AVO classes.

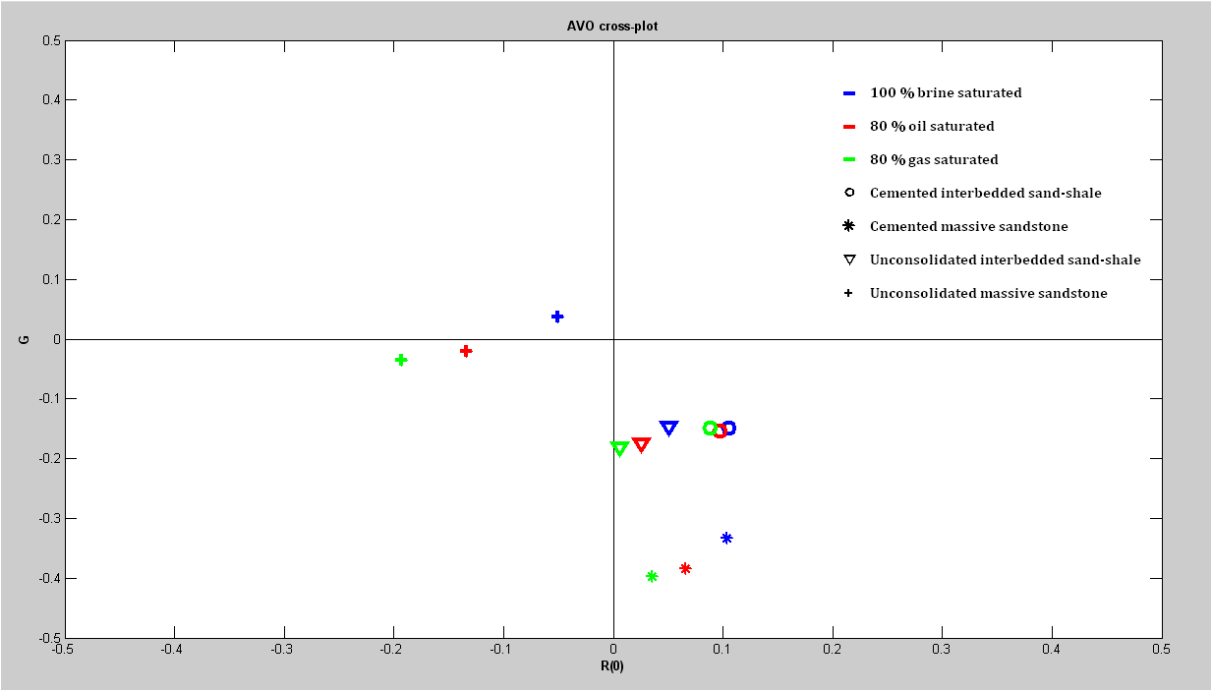

Figure 3. 1: AVO crossplot of all twelve modelled scenarios.
All the possible modelled scenarios in the Alvheim field are plotted in the same plot. The blue points are for 100 % brine saturation, the red points for 80 % oil saturation and the green points for 80 % gas saturation. (Eggen, 2012)

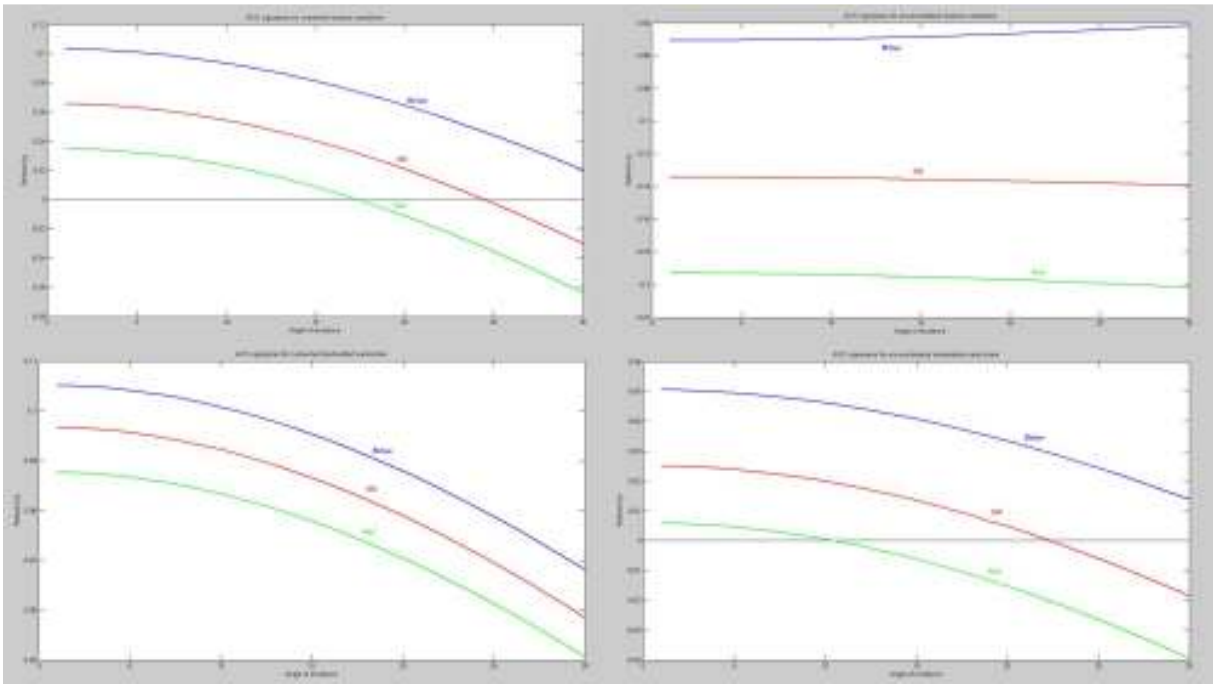

Figure 3. 2: AVO curves for all twelve modelled scenarios.
The two upper plots show the AVO curves for the cemented massive sandstone and the unconsolidated massive sandstone, respectively, while the two lower plots show the AVO curves for the cemented interbedded sand-shale and the unconsolidated interbedded sand-shale, respectively. (Eggen, 2012)

Figure 3. 2 shows the same results as Figure 3. 1 however here they are displayed as AVO curves. Here are the curves for the massive sandstone plotted in the upper two plots, where the cemented massive sandstone is plotted to the left and the

unconsolidated massive sandstone is plotted to the right. The cemented interbedded sand-shale is plotted in the lower left plot while the unconsolidated interbedded sand-shale is plotted in the lower right plot. Sometimes it can be easier to use AVO curves when defining the different AVO classes, but they should give the exact same result as the AVO crossplot. Starting with the cemented massive sandstone it is plotted as stars in Figure 3. 1. From both the crossplot and the AVO curves it is possible to observe that all three fluid saturations have a positive intercept and a negative gradient which gives that it will plot in the fourth quadrant in the AVO crossplot. Comparing this with the classification scheme made for AVO signatures, shown in Figure 2. 1 it can be seen that the cemented massive sandstone fit well with the class IIp AVO anomalies.

The same comparisons can be done for the rest of the scenarios. By doing that it is possible to see that the signatures for the unconsolidated massive sandstone, plotted as crosses in the AVO crossplot, is somewhat different than the others. While the oil and gas filled lithologies both have negative intercept and small negative gradients the brine filled lithology has negative intercept and small positive gradient. The oil and gas filled lithologies will, in the crossplot, plot in the third quadrant while the brine filled lithology will plot in the second quadrant. This gives that the unconsolidated massive sandstone plots as class IV to class III anomaly. The reason that the brine saturated sandstone plot as another class than the oil and gas saturated sandstones can be that the shale parameters used for the capping shale did not actually come from the capping shale but from shale located in between the sand sections. This could cause that the contrast between the cap rock, the sealing shale, and the massive sandstone reservoir was too small.

All three possible saturations for cemented interbedded sand-shale, plotted as circles, have positive intercept and negative gradient which make them to plot in the fourth quadrant and to be classified as a class I anomaly. The last three scenarios are for the unconsolidated interbedded sand-shale, shown as triangles. They have also a positive intercept and a negative gradient. On Figure 3. 1 they plot between class I and class IIp, but they most likely belong to the class IIp anomalies.

Regarding all twelve scenarios together on the crossplot in Figure 3. 1 it is possible to see that they all follow the cementation trend very well, using Figure 2. 2 as reference. The cases with unconsolidated scenarios have a clearly lower intercept than the cemented scenarios. Each lithology follows the hydrocarbon trend very well where the oil and gas scenarios have lower intercept and gradient than the brine filled scenarios. And by comparing the crossplot with the classification scheme shown in Figure 2. 1 it is possible to see that practically every brine filled scenario follow the background trend.

It should be said that the classification of AVO anomalies using only crossplots and plots of AVO curves should only be used as descriptive terms. It cannot be

concluded that the reservoir contains hydrocarbons only based on the classification of the anomalies indicating it. This can only be concluded if it already is known for a fact that there are hydrocarbons present.

This work which was started in the project work has been continued in this master's thesis. For this, only the one well, well 25/4-7, was used since this penetrates the hydrocarbon discovery which it is focused on in this thesis, the Kneler discovery. Two sets of seismic data have also been used, where an AVO analysis has been performed and the results are compared with the results from the project work to see if the modelled scenarios can be used as a substitute for the real data. Since most of the results in the project work are obtained by modelling and assumptions, it will not be given that the results of this master's thesis, which is based on real data, will show the same results even if it is the same area that is being considered.

4. Data description

Two sets of seismic data and data from one well have been available as sources of information for this thesis. The one set of seismic data consists of partial post-stack seismic which covers the entire Alvheim area. This set includes all three hydrocarbon discoveries located in the Alvheim field. The second set of seismic data consists of pre-stack seismic data from a small area around the one hydrocarbon discovery named Kneler which is the one it has been focused on in this thesis. The available well data comes from well 25/4-7 which penetrates this Kneler discovery and therefore give additional information to the seismic.

4.1 Post-stack data

The post-stack data from the Alvheim field is very well processed and is stacked in partial stacks, Near stack and Far stack. According to the processing report presented in Rimstad et al.'s article Bayesian lithology/fluid prediction (Rimstad, Avseth og Omre 2012) these stacked sections are generated from pre-stack-time migrated common-depth-point gathers from 1996. The data was reprocessed and normal-moveout corrected in 2004/2005. Radon demultiple was applied to remove multiples and increase signal/noise ratio, and the stacks were produced according to average angles. Three hydrocarbon discoveries located in the Alvheim field are visible on both partial stacks where they stand out from the background trend.

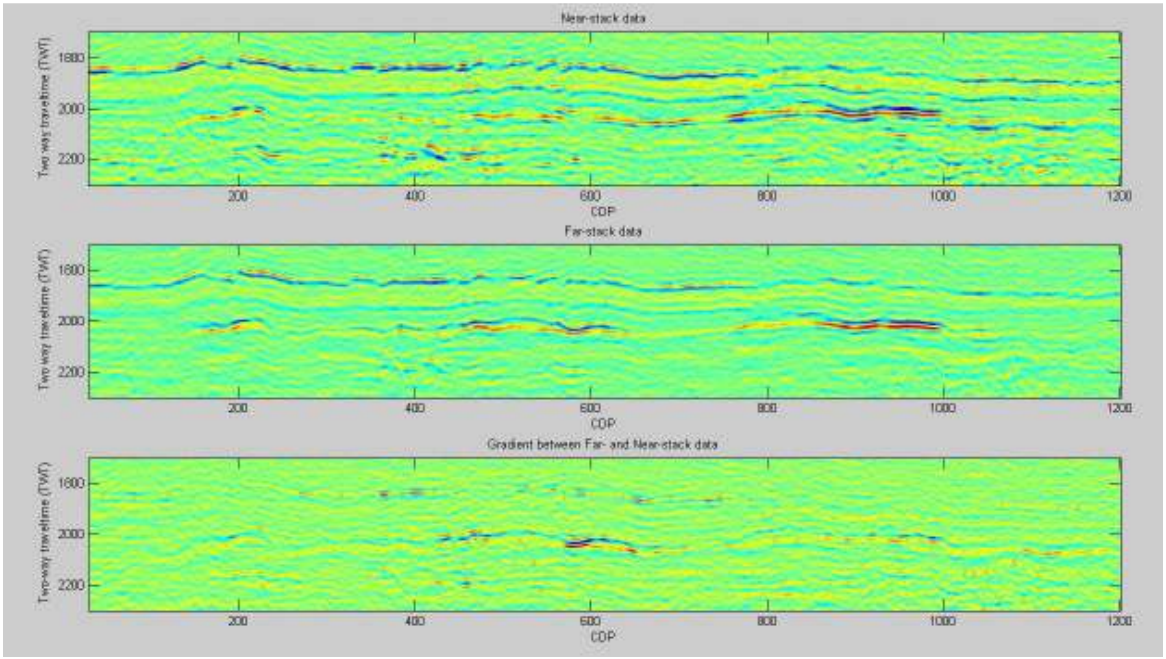

Figure 4. 1: Stacked seismic sections.
Upper section shows Near stack data, middle section shows Far stack data and the lower section shows Far-Near stack data. All sections are plotted as a function of two-way travel time and CDP.

Figure 4. 1 shows the Near and Far stacked sections in addition to a third section showing the gradient, Far – Near stack data. All the three stack sections are shown as a function of two-way travel time and CDP. By closer investigation it is possible to see that all sections show some interesting features standing out from the background trend, but with different clarity. The anomalies are most visible on the Far-stack data. All anomalies are located at approximately the same depth with a two-way travel time (TWT) of around 2000 ms. Prior to the analyses performed here it is already known that the anomalies refer to the three hydrocarbon discoveries that make up the Alvheim field; The Boa and Kameleon gas discoveries and the Kneler oil discovery.

In Figure 4. 2 the Far-stack section is presented alone where the three discoveries are emphasized by ellipses.

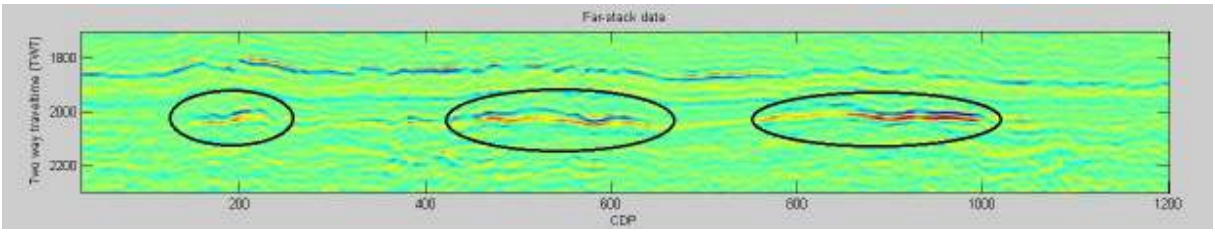

Figure 4. 2: Far stack section with marked hydrocarbon discoveries.
The three hydrocarbon discoveries in the Alvheim field are marked by ellipses; Boa to the left, Kameleon in the middle and Kneler to the right.

The discovery furthest to the left is located partly in the British sector (Petroleumsverksemnd 2011) and is referred to as the Boa discovery. The Boa discovery has been drilled, and it is found to be one of the two gas discoveries in this field. The other gas discovery is the one located in the middle, and is referred to as Kameleon. The discovery located furthest to the right is the one that it has been focused on in this thesis. This is the only oil discovery in this field, and it is referred to as Kneler. Above the three anomalies in the seismic, at slightly shallower depth, it is possible to observe another strong reflector that stands out from the background trend in the same manner as the hydrocarbon reservoirs. This reflector is most likely the base of the Balder Formation, which means that it is the transition between the Balder Tuff and the shale in the Sele Formation. This transition is a very good marker horizon since the change in acoustic impedance is large when going from the tuff to the shales.

4.2 Pre-stack data

The pre-stack data is, as previously stated, from the area around the Kneler discovery. This data is also processed data, however not as well as the post stack data. Since this data is concentrated around the Kneler discovery, it does not have the same extent as the post stack data and consists of 53 inlines, from 1084 to 978, and 60 crosslines, from 4865 to 4985.

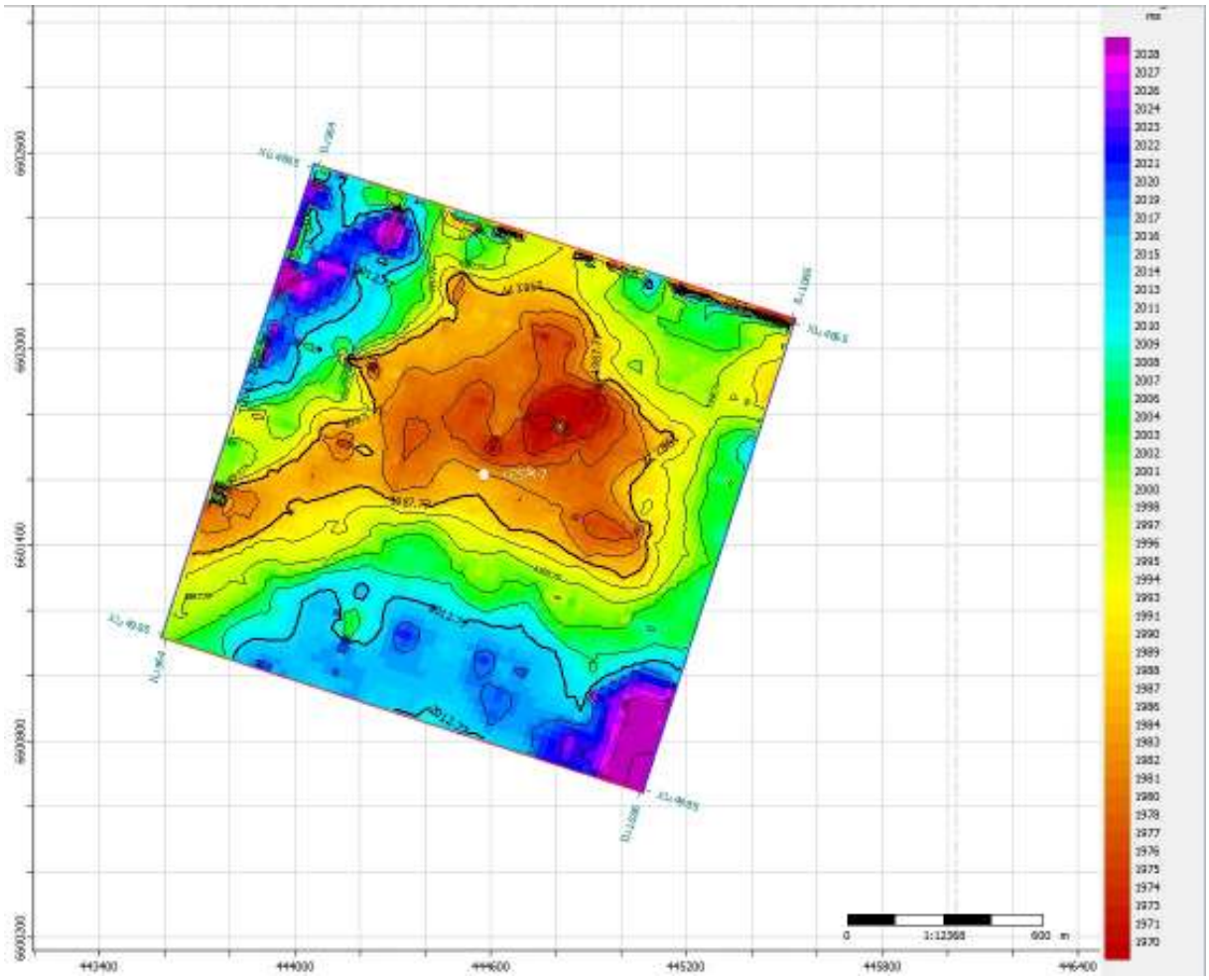

Figure 4. 3: Contour map over the Kneler area showing the top oil sand horizon. The contours are showing every 25 lines, and the Colourbar is showing the TWT.

Figure 4. 3 shows the contour map over the area around the Kneler structure. The contours show the top oil sand horizon. The map is created as a function of two-way travel time, and the colourbar shows how the two-way travel time is related to the colours shown in the map. The major contour lines are drawn for every 25 ms while the minor contour lines are drawn for every 5 ms. From this map, the geological structure is very clear, and it is easy to recognize that there is a sand lobe forming the reservoir. The location where the well penetrates the reservoir is also shown in the map marked by a white point close to the centre of the map.

Figure 4. 4 shows two seismic gathers and one seismic stacked section showing the pre-stack data. The gathers are taken from the provided data, whereas the stacked section has been stacked using Hampson-Russell. The seismic is taken from, and stacked on, crossline 4917, which is the crossline that crosses the well location. The colours put on the seismic are there to make it easier to distinguish between soft and hard events. The red colour marks the hard events, peaks on the wiggle traces, and the blue colour marks the soft events, troughs. The reservoir is located at approximately 2000 meters depth, and there are some observations that can make it possible to define parts of the reservoir only from the seismic data. The red ellipses shown on the gathers marks an AVO effect located neatly above 2000 ms. This is most likely the top of the oil sand marking the top of the reservoir. The seismic data will be investigated more thoroughly later in the thesis.

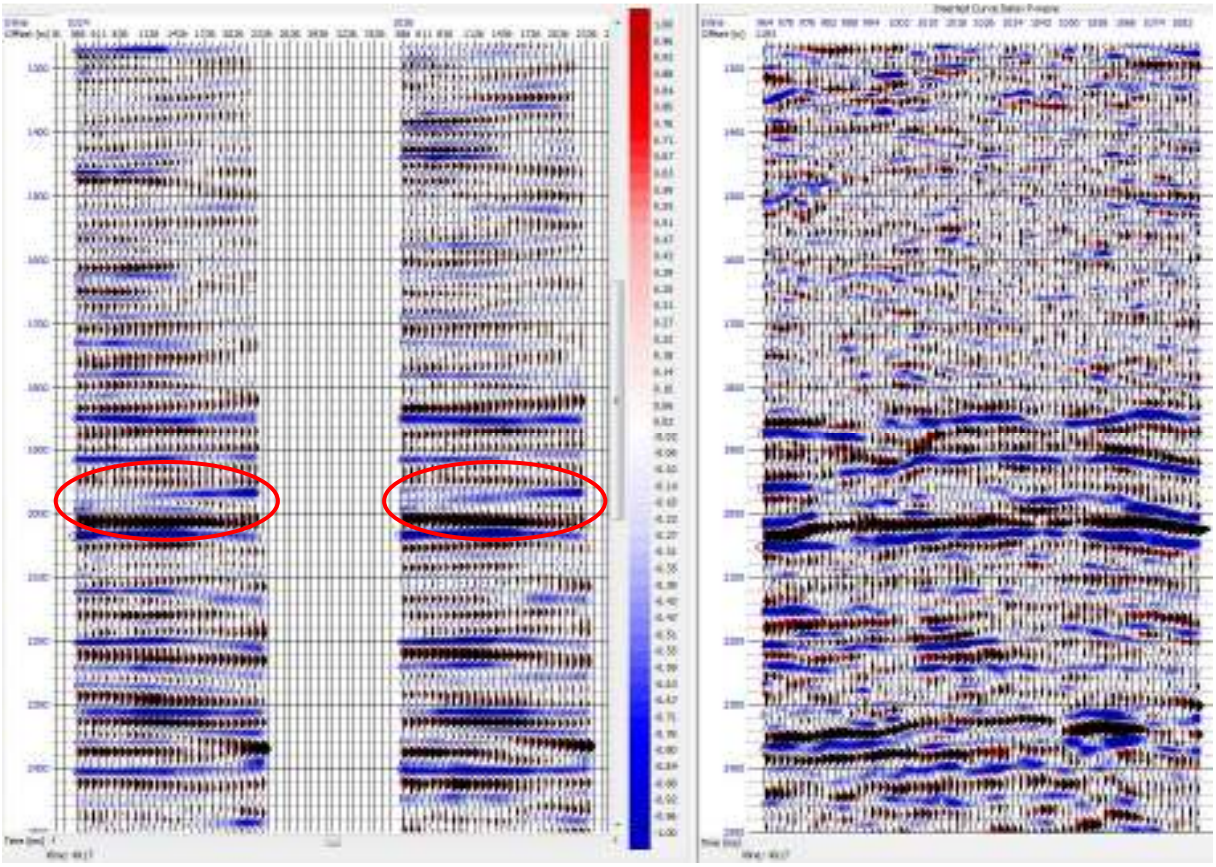

Figure 4. 4: Seismic data from crossline 4917.
Two seismic gathers are shown to the left and a stacked section is shown to the right.

4.3 Data quality control

The data quality is extremely important when performing analyses on the data. If the data does not have a certain quality the analyses can result in wrong answers which again, in this business, can result in serious consequences. In some instances there are certain requirements to the data quality that has to be fulfilled to be able to perform the desired analyses. There are ways to verify the quality, and to assure that the planned analyses can be performed.

One data type where there has to be performed a quality control before using them are the limited range stack sections. It will be shown that AVO attributes are a great addition that helps with the interpretation of the seismic data. To be able to create some of these attributes, it has to be certain that the Near and Far stacks are correctly balanced. To check this, a crossplot of Near stack versus Far stack data can be constructed. Such a plot is shown in Figure 4. 5.

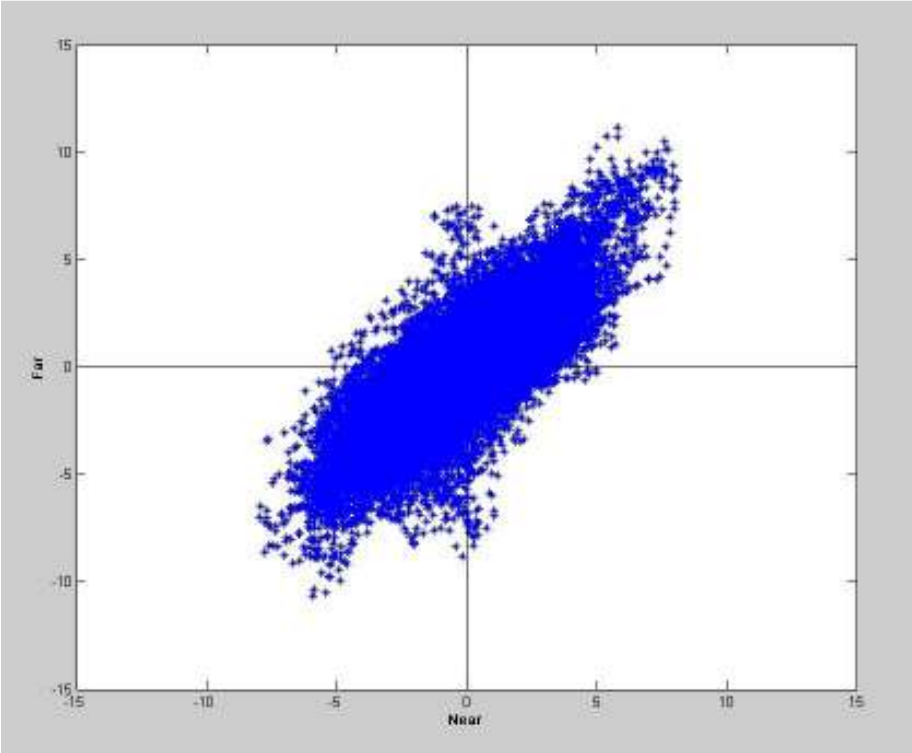

Figure 4. 5: Quality control of partial stacked data.
Plot showing quality control of limited range stack sections with crossplot of Near versus Far stack data.

This plot is composed of the same data which was used to create the three stack sections shown in Figure 4. 1. What can be observed from this plot is that high Near stack values are in accordance with high Far stack values and that low Near stack values are in accordance with low Far stack values. This means that the data are well balanced and that the Far-Near stack can be used as an approximation for the AVO gradient, which will be shown in chapter 5.2. The fact that the Near and Far

data are well balanced should not be surprising according to the processing report mentioned in Rimstad et al. (2012).

5. AVO Analysis

5.1 AVO modelling and well tie

5.1.1 Well data

The well data from well 25/4-7 are the same data that was used in the preceding project. It is possible to get a lot of interesting information from well logs, and they may help to understand the seismic data better. It was found that the well data did not correspond well with the seismic data, and that there were some differences concerning the two-way travel time. To be sure that the two-way travel time is correct throughout the well, check shots can be used to adjust the travel time.

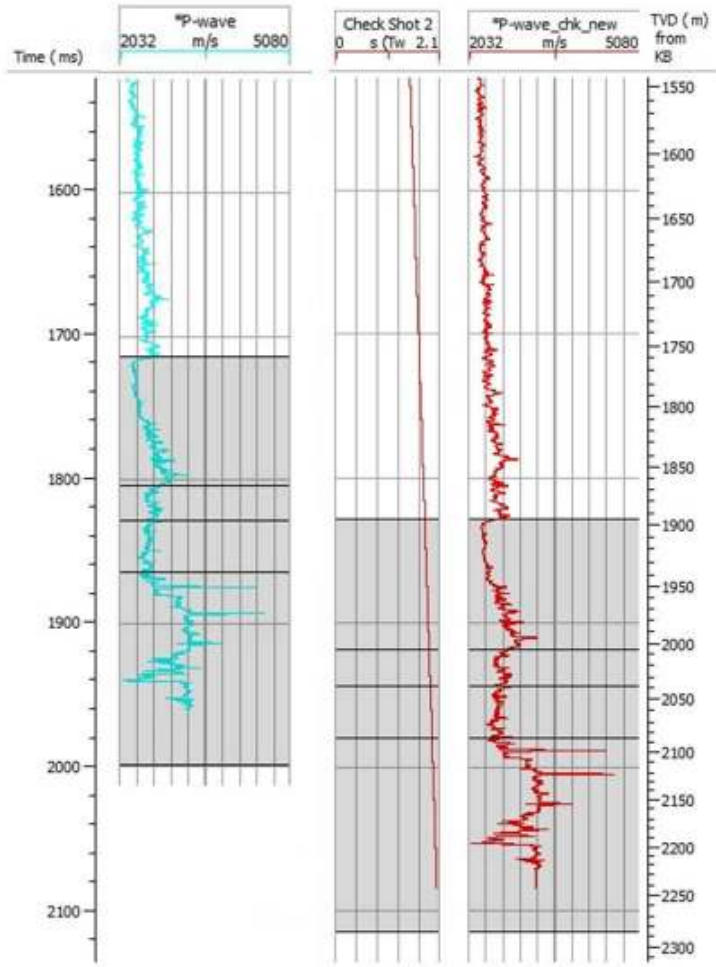

Figure 5. 1: Result from adjusting P-wave velocity using check shots.
Left log shows the P-wave velocity before performing check shot correction, midmost log shows the check shot log showing how the velocity increases with time, and right log shows the velocity after check shot correction has been performed.

Figure 5. 1 shows the result from the shifting of the logs when using check shots. The log furthest to the left shows the P-wave velocity from the well, while the log furthest to the right shows the P-wave velocity after it was adjusted using the check shot shown between the logs. The check shot log shows how the velocity increases with time. This log looks to be linear on this figure, but if the check shot log had been presented from the sea bottom it would be possible to see that it actually has a slight curvature to the right. When the P-wave velocity has been corrected, the other logs can be adjusted as well, and the well logs will correspond well with the seismic data from this location.

Figure 5. 2 shows the logs from the well after the check shot correction has been performed. All these logs contain invaluable information which can help defining both reservoirs and other important intervals in the well. The two last logs in the figure, acoustic impedance and Vp/Vs ratio are not logs that were measured in the borehole, but they have been calculated in Hampson Russell using the other logs from the well.

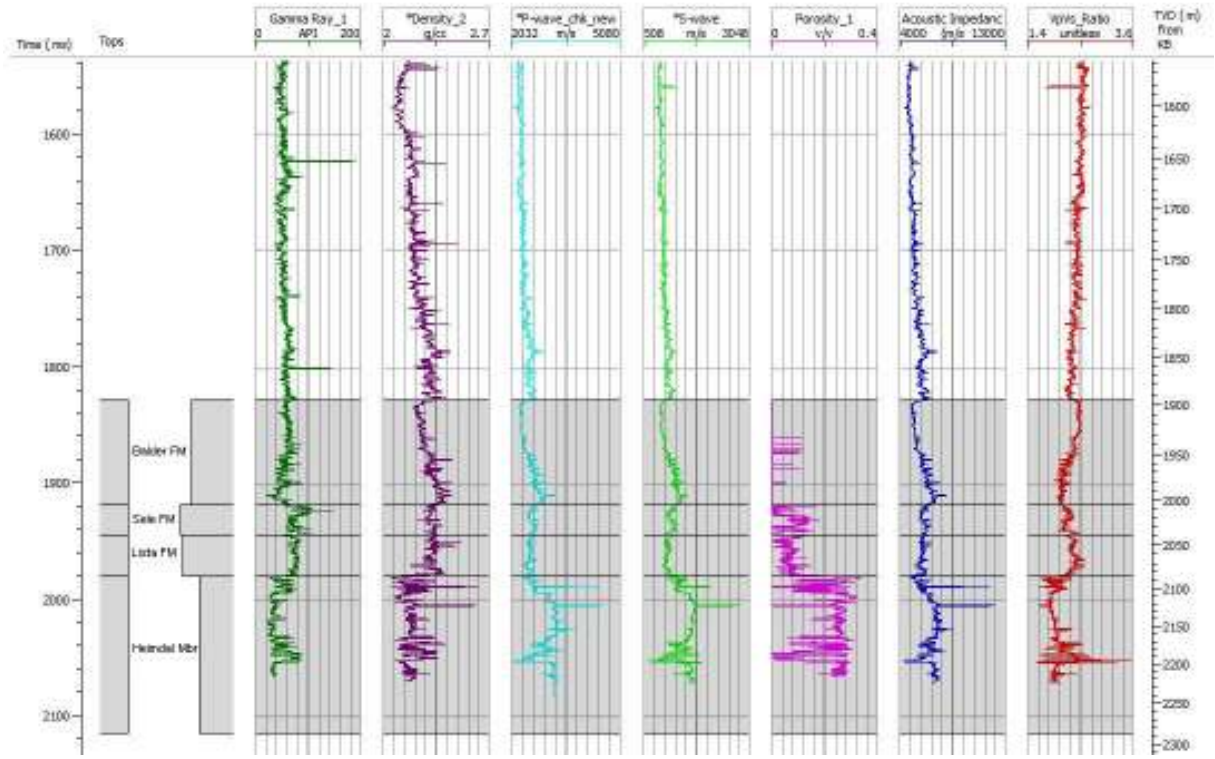

Figure 5. 2: Logs from well 25/4-7.
From left to right; Gamma ray log, Density log, P-wave velocity, S-wave velocity, Porosity, calculated Acoustic impedance and calculated Vp/Vs ratio. A larger version of this figure is shown in Figure B in the Appendix.

The lithostratigraphic column shown furthest to the left in the figure above shows the lithologies found in the well when drilling. They are placed on the well logs to get a better understanding of the information from the logs. From the geological history and previous analyses it can be shown that the base of the Balder Tuff is located just beneath 2000 meters depth. This can be seen on the gamma ray log where there is a sudden increase in log values while the velocity logs show a sudden decrease in

velocity. This is typical for the transition between the Balder Tuff and the shale in the Sele FM since there is a large change in acoustic impedance when going from tuff to shale. Another clear transition is the one between the shales in the Lista Formation and the top of the sands in the Heimdal Member in the lower part of the Lista Formation. This is the top of the oil reservoir, located at approximately 2090 meters depth. Just inside the reservoir the gamma ray log shows a somewhat corrugated signal which indicates that the top of the reservoir does not only consist of clean sandstone. This is because the upper part of the reservoir consists of unconsolidated sand-shale. There are also some fluctuations within the density values while the velocity increases downwards in the reservoir. Beneath the fluctuating interval on the gamma ray log the value is stabilizing and it is likely to presume that the log has moved into cleaner sandstone. Also the density log stabilizes and increases slightly beneath the interbedded part of the reservoir, and the velocity logs show a gradual increase in velocity downwards. The reason for increase in density value is that the reservoir becomes more cemented going downwards which matches the definition of the lithologies found in this well stating that the reservoir consists of unconsolidated interbedded sand-shale over a more cemented massive sandstone. The base of the reservoir can be said to be located at approximately 2132 meters depth which is where the oil-water contact (OWC) is found to be (Simm 2005).

In addition to just using the logs for interpretation, they can also be used for other purposes. The two calculated logs of acoustic impedance and Vp/Vs ratio was used to create a Rock Physics Template (RPT) plot. RPT's are templates of rock physics models for prediction of both lithology and hydrocarbons. The RPT plot from these logs is shown in Figure 5. 3.

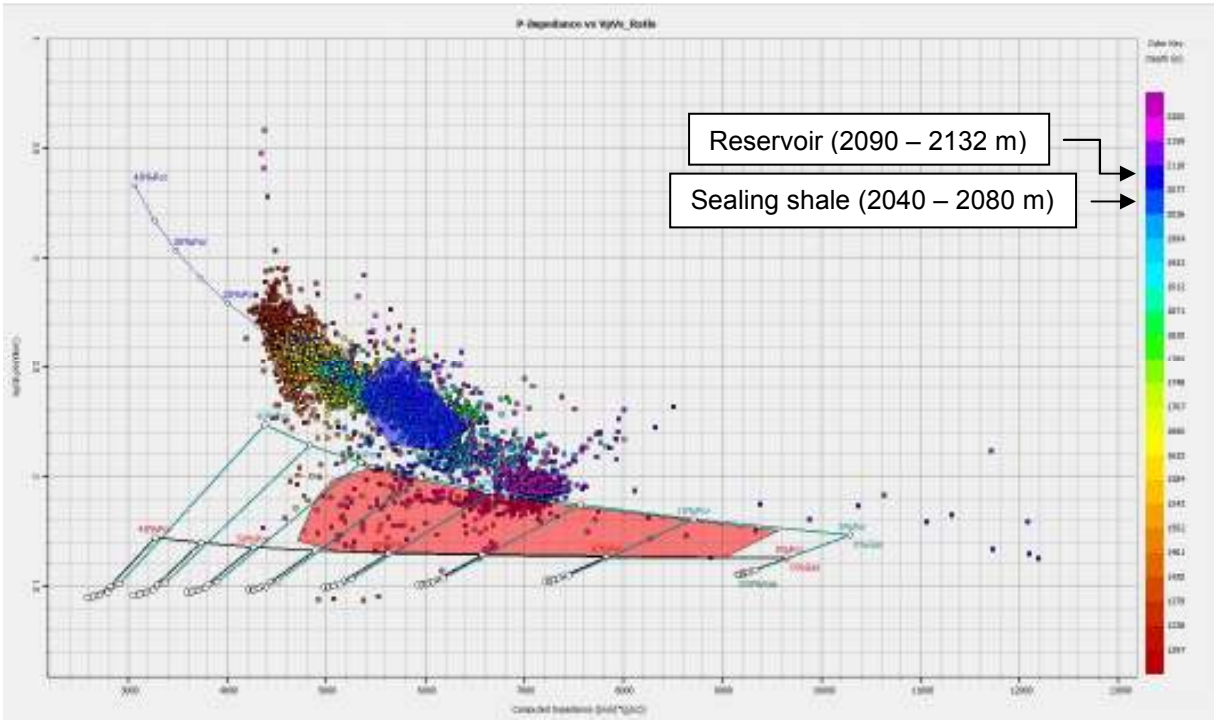

Figure 5. 3: RPT plot presented as crossplot of Acoustic Impedance versus Vp/Vs ratio. The red polygon marks the points taken from inside the reservoir and the blue polygon marks the points where the sealing shale is located. The reservoir polygon is bounded by two rock physics templates; the lower, black, template shows the oil to gas boundary while the upper, dark green, template shows the water to gas boundary. The third template in the plot is the shale template.

The points in the figure above are plotted as a function of depth which is shown on the colourbar. There are two polygons on the plot closing in points from two parts in the well. The polygon marked red represents the points that are taken from the reservoir, the part filled with oil. This polygon is chosen by creating the two rock physics templates placed on either side of the polygon on the plot. It is already known that the upper part of the reservoir is located in interbedded sand-shale. To make the templates represent these reservoir conditions the best, the lithology in the reservoir was set to contain 40% shale and 60% sandstone when creating the templates. The lower, black, template is the oil to gas boundary while the upper, dark green, template is the water to gas boundary. This means that the points that plot in between these two lines are points that have the Acoustic Impedance (AI) values and the Vp/Vs ratios that may come from an oil filled reservoir. There may be other parts in the well that also show the same AI and Vp/Vs values, and therefore were the points closed in the polygon matched with the known reservoir depth from the colourbar. The points that were found to not match the reservoir depth are the ones that can be found between the two templates but are not closed in by the polygon. There are several reasons for these points to have the same AI and Vp/Vs values as the reservoir. There may be some wrong measurements made in the well causing the points to plot between these templates, but there is also the possibility that there are brine saturated sandstones in the well where there also is a presence of diagenetic quartz cement. This cement will cause the points from this sandstone to plot in an

area with very low Vp/Vs values. This area may then interfere with the area where it is expected to find hydrocarbon saturated sandstones. But no matter what causes these points to plot in between the templates, it does not affect the result since the reservoir depth is known and the wrong points can be filtered out.

The blue coloured template is the shale template. There is a blue polygon shown somewhat lower than the lower end of the template. This polygon is closing in the points that are found to represent the shale working as a cap rock for this reservoir. Since there is a large cluster of points, the shale cap rock had to be found by using the depths in the colourbar. This showed that the points from the shale have a lighter blue colour than the points from the reservoir, and the polygon was created around these points.

The points that are located inside the reservoir polygon and the points inside the shale polygon can now be shown on the two logs used to create this crossplot to show what parts of the well these points represent. The AI log and the Vp/Vs ratio log with the markings from the RPT plot are shown in Figure 5. 4. The grey area marking the formation boundaries is still visible on these logs to give an idea of the location in the well.

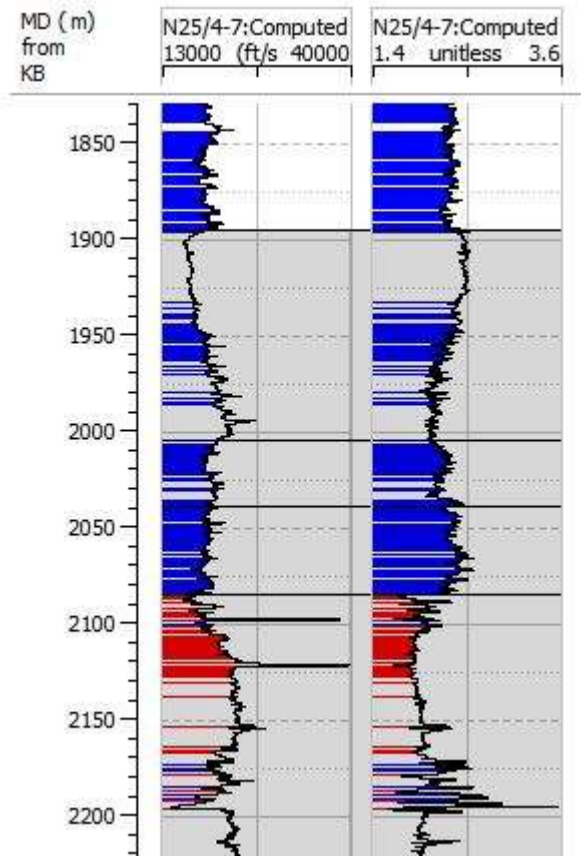

Figure 5. 4: Logs of Acoustic Impedance and Vp/Vs ratio with marked reservoir zone. Blue colouring shows the location of the points closed in the shale polygon and the red coloured area shows the location of the points closed in the reservoir polygon in the previous figure.

The points closed in the reservoir polygon in the RPT plot in Figure 5. 3 are marked with the red colour in the plot above and the points from the shale polygon are marked by the blue colour. By disregarding the smaller red coloured areas and focusing on the larger area, it is possible to recognize that the coloured area matches the area defined as the reservoir in Figure 5. 2 pretty well. The top reservoir is located at approximately 2090 meters depth, while the OWC is located around 2132 meters. The reason that there are many smaller areas marked with red marker is that, as previously stated, there may be some wrong measurements, but there is also the possibility that some points have the same AI value and Vp/Vs ratio as points located inside the reservoir even if they are not. This may lead to the misleading colouring. Regarding the blue colouring it can be seen that there is a much larger area that is coloured here. What has to be remembered is that the polygon for the shale was created over a large cluster of points where the wanted points were placed on top. This means that all the areas coloured blue on the logs above do not necessarily contain shale since all the points located under the intended points will plot on the logs as well. But what also can be seen is that the shales in the Lista Formation located over the reservoir area are marked blue, and these are the shales that work as a cap rock for this reservoir.

5.1.2 Synthetic seismic data

In addition to having real seismic data, it is also possible to create synthetic seismic, and when doing so, the data from the well is used to create artificial seismic data from the area where the well is drilled. It should be possible to recognize the similarities between the two seismic sections, the real seismic and the synthetic seismic created from the well data. Especially the interesting features, such as the top of the reservoir shown by the AVO effect, mentioned in chapter 4.2, should be found visible also on the synthetic seismic data. Depending on the information taken from the well before creating the synthetic seismic, there is often an evident reduction in noise related to the real seismic. This can result in the fact that some features are more visible on the synthetic seismic because there is no noise affecting the picture. When first creating synthetic seismic a wavelet is needed. This creation of synthetic seismic was done in Hampson-Russell and there were several possibilities to create a wavelet; one could be extracted from the well, or it was also possible to just create a standard wavelet. First it was tried to extract a wavelet from the existing well. This wavelet is shown in Figure 5. 5 on the next page.

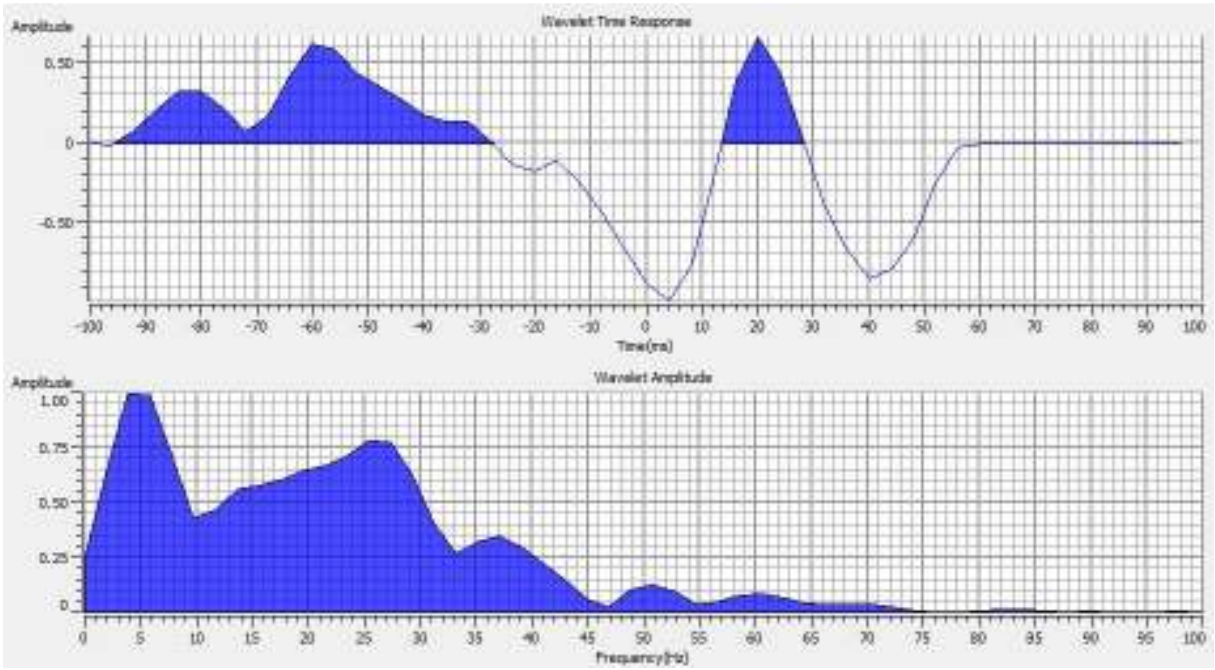

Figure 5. 5: Wavelet extracted from well 25/4-7.
The wavelet contains noise that could affect the quality of the synthetic seismic data if it was used to create it.

What can be seen from this figure is that this wavelet contains a great deal of noise. This can lead to noisy synthetic seismic, and the advantage of being able to see some of the important features more clearly on the synthetic seismic is no longer evident. But it can also be seen that, when disregarding the noise in the beginning of the wavelet, the main wavelet is very similar to a Ricker wavelet, which is a normal zero-phase wavelet. Therefore, to avoid the noise in the synthetic seismic which this wavelet could cause, a normal Ricker wavelet was constructed to be used when creating the synthetic seismic instead of the wavelet extracted from the well. When creating this Ricker wavelet the dominant frequency was set to be 25 Hz. The wavelet that in the end was used to create the synthetic seismic is shown in Figure 5. 6.

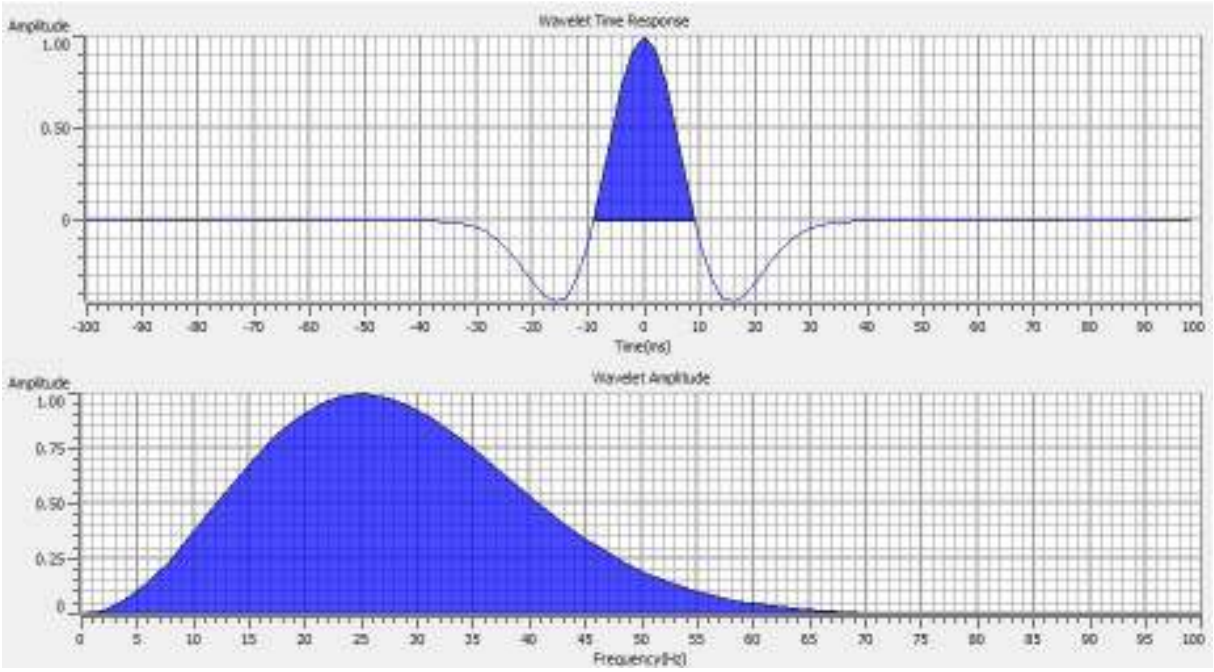

Figure 5. 6: Ricker wavelet.
The wavelet used when creating the synthetic seismic. Both the time response (top) and the amplitude (bottom) are shown.

Since this wavelet is nice and noise-free it could be used to create the synthetic seismic which would resemble the real seismic by containing the important features visible on the well log data but at the same time contain much less noise. The seismic that was created by using this wavelet is shown in Figure 5. 7. The reflectors shown in the seismic are clear to see and there is no noise to affect the reflectors behaviour. The seismic will have the same two-way travel time (TWT) as the well log data since the velocities for the seismic are taken from the logs. Since there was performed a check shot correction on the logs, the TWT should match the one on the real seismic data and the special features should be located at the same depth. Thinking back to the gathers from the real seismic data shown in Figure 4. 4 there was a pretty clear AVO effect representing the top reservoir visible on the gathers at 1980 ms. By looking at the newly created synthetic section is it possible to observe the same AVO effect here at approximately the same depth. However, as an effect of the lack of noise in the synthetic seismic, it is easier to see that there is a gradual increase in amplitude in this section in relation to the real seismic. There is nothing that states that a synthetic section will give the correct answers when using it as the only information, but using it as a supplement to the real seismic to show how the noise affects the seismic data can be of great value.

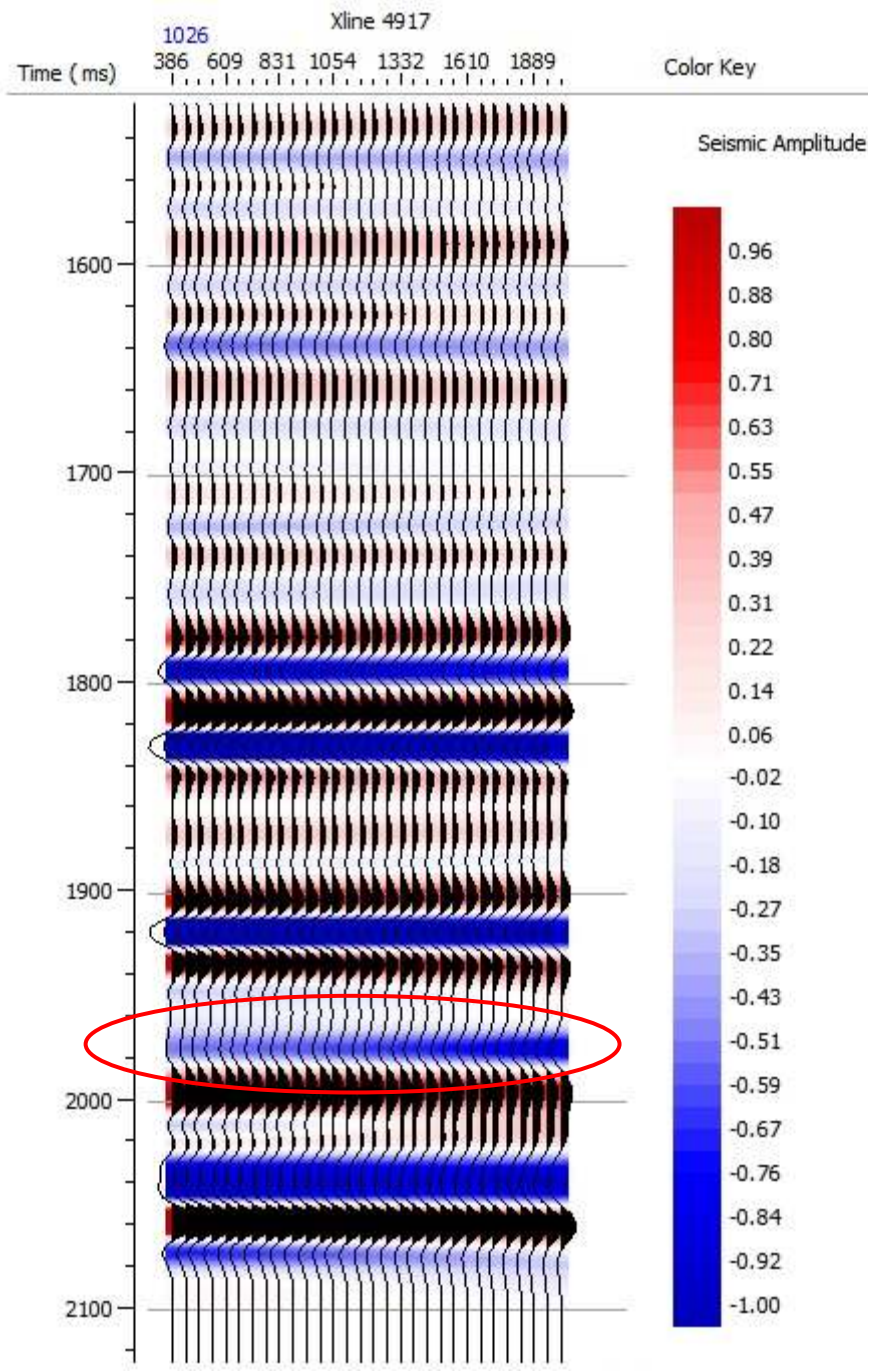

Figure 5. 7: Synthetic seismic gather.
The AVO effect marking the top oil sand is marked by a red ellipse.

5.2 AVO attributes

To make it easier to discover new hydrocarbons, the AVO data should be interpreted correctly. To help with the interpretation, it is possible to use AVO attributes. There are several AVO attributes that can be used for this purpose.

An often used attribute is the crossplot between intercept (R(0)) and AVO gradient (G). As an approximation to this crossplot it is possible to use a crossplot of Near versus Far – Near stack data. This is an AVO attribute that is created from limited-range stack sections. The Near stack data can be used as an approximation of the intercept while the Far – Near stack data can be used as an approximation to the AVO gradient. For this attribute to be legitimate, both the Near stack and the Far stack data have to be correctly balanced (Avseth, Mukerji and Mavko 2005). A test of this was performed in chapter 4.3 where it was found that the data are correctly balanced and the crossplot of Near versus Far stack data is a good approximation of the crossplot between intercept and AVO gradient.

Now this crossplot can be created from the Near and Far stack data. However, if a crossplot is made from the whole area, it will not be possible to distinguish the trends of each of the hydrocarbon discoveries since there are both oil and gas discoveries in the area. To separate the different trends from each other, smaller areas around the interesting areas were picked. Plotting these areas separately on top of each other can make it possible to see how the trend of one of them varies in relation to the others.

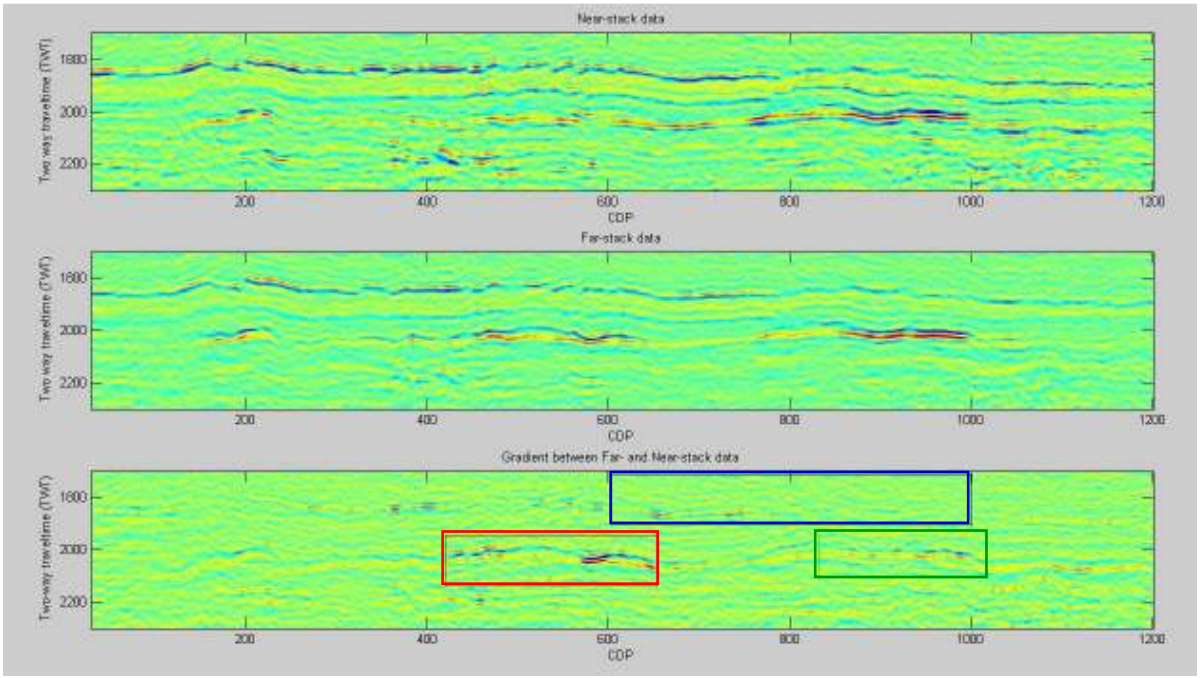

Figure 5. 8: Stacked sections with marked anomaly areas.
The marked areas are the areas used when the anomalies were plotted in a crossplot. The blue marks the area used for the shaly background trend, the red marks the gas anomaly and the green marks the oil anomaly.

Figure 5. 8 shows the same figure as in Figure 4. 1 however in this figure an area around the anomalies of the Kneler and Kameleon discoveries have been marked by boxes. The red box marks the Kameleon discovery; the green box marks the Kneler discovery while the blue box marks an area somewhat above the hydrocarbon discoveries. The area within the blue box is representative for the shaly background trend, and was used to show how the trends from the hydrocarbon discoveries stand out in comparison to the background trend.

Figure 5. 9 shows two crossplots where the Near stack data has been plotted against the Far – Near stack data with respect to the two-way travel time. The crossplot to the left is the crossplot from the whole Alvheim area as a function of the two-way travel time, and the crossplot to the right shows the three areas marked in the figure on the previous page plotted on top of each other to show how they differ from the background trend.

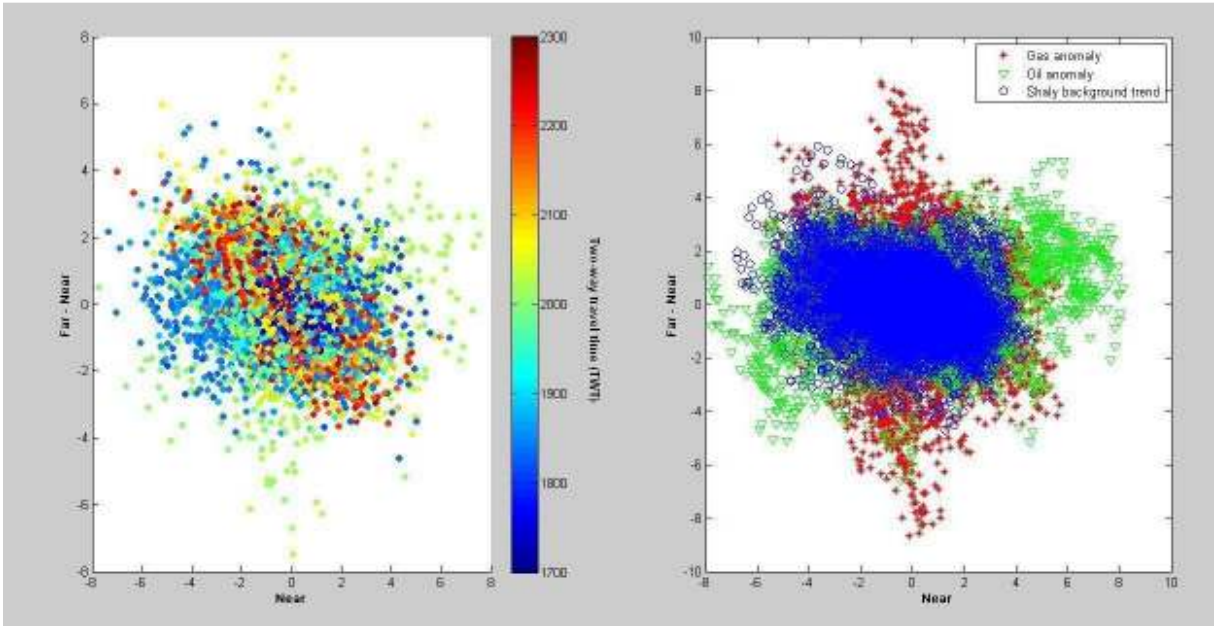

Figure 5. 9: Crossplot of anomalies.
Crossplots where the near and far-near stack data are plotted against each other. The plot to the left is a plot of the whole area where the Alvheim field is located. The colourbar shows the two-way travel time. In the plot to the right it has been separated between the different anomalies. The blue circles represent the shaly background trend, the red stars represent the gas anomaly while the green triangles represent the oil anomaly.

As previously stated, the plot to the left showing points from the whole area does not give so much information since it only is one big cluster of points. But the plot to the right, showing only the marked areas, can tell a lot more about the hydrocarbon discoveries. It can be seen that the Kameleon gas discovery, represented by the red points, and the Kneler oil discovery, represented by the green points, stand out from the shaly background trend, shown in blue. According to the classification scheme in Figure 2. 1 the anomalies are located on the lower left quadrant of the crossplot. The crossplot above shows the top of the anomaly on the lower left side, while it also

shows a deviation from the background trend in the upper right quadrant. This deviation represents the base of the AVO anomaly. It is therefore possible to observe both top and base anomaly on an AVO crossplot. By classifying the shown anomalies it can be found that the red points, the gas discovery, plot as a class II AVO anomaly while the green points, the oil discovery, plot more in line with a class III AVO anomaly. The areas that are chosen when making this crossplot are chosen by hand and they may therefore not be as closely centered to the reservoir as preferred, but they still show clear anomalies that stand out from the background trend. For this thesis it is the oil discovery that is most interesting, and since the class III AVO anomalies represent soft sands saturated with hydrocarbons, the classification made fit well with this reservoir where there are unconsolidated sands in the upper part.

Another type of attributes that can be useful is Far – Near times Far and Far – Near times Near. A plot of these attributes is shown in Figure 5. 10. The Far – Near times Near attribute is a good attribute to enhance class III hydrocarbon-related AVO anomalies. At the same time as this enhances the hydrocarbon it will reduce the corresponding brine-saturated class II AVO response. In the Far – Near times Far attribute the Near stack is weak while the far stack is a strong negative, and this gives that this attribute is good for the opposite, enhancing class II AVO anomalies (Avseth, Mukerji and Mavko 2005).

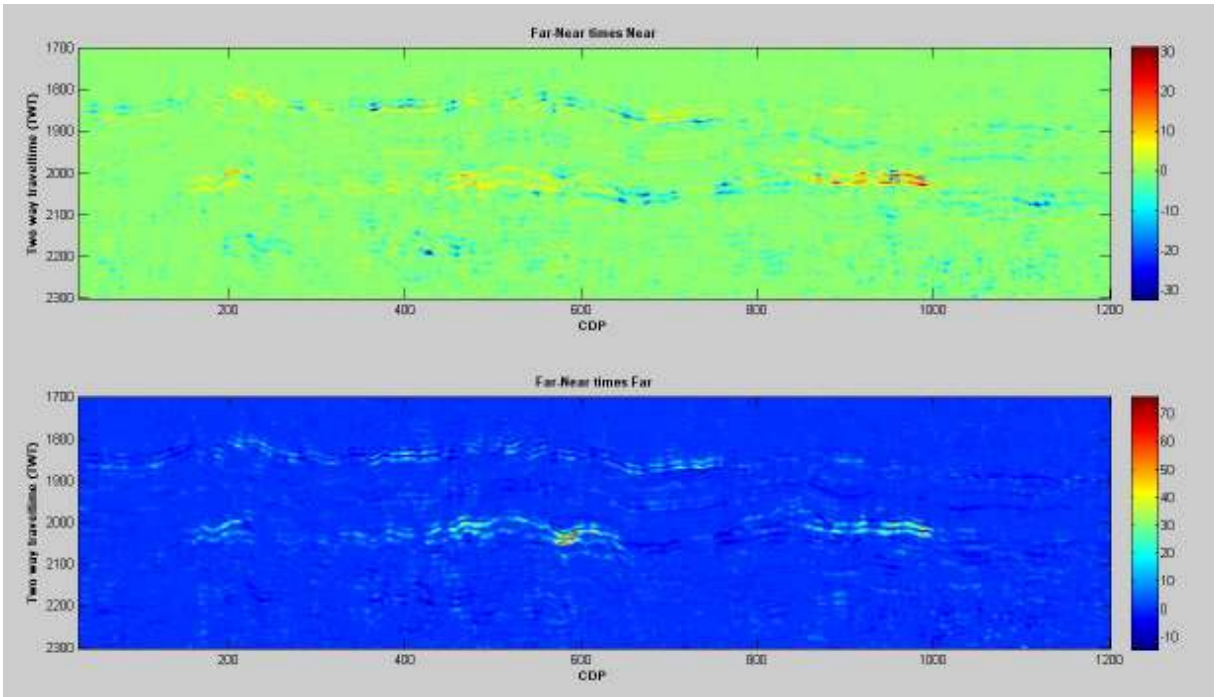

Figure 5. 10: AVO attribute plot of FNxN and FNxF.

The upper plot in this figure shows the Far – Near times Near attribute. Here it can be seen that it is the Kneler oil discovery which is enhanced the most. Since this attribute enhances class III AVO anomalies, this attribute gives the same result as the crossplot shown in Figure 5. 9. This kind of plot can also be used as an

approximation to the product stack. The lower plot shows the Far – Near times Far attribute. On this plot it is not the Kneler oil discovery which is enhanced but the Kameleon gas discovery. The discovery itself is positive while the background trend is negative. This attribute enhances the class II AVO anomalies, and this result also confirms the classification in Figure 5. 9.

Watching both sections it can be seen that on both plots, and on all three discoveries it is possible to see the top and the base of the reservoir. All discoveries are shown by two reflectors where the upper reflector represents top reservoir and the lower reflector represents the base. The reason that all discoveries show a positive signal is that they all have a negative intercept and a negative gradient, and since negative and negative becomes positive, they stand out in that manner.

The previous shown AVO attributes are all performed on the post stack seismic which covers the entire Alvheim area. It is also possible to make several AVO attributes from the pre-stack data set, given that the data have been stacked first. Figure 5. 11 shows the crossplot made from the pre-stack seismic concentrated around the Kneler discovery after stacking. The plotted area is well focused around the reservoir. Here there are no limited range stack sections available, so for the construction of this plot the intercept and gradient were calculated from regression of the seismic gathers using Hampson-Russell. This will cause the gradient to contain more noise than the approximation to the gradient, the Far-Near stack used for the crossplot from the post-stack data. Matching the coloured points in the plot with the colourbar, it can be found that the green and yellow coloured points represent the reservoir interval. Analysing the plot it is possible to see that there is a small deviation from the background trend also here, but it is not as clear as the one shown in Figure 5. 9. It also looks like this crossplot is somewhat rotated in relation to the other crossplot causing the deviation not to be so prominent. Knowing the area where the data are from can give an indication of what answer is expected when the data are not obvious enough, and it is difficult to make a classification from one plot alone. It should preferably give the same answer as was obtained from the other set of seismic data from the same area.

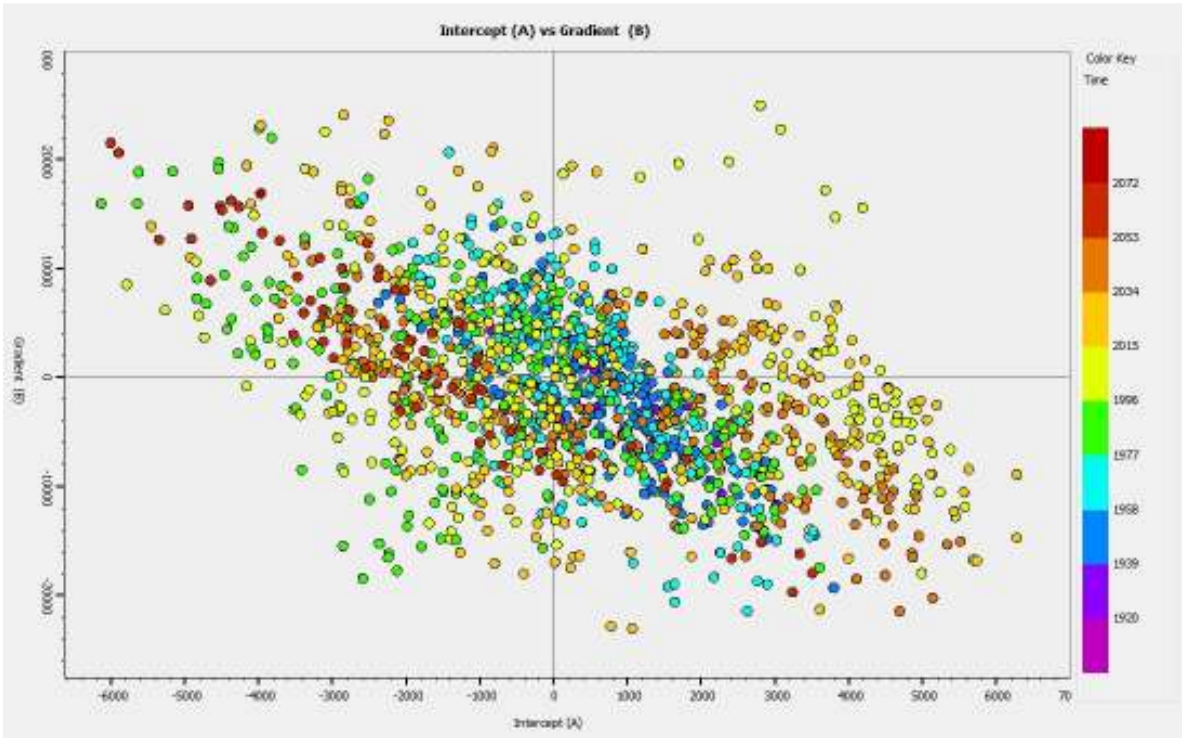

Figure 5. 11: Crossplot of Kneler discovery.
The plot shows points from the reservoir as a function of two-way travel time.

To help classifying the anomaly it is possible to perform an AVO gradient analysis on the data. As was done for the several modelled scenarios in the project work finished in January 2012 (Eggen 2012) AVO curves can make it easier to place an anomaly in one of the AVO classes. Figure 5. 12 shows the AVO gradient analysis performed on the crossing inline and crossline from the real data where the drilled well is located. The gradient analysis itself is performed on the visible AVO effect which marks the top of the oil sand.

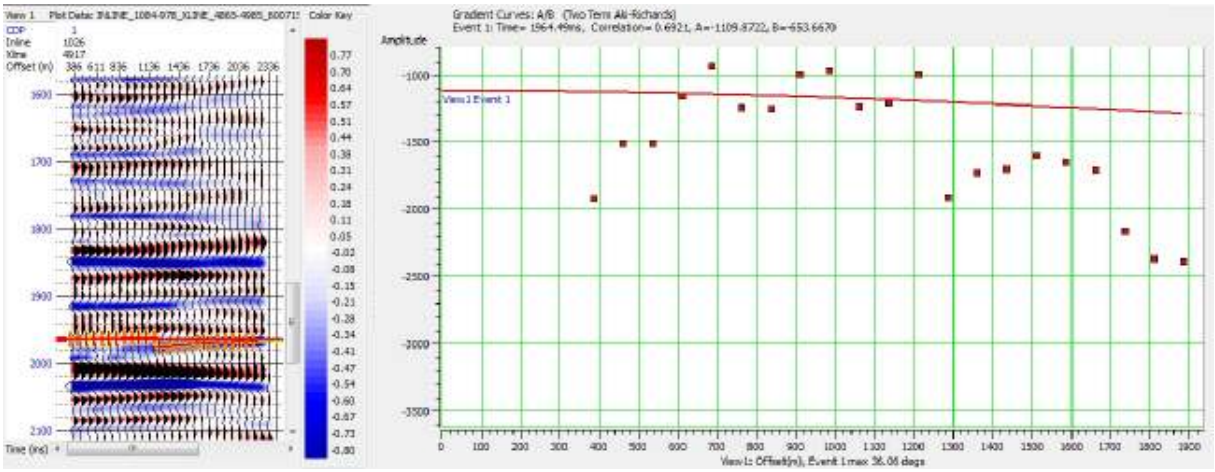

Figure 5. 12: AVO gradient analysis of the real seismic data.
The yellow and red crosses on the seismic to the left show the separate traces where the gradient analysis has been performed. Every cross represents one point in the plot to the right which shows the amplitude from the exact location of the red and yellow crosses. The solid line has been adapted on the points to find the most suitable AVO curve. A larger version of this figure is shown in Figure C in the Appendix.

The seismic to the left shows the reflector where the gradient analysis has been performed, marked by red and yellow crosses. It is possible to see that there is a break approximately in the middle of the marked line. This is done because it looks as if there may be some tuning effects in the seismic. It is difficult to say exactly what the reason for this is, but it looks like there is a thin, stiffer, layer which is not thick enough to be observable on the seismic that is located in between two soft events. So, when it was chosen where to perform the gradient analysis the best fit was chosen. It is also possible that there is interference between the soft, blue, event and the underlying hard, red, event. The lower reflector of the soft event can be the side lobe of the underlying hard event.

The plot to the right displays the result of the gradient analysis. The separate points show the amplitudes from each trace whereas the solid line is adapted to the points to find the best fit AVO curve. It is very clear to see from this figure that the AVO effect is not represented by a clear gradual increase in amplitude, but rather a more fluctuating increase by the way the separate points are spread. It is possible that it is the noise in the data that causes the amplitudes to vary that much. Even if the AVO effect was nicely visible, this AVO curve shows that the amplitude varied a lot more from one trace to another than what was possible to see from the seismic. Now it is possible to compare this curve with the classification scheme in Figure 2. 1. The line has a negative intercept and a negative gradient which again gives that this fits well with a class III AVO anomaly. A class III AVO anomaly represents, as earlier mentioned in chapter 2.1.3, soft sands with high fluid sensitivity. This AVO class is also located far away from the background trend and should be easy to detect on seismic data, which it is in this case where the gradient analysis has been performed on the easily visible AVO effect. The result obtained from this gradient analysis matches the result obtained from the crossplot of Near stack data versus Far – Near stack data from the post-stack data.

The AVO gradient analysis above was performed on the real seismic data which contains a great deal of noise. The same analysis can also be performed on the synthetic seismic. Since the synthetic seismic is created by using values from the well that penetrates the Kneler reservoir, it is expected that this analysis will give the same result as the analysis performed on the real seismic.

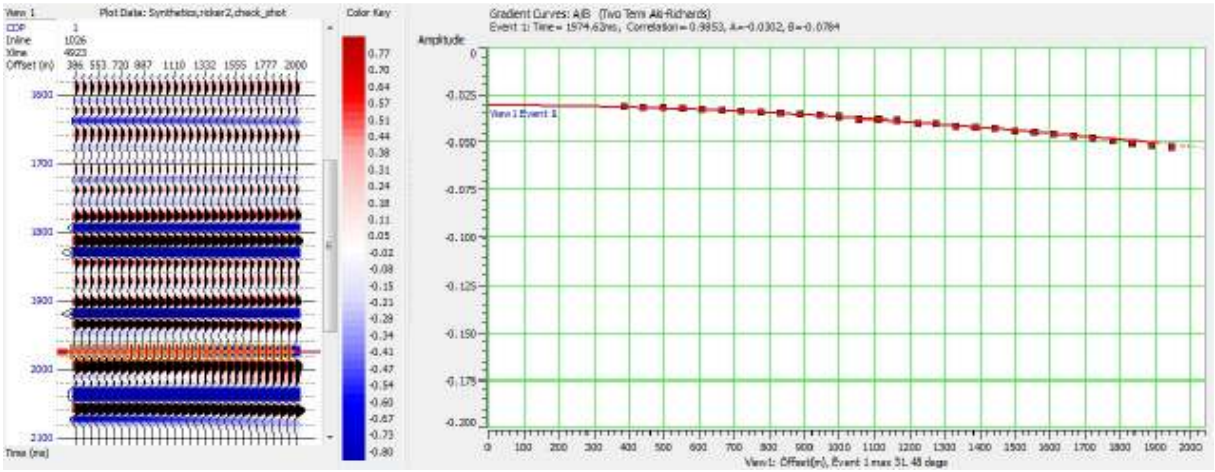

Figure 5. 13: AVO gradient analysis of the synthetic seismic data.
Also here the crosses on the gather to the left represent the amplitudes from the several traces plotted as points in the crossplot to the right. A larger version of this figure is shown in Figure D in the Appendix.

Figure 5. 13 shows the results from the gradient analysis performed on the synthetic seismic. Here again the seismic to the left shows where the gradient analysis has been performed. It is possible to observe the AVO effect on this seismic as well, here also marked by the red and yellow crosses. This seismic is more or less noise free which leads to the AVO effect being easier to detect and to follow. Even if this gather does not show any signs of tuning effects where the AVO effect is located, does not mean that there is no thin, stiff layer located between two soft layers. Tuning effects may also appear on synthetic seismic, however this is not the case for this exact location on the gather. The plot to the right shows the result from the gradient analysis. What can be seen from this plot in relation to the plot from the gradient analysis performed on the real data is that the adapted solid line fits the separate amplitude points almost perfectly. The amplitudes from each trace do not vary that much from one trace to another either. The result of this gradient analysis shows the same as the analysis performed on the real data; a curve with both negative intercept and gradient that can be classified as a class III AVO anomaly.

5.3 Observations

In the following chapter are the observations that were made when performing the different AVO analyses on the seismic data shown. Both sets of seismic data and the data from the well have been considered and compared. Both similarities and differences between the different analyses are found and discussed.

5.3.1 Inside reservoir area

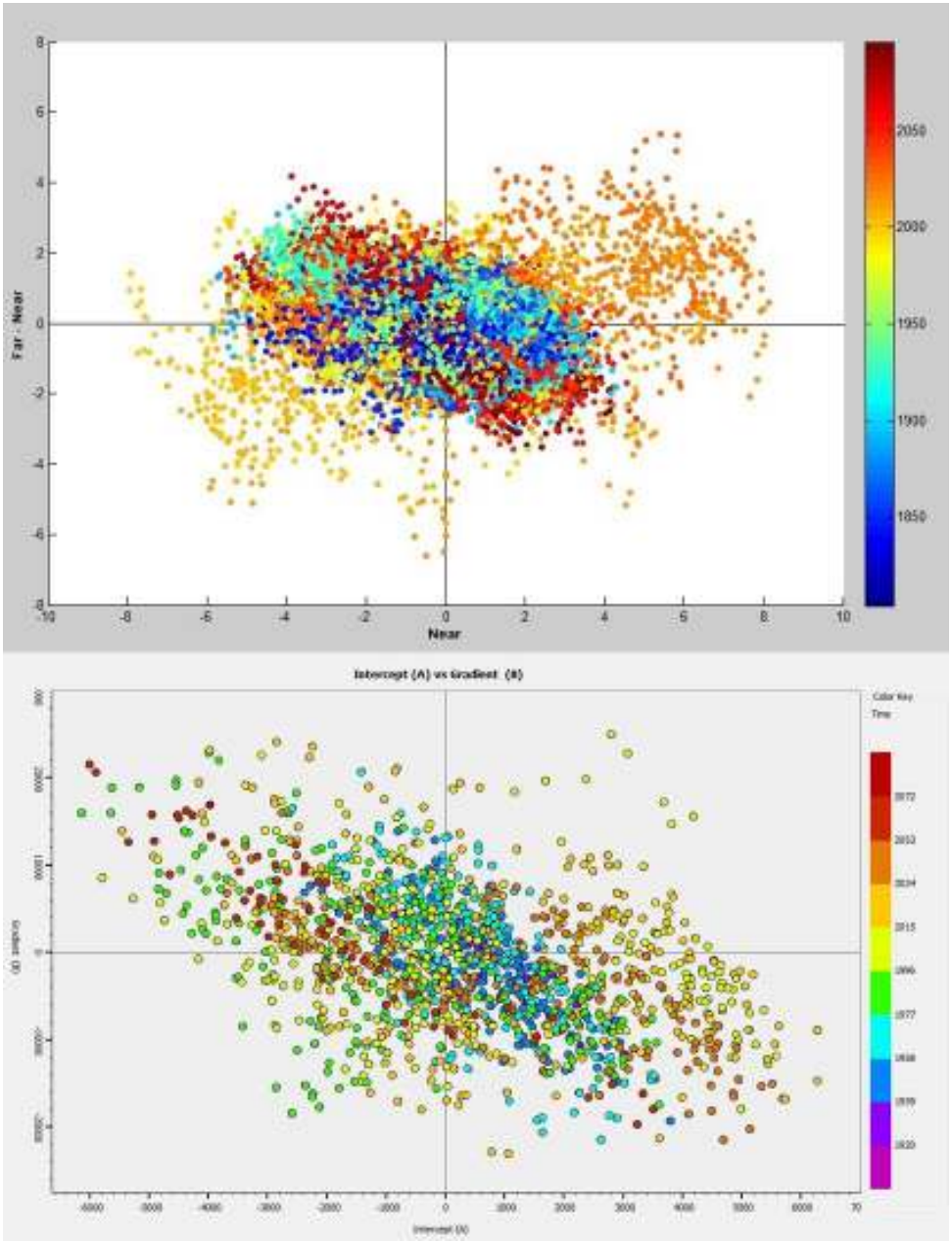

Figure 5. 14: Comparison of crossplots.
The upper plot is the same as what is marked by green triangles in figure 4.3. These are the points around the Kneler structure chosen by hand from the seismic that shows the entire area. The lower crossplot is created from the seismic located around the Kneler discovery.

Figure 5. 14 shows a comparison of crossplots created from the two different sets of seismic data mentioned in chapter 4. It is intended that the two plots show points from the same area. The upper plot is the crossplot from the post-stack seismic data and the plotted area was marked by a green rectangle in Figure 5. 8. The same crossplot is shown in Figure 5. 9. The lower plot is created from the pre-stack seismic only located around the Kneler oil discovery, previously shown in Figure 5. 11. It is already known that this Kneler oil discovery is an AVO class III anomaly, and that the two plots all in all show the same trend. On the upper plot the oil trend is very clear and easy to recognize. The yellow and orange points show a clear deviation from the background trend, and it can easily be said to be a class III AVO anomaly. The lower plot does not show the same deviation as the upper plot even if the data are taken from the same area. This can be caused by the large amount of noise in the data, or by the lack of data points. However, looking very closely at the lower plot it is possible to see that there is a deviation also there, but the trend looks to be slightly rotated clockwise in relation to the upper plot. The rotation of the data points can be caused by the larger amount of noise in the AVO gradient than in the Far-Near stack data which probably is due to the fact that it is the Least Square Inversion which has been used to calculate the Intercept and AVO gradient, and this is very sensitive to noise in the seismic gathers.

It is also possible to relate the classification done from an AVO crossplot to the observations made from the RPT plot in Figure 5. 3. The direction in which the points are “moving” when going from the sealing shale to the reservoir sands in the RPT plot can be related to the AVO class the top reservoir will plot as in the AVO crossplot. Figure 5. 15 on the next page shows the same RPT plot as in Figure 5. 3 to the left, but here are two arrows added onto the plot to show the direction of the points when having unconsolidated sandstone (yellow arrow) and cemented sandstone (red arrow) as reservoirs. The figure below the RPT plot is a schematic figure of an AVO crossplot. This crossplot shows how the movement of the points in the RPT plot can be related to the AVO classes in an AVO crossplot.

From the analyses performed in this thesis it was found that the top reservoir plots as a class III AVO anomaly. The reservoir sands in the upper part of the reservoir are unconsolidated, and the transition from the sealing shale into these sands is shown by the yellow arrow in Figure 5. 15. The unconsolidated sands have a large fluid sensitivity and it can be seen that following the yellow arrow gives a decrease in Acoustic Impedance. Relating this movement to the AVO crossplot it can be seen that this gives a larger negative intercept than the shaly background trend and the top reservoir plot in line with the class III AVO anomalies. The red arrow shows the movement of the points when going from the sealing shale to cemented sandstone. The points from the more cemented sandstone in this RPT plot are not located directly beneath the cap rock but rather at a somewhat deeper depth beneath the diagenesis contact. However, moving away from the well it is possible that the transition from cap rock to reservoir does not longer include the unconsolidated

sandstones and that the reservoir only consists of cemented reservoir sands. The cemented sands have low fluid sensitivity, and from the schematic plot it can be seen that this transition results in an increase in Acoustic Impedance. This shows that if the AVO analyses would have been performed on these cemented sands instead of the unconsolidated sands, it would have resulted in an AVO class ranging from class II to class IIp. This shows that even if there are scale differences between these two plots there is a good accordance between what the RPT plot shows and the results that can be obtained from the AVO crossplot.

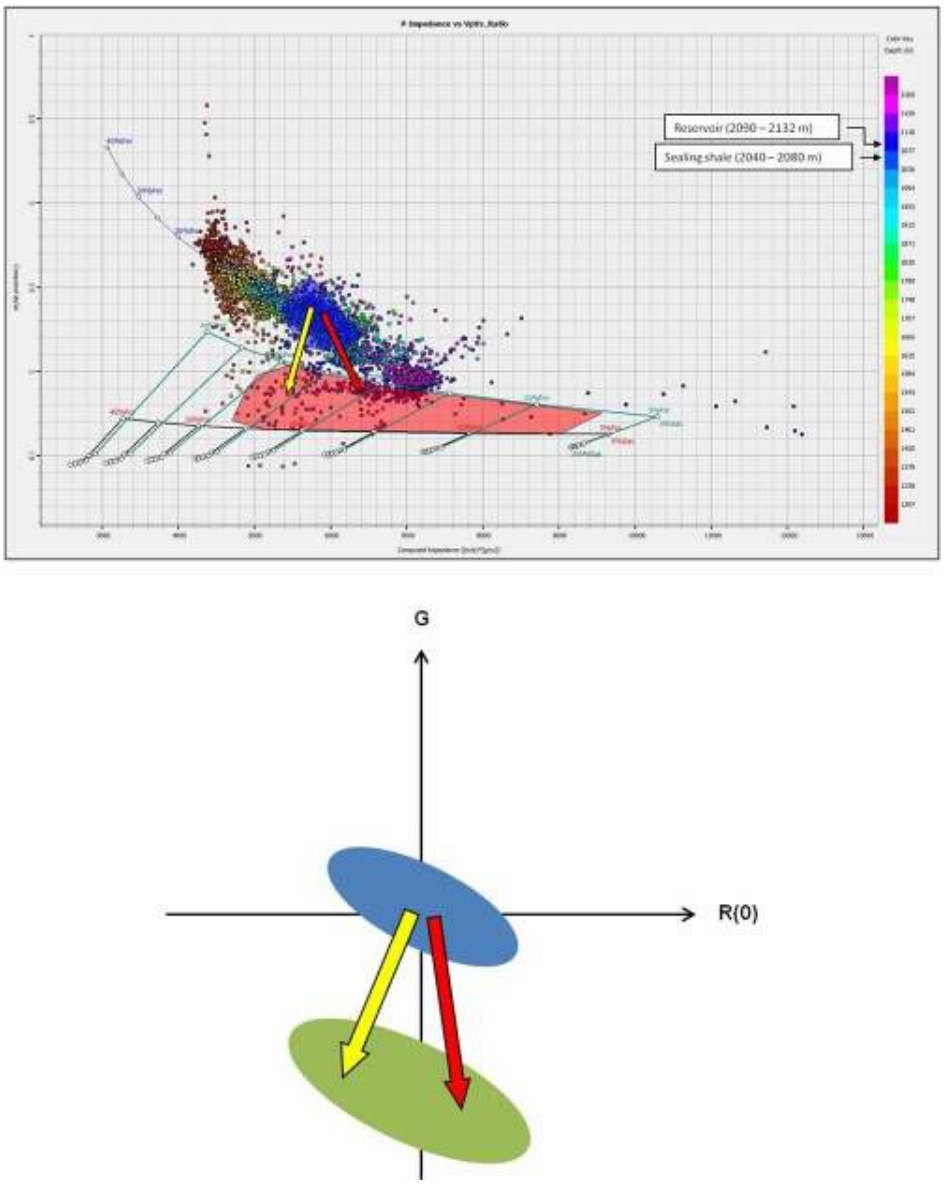

Figure 5. 15: Explanation of how the RPT plot can be related to the AVO crossplot. The arrows in the RPT plot show the movement of the points in the transition between the sealing shale and the reservoir.

As explained in Chapter 4, two different sets of seismic data have been used to analyse the Alvheim reservoir, one post-stack seismic data set and one pre-stack seismic data set. Synthetic seismic was also created based on information from the well penetrating the Kneler discovery. This means that by comparing the pre-stack

data set with the synthetic seismic and the well logs it should be possible to find some of the same features in all three. In Figure 5. 16 four different pictures are shown. From the left to right, the first picture shows a section of stacked seismic which has been stacked from the pre-stack seismic using Hampson-Russell; the second picture shows one CDP gather from the pre-stack seismic, where it is the seismic from the well location that is shown; the third picture shows synthetic seismic created by using a normal Ricker wavelet and velocities taken from well 25/4-7; while the last picture shows logs from the well penetrating the reservoir, well 25/4-7. The three log curves that are shown are the Gamma Ray log, and the calculated Acoustic Impedance and Vp/Vs ratio. These pictures can now be compared to find the similarities and the interesting features which are visible in several of the pictures.

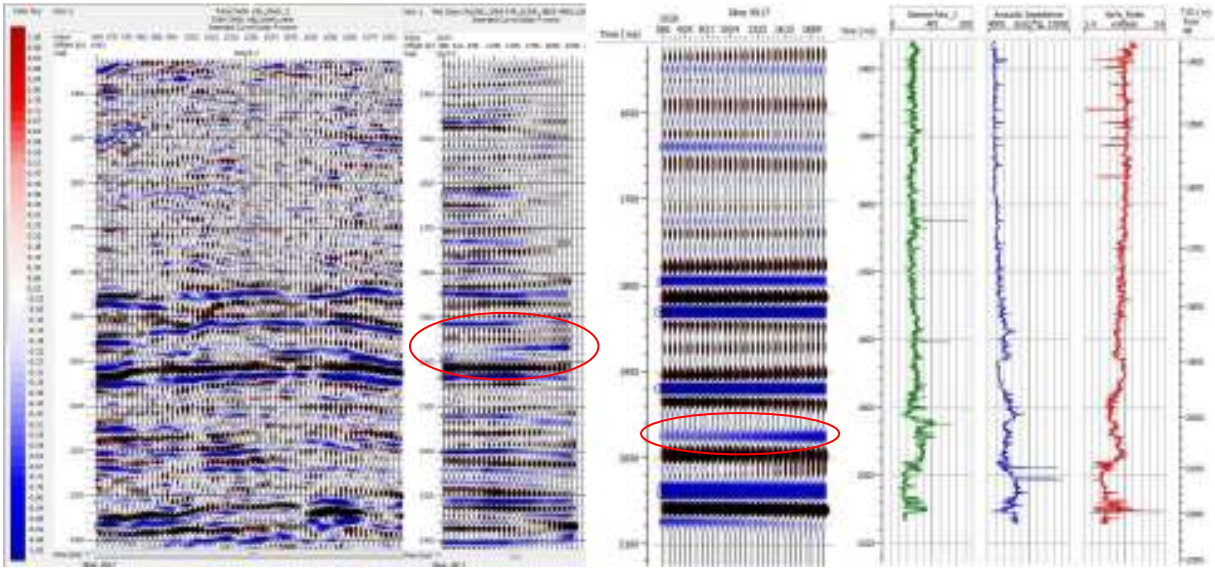

Figure 5. 16: Comparison of synthetic and real seismic data.
Furthest to the left is a stacked section of the seismic from the Alvheim field. The next picture is a figure of one gather which is located around where the available well is located. The third figure is synthetic seismic which has been created by using well 25/4-7. The final figure shows the logs for the gamma ray, acoustic impedance and the Vp/Vs ratio. A larger version of this figure is shown in Figure E in the Appendix.

Even if the stacked section is very important it can be better to start looking at the single gathers first when looking for special features. This can be better because if the features change from one gather to another, and also if there are changes within the separate gathers such as changes in amplitude from near to far offsets. Features related to change in amplitude with offset will not be visible on the stacked seismic due to the cancelling of the signal when the gathers are stacked for all offsets. Therefore, by starting looking at the second picture in Figure 5. 16 it is possible to observe a clear AVO effect at approximately 1980 ms, where there is a distinct increase in amplitude with offset. On near offsets it can be seen that the amplitude is weakly negative which means that this anomaly has a negative intercept. At far offsets the reflector shows an even stronger blue colour which represents stronger negative amplitudes. This gives that this reflector also has a negative gradient since the negative amplitude increases with offset. It has already been mentioned that this

AVO effect represents the transition from the shales in the Lista Formation to the oil sand in the Heimdal Member, which also is a part of the Lista Formation. When the gradient analysis was performed it was said that this effect gives a class III AVO anomaly representing soft sands with high fluid sensitivity. This gives good reasons to believe that this is the top reservoir consisting of soft sands filled with oil.

Directly beneath this AVO effect, there is a hard red (positive) event. By taking a closer look at this it can look like this one event actually consists of two different reflectors. At near offsets it looks like there is one large, very clear, reflector, but moving to far offsets it is possible to see that the reflector divides into two events. The reason that this phenomenon becomes clearer with offset is that at near offset the waves are proximate vertical, and that the distance between the two events is smaller than the minimal of what is possible to observe on seismic, which means it is thinner than one fourth of the wavelength. When going from near offsets to far offsets the waves will no longer be vertical, but they will be more diagonal. This will cause the waves to travel through the thin layer for a longer distance, convincing the seismic waves that the layer has become thicker. If the distance is larger than one fourth of the wavelength, it will be possible to observe the event on the seismic as two separate reflectors. This means that this event can actually consist of two separate events but the seismic resolution is not good enough to separate them. Relating this event to the geology of the subsurface, it can represent the transition from unconsolidated to more cemented sand, i.e. a diagenesis contact since the reservoir is located in the transition zone between mechanical and chemical compaction. At the same time as it can be the diagenesis contact, this event can also represent the transition from an oil-filled to a water-filled reservoir since both these transitions are located at the approximately same depth. What can be the case here is that the upper weak hard event that is only observable on far offsets is related to the diagenesis while the lower, much stronger hard event is due to the fluid changes. This is one explanation, but there are also other factors that can play a role in the way the events show up on seismic, one of them might be that at far offsets the waves will be attenuated to a lower frequency which may affect the resulting signal.

The two discussed features, the AVO effect and the soft layer beneath, are the two events that stand out the most when taking a quick look at the seismic. Now, this seismic section can be compared with the synthetic seismic, located one picture to the right, which is created based on information from the well. Since the seismic gather that has been discussed is located where the well penetrates the reservoir, this gather and the synthetic seismic should have several similarities. Figure 5. 17 shows two seismic gathers, one of the real seismic and one of the synthetic seismic where it has been focused on the part where the lithologies are known. This is the interesting part of the seismic relevant for this comparison.

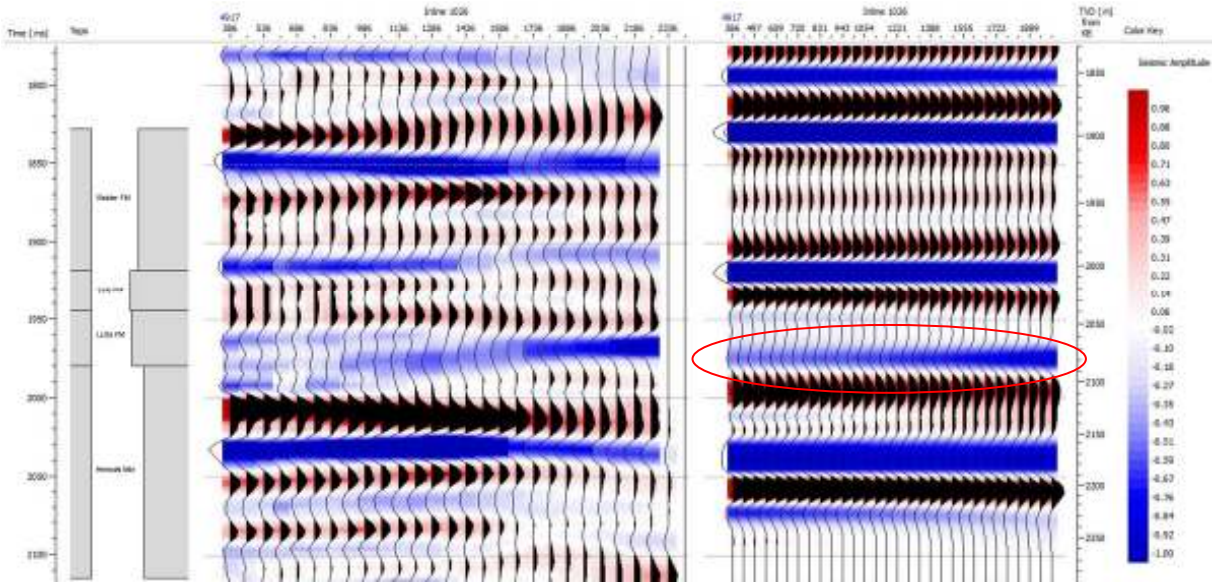

Figure 5. 17: Comparison of real and synthetic seismic sections.
Only the interesting part of the well is shown; where the lithologies are known.

By looking at the synthetic seismic to the right in Figure 5. 17, it is possible to see that the AVO effect is observable also here. Following the AVO effect over to the real seismic it can be seen that the check-shot correction performed on the logs was successfully performed and that the synthetic seismic now corresponds well with the real seismic. Since the synthetic seismic does not contain any noise, it is easier to see the AVO anomaly as one clear reflector where the amplitude clearly increases with offset. In contrast to this clear effect on the synthetic seismic, the effect on the real seismic is not as clear and cannot so easily be interpreted as one clear reflector.

The other interesting feature on this seismic set was the large hard (positive) event located beneath the AVO effect. It is also almost more distinguishable on the synthetic seismic than on the real seismic. However, here it is possible to see that it looks like it consists of two separate events already at near offsets. There is a small indication that there is a thin soft layer in between the two hard events. This can be caused by tuning effects, but it may also just be the side lobe to the upper hard event that appears as a separate reflector. From these seismic images alone it is not possible to say which event that represents the diagenesis changes and which event that represents the fluid changes, but maybe when comparing them with the well logs it is possible to give a better answer to this interpretation. What can be said from the comparison between the synthetic seismic and the real seismic is that the synthetic seismic gives a good picture of the real seismic and can easily be used to help with the interpretation. Since the synthetic seismic is created by using a normal Ricker wavelet together with the velocities from the well, the well-logs should reflect the same features that have just been discussed.

A larger version of some of the logs from the well is shown in Figure 5. 18 on the next page. In addition to the three logs shown in the comparison picture in Figure 5. 16

the density log has been added as a fourth log. It has also here been focused on the important part of the reservoir, and the logs are therefore only showing the part where the lithologies are known. From previous analyses it is known that the OWC is located at 2132 meters depth. This represents a TWT of slightly higher than 2000 ms, and the OWC is approximately marked by the cyan coloured line in this figure.

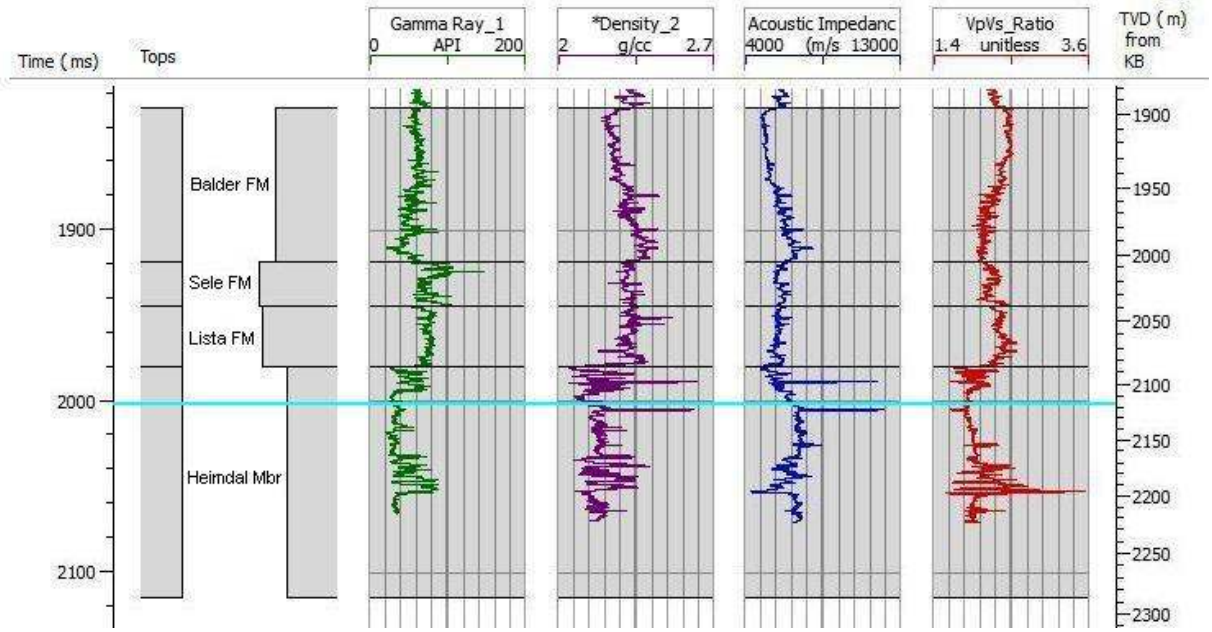

Figure 5. 18: Sample of logs from well 25/4-7.
Logs showing Gamma Ray, Density, Acoustic Impedance and Vp/Vs ratio. The known lithologies are added to show the formation boundaries in addition to the cyan coloured line which represents the OWC.

The comparison between the synthetic seismic and the well-logs can start by looking at the well-logs around a two-way travel time of 1980 ms which is where the AVO effect was located on the synthetic seismic. It can be seen that the gamma ray log decreases somewhat before it goes into the reservoir. This is a clear sign that the amount of radioactive material in the lithology decreases. This supports the statement that the AVO effect represents the transition from the shales in the Lista Formation to the reservoir sand in the Heimdal Member, also located in the Lista Formation. When coming into the reservoir, the gamma ray log does not show a stable signal, but it is rather fluctuating. The reason for this is that the upper part of the reservoir consists of interbedded sand-shale. Normally shale will have a higher radioactive content than sandstone and this gives a reason to believe that the shale sections are the ones which make the Gamma Ray log fluctuate. It can also be seen from the density log that there is a lithology with varying density located in the upper part of the reservoir; normally, unconsolidated sandstone will have a lower density than shale. Following the logs deeper it looks like the Gamma Ray log stabilizes when coming into a lithology with lower radioactive content at a TWT of approximately 1995 ms. This is most likely a fairly clean sandstone. The density log shows a short interval with quite low density before increasing slightly and stabilizing for an interval of about 40 ms. This increase in density can be a result of the

transition from mechanical to chemical compaction, which means that the sandstone the logs have moved into is a more cemented, massive sandstone. By looking closely at the density log it is possible to see that this increase in density happens just above 2000 ms, and is at approximately the same depth as where the OWC is located.

The transition from mechanical compaction to chemical compaction is together with the OWC said to be represented by a hard event located beneath the AVO effect on the seismic data. Figure 5. 19 below shows a figure where the logs in the previous figure are put together with the synthetic seismic to see how the interpretation from the logs fit together with the interpretation of the seismic performed earlier.

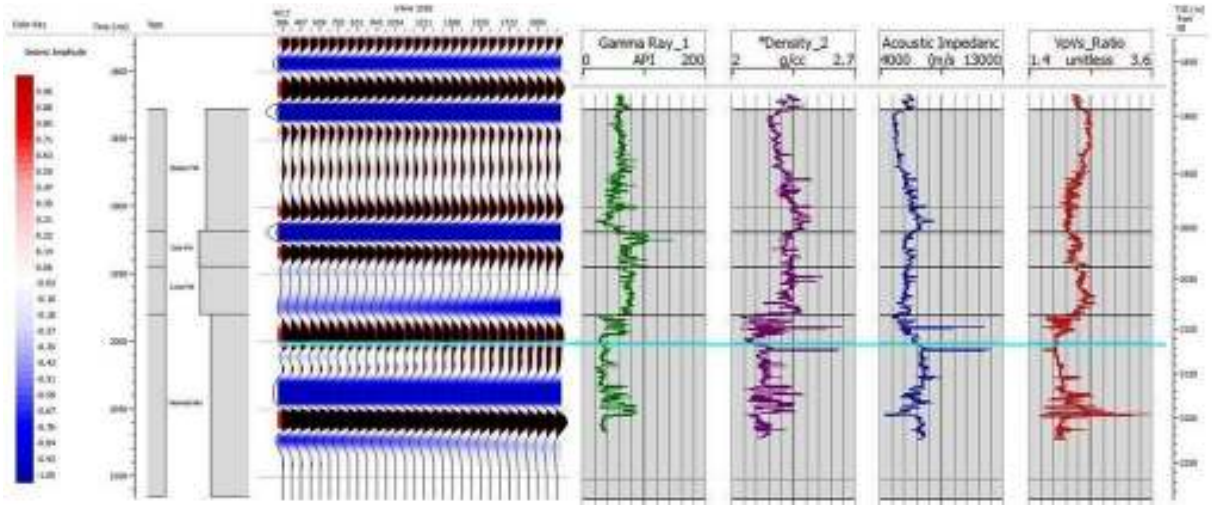

Figure 5. 19: Comparison of synthetic seismic with well logs.
Picture shows a closer comparison of the events on the synthetic seismic with the fluctuations on the logs. The cyan coloured line representing the OWC has been drawn all the way over the synthetic seismic as well as on the logs.

From the figure above it can be seen that the OWC matches well with the red hard event located beneath the AVO effect. However, it is very difficult from this figure to see that the diagenesis contact is located just slightly above the OWC. It can then be said that the hard event, which looks to actually consist of two separate events, do represent the diagenesis contact and the fluid contact.

The reservoir with the interesting fluctuations on the logs and the events showing up on the seismic has now been discussed. It is the reservoir interval which is most interesting for this field, but there are several other features which are not located in the reservoir interval that can be found on both the seismic and on the logs. For this it should be looked at shallower depths. Observing the lithology column and following the transition from the tuffaceous shales in the Balder Formation into the shales of the Sele Formation, located at approximately 1920 ms, over to the synthetic seismic it is represented by a clear soft (blue) event. On the logs this transition causes an increase in both Gamma Ray and Vp/Vs ratio while it causes a decrease in Density and Acoustic Impedance. The drop in Acoustic Impedance is characteristic for this

transition when going from the high velocity tuffaceous shales in the Balder Formation to the shales of the Sele Formation which have a considerably lower velocity (Sele Formation n.d.). The radioactive content is higher in the shales of the Sele Formation which results in the sudden increase in Gamma Ray readings. The top Balder Formation is very difficult to define since there often are no clear indications of this transition, but if it can be found it has to be represented by a hard (red) event since the transition is from shale in the Hordaland Group to the more tuffaceous shales in the Balder Formation. On the logs this is often shown by positive Acoustic Impedance that varies in strength, and is difficult to pick. Since there are cores that are taken from the well and are available for this interpretation it is possible to find this transition from the lithology column. From this lithology column in Figure 5. 19 the transition should be found at 1830 ms. At this TWT the logs show a decrease in Acoustic Impedance and an increase in Vp/Vs ratio. The synthetic seismic does also show a hard event in that area, however it is located slightly higher, at approximately 1815 ms. Here it is important that this shift in the synthetic seismic does not overrule the information from the logs, because when going back to Figure 5. 17 and taking a look at the comparison between the real seismic and the synthetic seismic it is possible to see that the real seismic actually does show a hard event at 1830 ms. This shows that the synthetic seismic does not always show the correct answer, and that it should mostly just be used as an additional information. The reason that the synthetic seismic does not match the logs or the real seismic, can be that the well tie outside the area of interest in a well is not always perfect. When creating synthetic seismic it is often done to get another set of information when interpreting the reservoir interval. The area above the reservoir and cap rock is not that important and there can often be found some small well tie errors in those areas. It is possible to perform a manual stretch of the synthetic seismic to force the current reflector to match the same reflector on the real seismic data. However, this is often not such a popular move since it almost can be said to tamper with the seismic gathers.

The top Balder Formation is not the only boundary above the reservoir which can be found from the logs and the seismic gathers. Since the Balder Formation can be divided into two sections, where the lower section is more tuffaceous than the upper section, it is also possible to look for the top of the Tuff zone. This does often show up as a pronounced seismic reflector with an increase in velocities due to an increase in cementation and a decrease in gamma ray values due to larger tuffaceous content. All these changes can be found on the logs at a TWT of 1870 ms. Looking at the synthetic seismic at the same TWT it is possible to see that it fits with a weak hard event. In the area where this hard event is found there are also two other hard reflectors located above and below the one that matches the top Tuff zone. The reflector representing the top Balder Formation was found to be located somewhat shallower than what the logs showed, and this may also be the case for this transition. This means that the reflectors should have been shifted slightly downwards which would show that it is most likely the upper hard event, of the three

shown together, that fit with top Tuff zone. Here again, the synthetic seismic cannot be relied on alone, but should rather be used as an additional source of information.

When it is found that there is a possibility that the synthetic seismic most likely does not show the correct reflector, it is interesting to see what answer the real seismic gather gives. Again going back to look at Figure 5. 17 it can be seen that the real seismic gives a more unambiguous answer; the top tuff zone from the well logs do fit with a hard, quite pronounced, reflector located beneath a quite clear soft reflector. This reflector would match the upper reflector, of the three, in the synthetic seismic, and this gives reason enough to believe that the part above the reservoir has been shifted somewhat on the synthetic seismic. The seismic alone would not have been enough to locate the transition into the more tuffaceous Balder Formation, but together with information from the well logs it is possible to do so.

Now the main features that are observable on the real seismic gather, the synthetic seismic and the well log data have been discussed. The remaining picture is the one of the stacked seismic section. Figure 5. 20 shows the stacked section put together with the real gather to show where the events found on the gathers should be located on the stacked section.

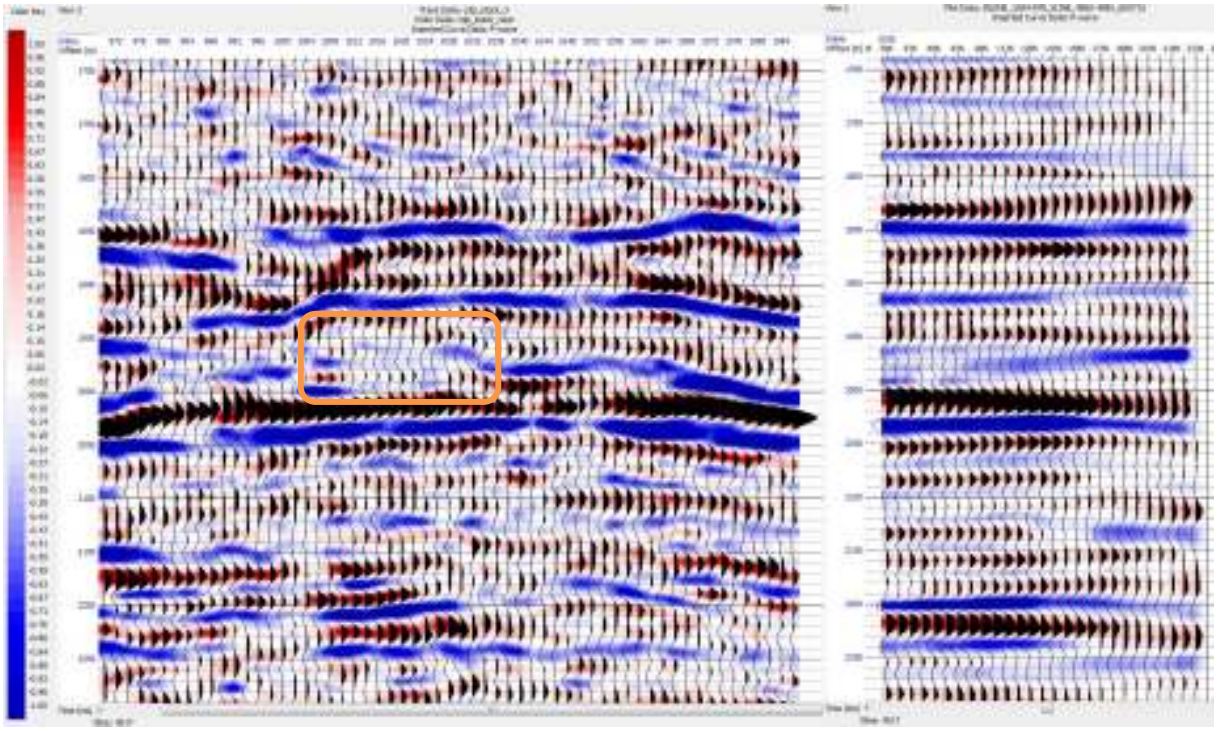

Figure 5. 20: Seismic stacked section and seismic gather.
The centre of the reservoir in the stacked section is marked by the orange rectangle.

As can be seen from the figure above, the reflectors shown on the seismic gather that have an almost constant amplitude signal for all offsets are also visible on the stacked section, but as for the AVO effect where the amplitude increases with offset, it cannot be discovered on this section because the signal will be cancelled out when

the gathers are added together. The seismic gather where the AVO effect has been discovered is taken from the gather where the well penetrates the reservoir. This seismic gather is located closely to the middle of the stacked section, which means that that is where the AVO effect should be located if it was visible. But even if the AVO effect is not visible, it is possible to find some indications of the reservoir on the stacked section.

Since the Alvheim reservoir is a turbidite reservoir there are sand lobes and shales interchangeably. When the reservoir gets compacted the shales will get more compacted than the sands. This will again cause the sand lobes to stand out in relation to the shales surrounding them. Looking at the area marked by the orange rectangle on the stacked section in Figure 5. 20 it can be seen that the soft (blue) reflector, which is most likely the same reflector as where the AVO effect is visible on the seismic gather, is located at somewhat shallower depth inside the rectangle than outside. The reason for this can be that the main lobe of this reservoir is located inside that rectangle while the outside of the rectangle is where the shales surrounding the sand lobe are located; the shales around the reservoir will be compacted more than the reservoir itself, which again will cause the reservoir sands to stand out. So, even if it is not possible to observe the AVO effect, it is possible to find some indications of the reservoir as long as the approximate location is known.

The red event located beneath the AVO effect is still very clear and very easy to notice. When taking a closer look around the middle of the stacked section this event looks very flat. This supports the statement that both the fluid contact and the diagenesis contact can be represented by this event. A fluid contact will be horizontal, but so will also a diagenesis contact and therefore both of these contacts can be an explanation for this reflector. Slightly over the main hard event, a little to the right there is another hard event which is possible to see. It is not as strong as the lower event, but it has the same curvature. This can be of help when defining where the two contacts are located in relation to each other. The interpretation of the seismic gather and the well logs concluded that the diagenesis contact might be located slightly shallower than the fluid contact, and it is therefore feasible to assume that this higher lying event could come from the diagenesis changes, while the stronger, lower event is due to the fluid changes in the reservoir.

The last reflectors that were discussed when interpreting the real and synthetic seismic gathers and the well logs; top Balder FM, top Tuff zone and the transition between base Balder FM and top Sele FM can all be observed on the stacked seismic section. The transition between base Balder Formation and top Sele Formation is the one out of the three that is the clearest. The reflector representing the transition into the tuff zone in the Balder Formation is also pretty clear, but in two places there looks to be some interference between this and another reflector, and this may disturb the interpretation of this reflector. It can also be seen that this reflector seems to follow the same curvature as the reflector for the top reservoir.

This can mean that within the short interval between the top of the Tuff zone and the top of the reservoir there are no surprises concerning the lithologies directly above the reservoir. Looking at the left side of this stacked seismic section it looks like there is some interference within the seismic. The probability of this being due to lithology changes is large since this is a turbidite reservoir, but to say exactly what is happening is difficult without any further information.

5.3.2 Outside reservoir area

Until now it has only been looked at the reservoir and the changes that are possible to observe there from the well logs and the available seismic data. What also can be interesting, is to see how the area outside the main reservoir looks on the seismic, especially the AVO effect and how far away from the well location it will be visible on the gathers. It is known that the reservoir is located in a sand lobe and that the well location is located towards one side of the lobe, shown in Figure 4. 3. This means that when moving away some distance from the well it should be possible to see that the AVO effect will fade away. And what about the other lithology boundaries, since this is a turbidite reservoir the lithologies may change a lot within a small area and maybe this can be seen on the seismic. To make it easier to look at the seismic gathers away from the reservoir it is possible to create super gathers. When doing this a certain number of gathers are added together to highlight the strong events and to minimize the noise. Even if the events change throughout the gathers, the change will not be sufficient enough to cancel an event when only summing five gathers; it will rather enhance them since the random noise will be more or less cancelled out. Doing this may cause some of the weaker events to get dimmer and make it difficult to define them, but in this case the interesting reflectors are of a certain strength and will not be affected that much.

Figure 5. 21 shows a series of super gathers made over the entire volume of the seismic data. All these gathers are shown for inline 1026 which is the inline where the well is located. In this figure, the fill of the wiggle traces have been removed to make it easier to see the changes in the seismic showed by change in colour. The colours still represent the same as earlier; the blue events are soft events, troughs, and the red events are hard events, peaks.

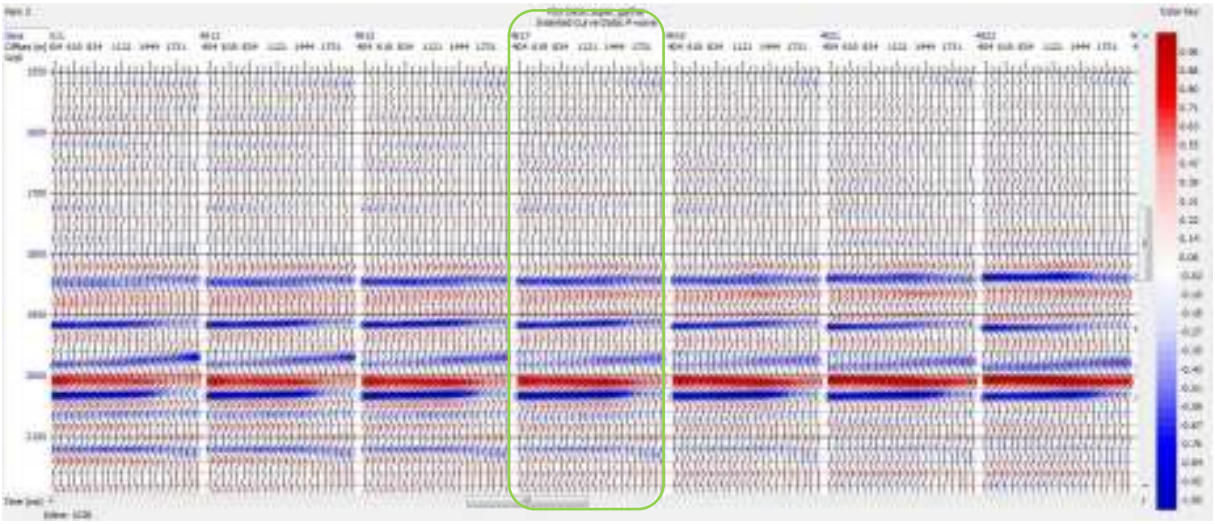

Figure 5. 21: Super gather showing the seven gathers closest to the well location. The super gathers are created over the entire area. The gather in the middle, marked by a green rectangle, is from the location where well 25/4-7 penetrates the reservoir.

In the figure above, the gather shown in the middle is the crossing with inline and crossline at the well location. The AVO effect is still visible at 1980 ms after creating the super gathers. So is also the hard event beneath representing the diagenesis and fluid contact. Of the other three discussed reflectors, located above the reservoir, the transition between the base Balder Formation and top Sele Formation is still pretty clear and easy to find while to top Balder Formation and top Tuff zone are somewhat weakened. However, this does not matter that much since it is the reservoirs development that is the most interesting. Observing the AVO effect in the midmost super gather it looks like the reflector is split in two at near offsets and represented by one reflector at far offsets. Regarding the lower reflector at near offsets, it looks like there can be an interference between the soft reflector representing the top Heimdal reservoir, the AVO effect, and the hard event beneath, representing the diagenesis contact and the OWC. This lower soft reflector may actually just be the side lobe of the hard underlying event, and the interference can make the soft event look somewhat stronger than it actually is. When taking this into consideration, it can be said that it is most likely the upper soft event that belongs to the AVO effect. This statement can also be supported by the fact that the AVO effect has to be observed for one time only.

Observing the seven gathers in Figure 5. 21 it is possible to see that there are some minor changes regarding the AVO effect. The AVO effect is observable on all gathers, however it looks to be most clear on the three gathers in the middle. These gathers do not cover a large area, and this gives reason to believe that the outer gathers are well within the reservoir. But there is a change regarding the AVO effect that should be discussed. Observing the gather located furthest to the right it can be seen that at near offsets, the amplitude is more faded, it shows less negative amplitude. If the AVO analysis was to be performed on this gather instead this change would have resulted in a less negative intercept. By still having the same

gradient, this would cause the top reservoir to plot more in line with a class II AVO anomaly. A possible explanation why this happens can be found.

Figure 5. 22 shows a schematic figure of how the reservoir may look like. This figure shows a possible answer to why the amplitudes of the AVO effect at near offsets is becoming less negative when moving towards higher numbered crosslines. The scale of this figure should not be compared with the super gathers shown in the previous figure since this only is a schematic figure used for explanations. The yellow coloured area is to represent the sand lobe functioning as a reservoir while the brown coloured areas represent dirty levee deposits with higher shale content deposited on top and beside the reservoir. This chaotic deposition is a function of the turbiditic currents that created this reservoir. The super gather observed in the middle is from the well location, and this can be showed by the black line in the figure below representing the well. Performing an AVO analysis on the top reservoir at this location means performing the analysis on unconsolidated sandstone. This is what has been done in this thesis and this gave the result that the reservoir could be classified as a class III AVO anomaly. The red line represents the possible location of the gather located furthest to the right. From the figure beneath it can be seen that if the AVO analysis was to be performed here it would be performed on the top reservoir consisting of cemented sandstone filled with oil instead of unconsolidated sandstone. The possible outcome of such an AVO analysis was shown in Figure 5. 15 in chapter 5.3.1. Here it was showed that this analysis could result in a class II AVO anomaly.

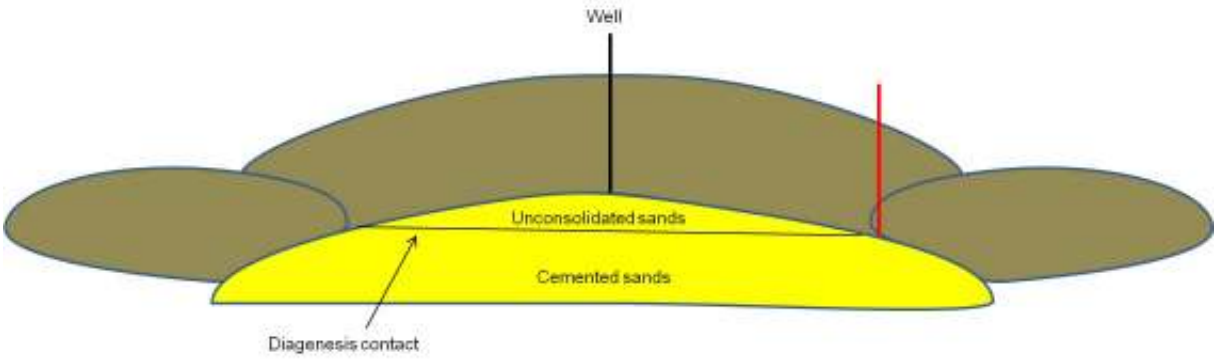

Figure 5. 22: Schematic reservoir figure.
The yellow coloured area represents the sand lobe working as a reservoir and the brown coloured areas represent dirty levee deposits with higher shale content surrounding the reservoir.

From the contour map in Figure 4. 3 it is possible to see where the well is located, and that it is located more to one side of the lobe. This means that moving towards higher numbered crosslines will most likely faster leave the reservoir behind than moving towards lower numbered crosslines. Since the seven super gathers closest to the well show no significant change in the AVO effect either way it is possible to look at the next seven super gathers following higher crossline numbers (Figure 5. 23) to see what happens to the AVO effect when moving further away from the well.

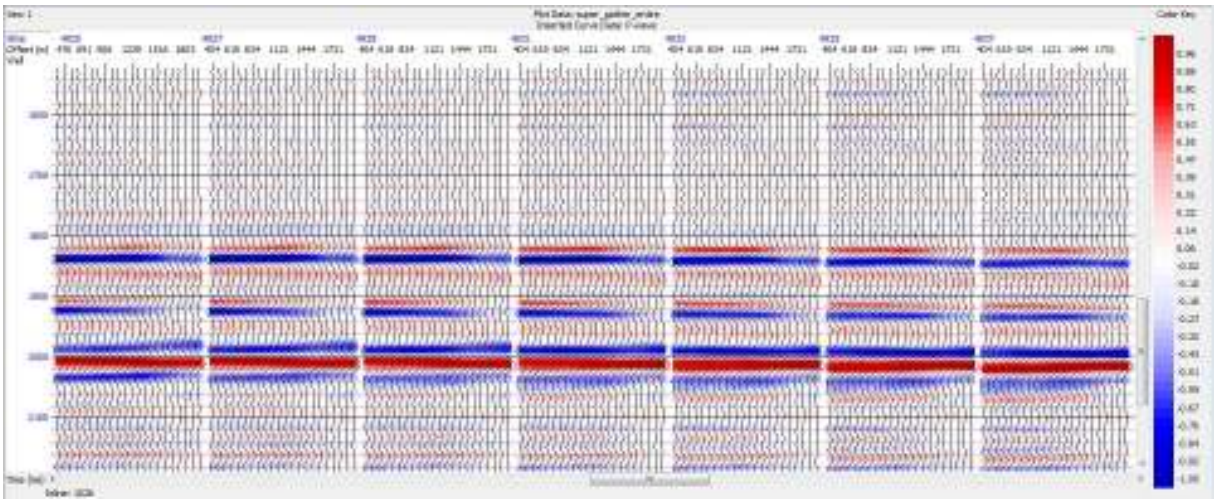

Figure 5. 23: Super gathers showing gathers at some distance away from the reservoir. These are the next seven gathers moving towards higher numbered crosslines.

Observing the figure above, it is possible to see that there are more things happening in the area covered by these gathers than in the preceding figure, and several of the reflectors change within the seven gathers that are shown. The interesting reflectors here are the AVO effect and the hard reflector beneath representing the cementation and fluid contact. Starting with the AVO effect and observing the gathers from left to right shows that the effect fades rightward. It can also be seen that the trend that started in the figure showing the other seven super gathers where the reflector showing the AVO effect gets less negative amplitudes at near offsets when moving towards higher numbered crosslines continues on these gathers. This means that there is a big chance that the following gathers are approaching the outer part of the sand lobe. It is still possible to observe a weak AVO effect on the two first gathers, from the left.

Looking at the third gather from the left it is possible to see that it looks like the AVO effect has completely faded away. To see where this gather is located in relation to the well, a look should be taken at the contour map in Figure 5. 24. This figure shows the same contour map as was displayed in Figure 4. 3, but here the contour lines are removed to show the outline of the sand lobe better. The well location can still be seen inside the lobe by the black circle. The solid black dot represents the midmost super gather in Figure 5. 23. This map shows that this gather is from the outer edge of the lobe which can mean that the gather actually shows seismic from outside the reservoir. If this is the case it makes sense that the AVO effect no longer is visible on the seismic gathers, and that this reflector shows a lithology with much higher shale content.

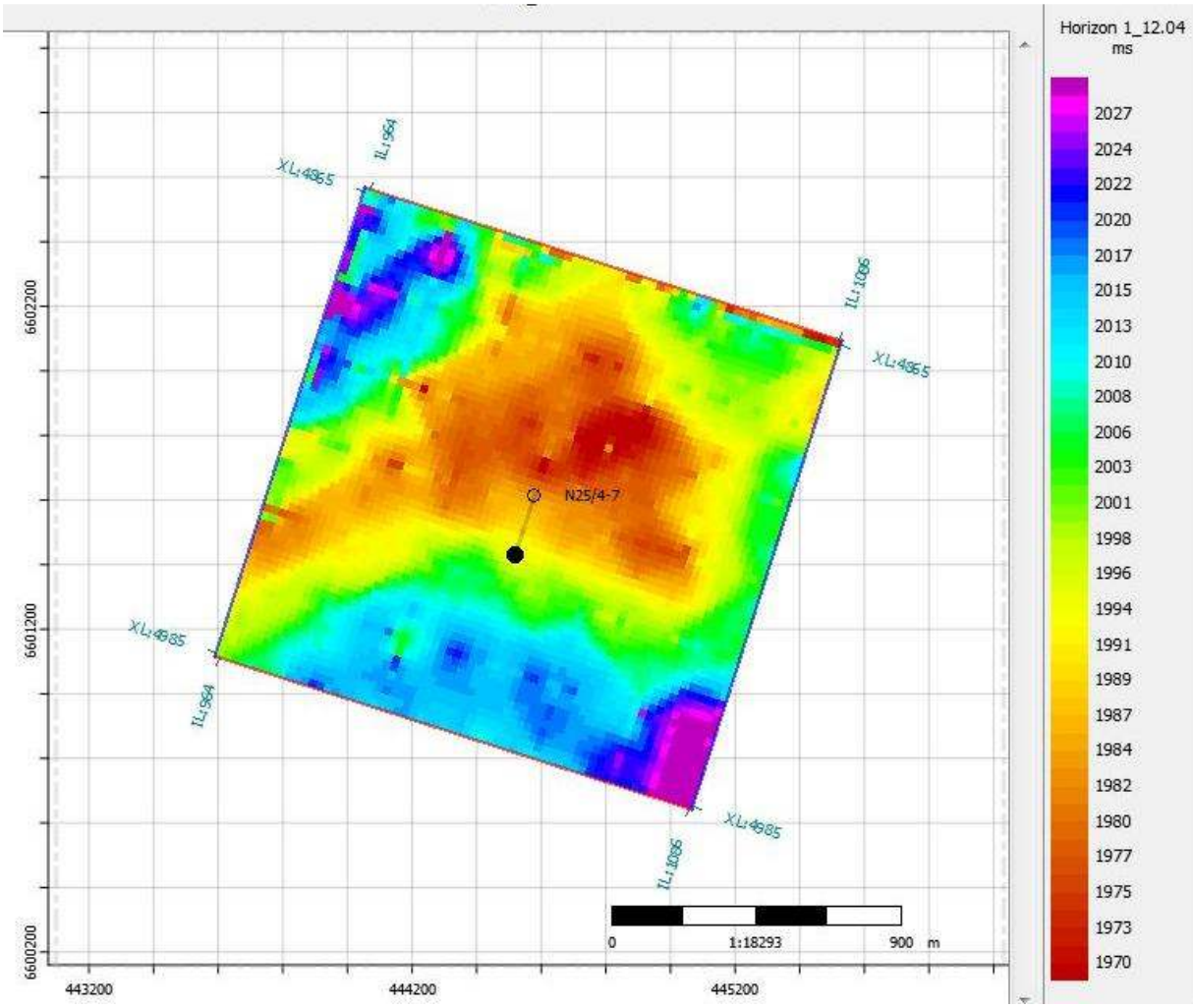

Figure 5. 24: Contour map showing location of super gather in relation to well location.

Observing the hard event, located beneath the soft event that represents the AVO effect in both figures, it can be seen that it does not look like this reflector consists of two separate reflectors any more. This may be a result of the stacking of the gathers; slight changes from one gather to another may have caused cancelling of the weakest reflector. When observing the real gathers it was always difficult to define if this reflector actually consisted of two separate reflectors or if it was a tuning effect. This means that this one reflector actually represents both the diagenesis contact and the fluid contact. However, when coming to the gather where the top reservoir reflector shows the transition from the sealing shale to the cemented sands, this reflector only represents the fluid changes.

It is also possible to observe how the other, previously discussed, reflectors behave away from the well. Starting by looking at the soft event representing the transition between base Balder Formation and top Sele Formation it can be seen that there are no large variations in how this reflector is displayed on the different super gathers. There are also no large variations in the other reflectors that have been discussed earlier either. It is the reservoir which is important for this thesis, and it has been found that there are no large variations there until moving out of the reservoir. Since

this is a turbidite reservoir there are many possibilities of what can have happened to cause the different variations that actually are observable on the seismic.

5.3.3 Modelled data versus real data

Several of the AVO analyses that now have been performed on the data from this area have given satisfying answers. Both the crossplot from the post-stack data, where the area around the Kneler discovery was chosen by hand, the AVO gradient analysis performed on the seismic gather from the pre-stack data and the AVO gradient analysis performed on the synthetic seismic, created from the logs, concluded that the anomaly from the reservoir belonged to the class III AVO anomalies. There was also a crossplot made from the pre-stack data that was only from around the Kneler discovery, which gave an indication that the data belonged to the class III anomalies, but did not give an unambiguous answer.

The results obtained in this thesis can now be compared with the results obtained in the project work preceding this thesis. In the project work it was found that a total of twelve different scenarios could be present in the reservoir even if the available wells only could conclude with three out of the twelve. After rock physics modelling, extracting to the unknown scenarios, and performing AVO analysis on these scenarios, they could be classified into the different AVO classes. Well 25/4-7, which was used as a source of information both for the project work and for this master's thesis contained two out of the three already known scenarios; unconsolidated interbedded sand-shale and cemented massive sandstone, which means that it would be expected that the results from this thesis would match with the results obtained from the analyses performed on these lithologies.

When performing the AVO analyses in this thesis, both AVO crossplots and AVO gradients were obtained. Since there were two available sets of seismic data, a crossplot could be created from both of them. The comparison between these two crossplots was shown in Figure 5. 14 in chapter 5.3.1 where the similarities and differences were discussed. The same figure is shown once more in Figure 5. 25 where it is compared with the crossplot obtained from the analyses performed in the project work.

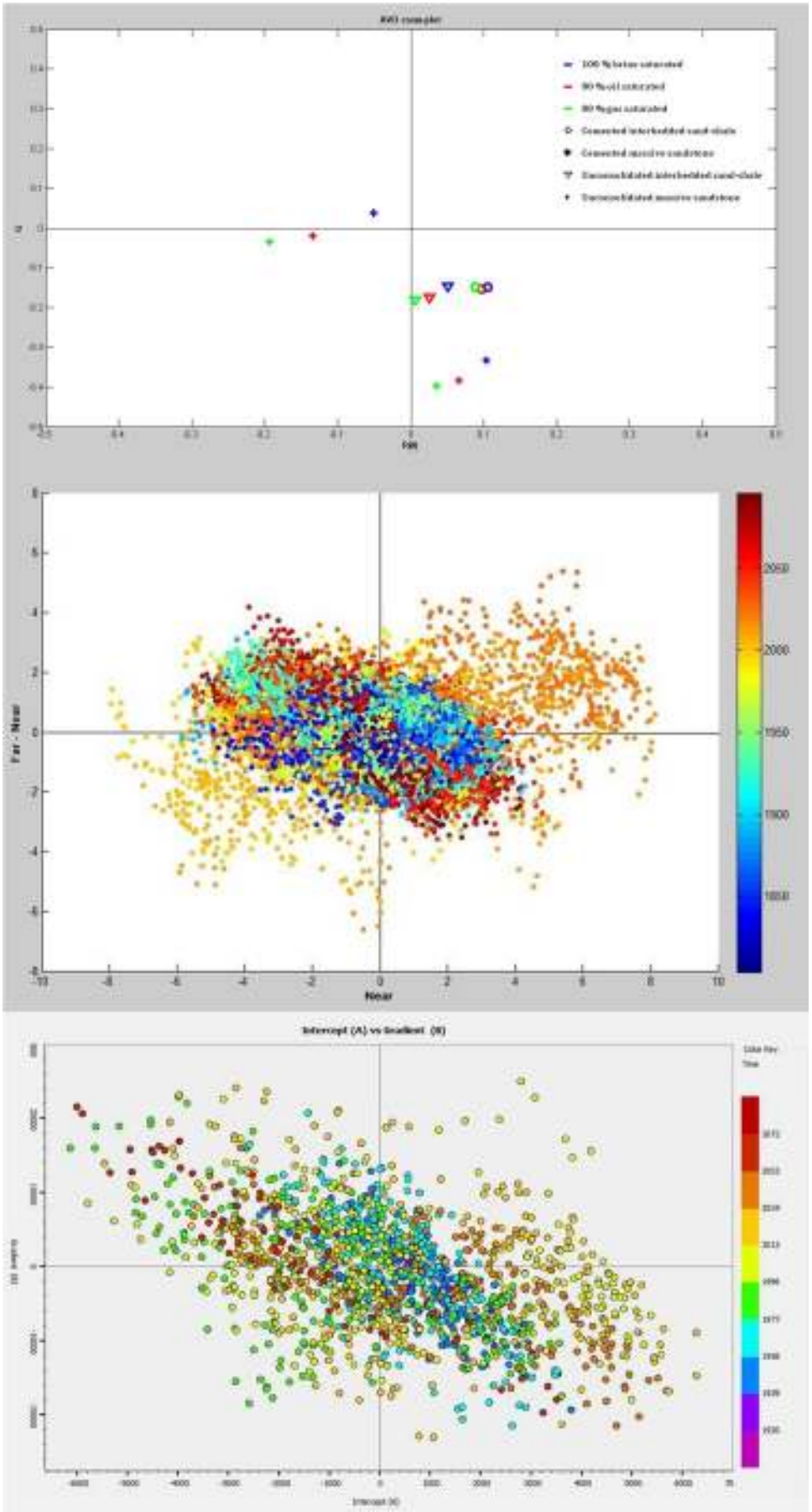

Figure 5. 25: Comparison of crossplots from modelled data and real data.

The comparison made earlier showed that both crossplots show a deviation from the background trend, and that the anomaly could be classified as a class III AVO anomaly, but it is the crossplot made from the post-stack data where the plotted area is chosen by hand that gives the best result. The upper plot in Figure 5. 25 shows the results from the project work. Based on the anomaly trend in the midmost picture it should plot in the third quadrant in the upper plot. The crossplot taken from the project work shows that there are two crosses that plot in the third quadrant. These crosses represent oil and gas filled unconsolidated massive sandstone. This does not quite match the expected answer which would be unconsolidated interbedded sand shale, since this is what the upper part of the reservoir consists of. But the results may still be correct.

The other analysis performed in this thesis which could be compared with results from the project work is the gradient analysis. The AVO gradient analysis has been performed on both the real seismic data and on the synthetic seismic data and the reflector chosen to perform the analysis on was the top reservoir. The comparison between the gradient analysis performed in this thesis and the analysis performed on the modelled scenarios in the project work is shown in Figure 5. 26. In this figure the gradient analysis performed on the synthetic seismic is left out because it was shown in chapter 5.2, and it showed the same result as the gradient analysis performed on the real pre-stack data, which is shown in the lower plot in Figure 5. 26. The upper picture is the one from the project work and it shows the AVO curves obtained for all twelve scenarios. It can now be found which of the twelve curves in the upper plot that match the curve obtained from the top reservoir. This AVO curve shows both a negative intercept and a negative gradient. The only modelled curves that match this description are the curves for the gas and oil filled unconsolidated massive sandstone. Logically this is the same result as was obtained from the crossplots, which not entirely match the result expected for this reservoir.

As previously discussed in this thesis the results show that the top reservoir is a class III AVO anomaly. From the modelled scenarios it was found that it is the hydrocarbon filled unconsolidated massive sandstone that gives a class III anomaly. So, how is it possible that these analyses match when it is known that the top reservoir consists of unconsolidated interbedded sand-shale?

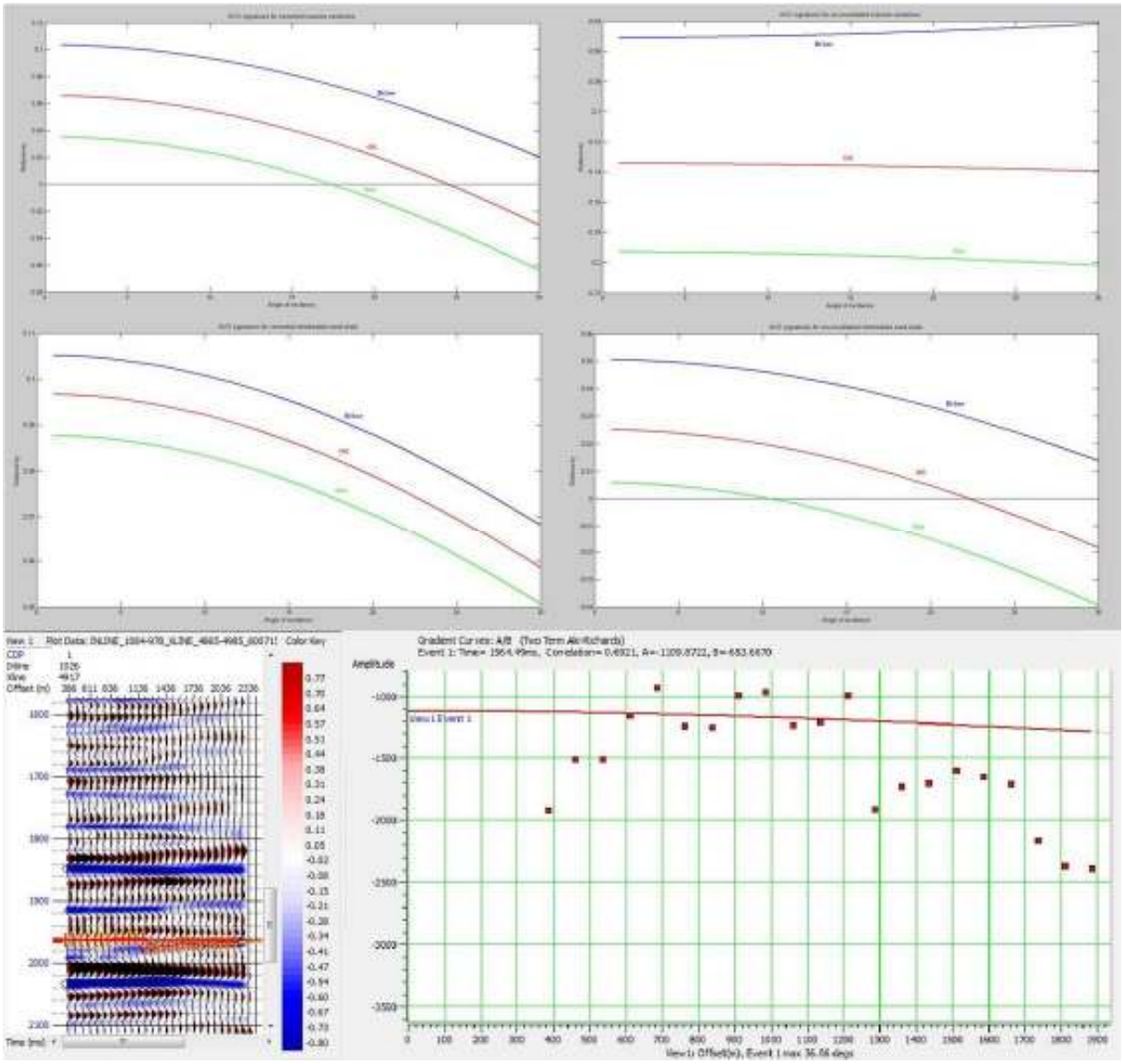

Figure 5. 26: Comparison of AVO curves from the modelled scenarios and real seismic data. The upper picture shows the four sets of AVO curves obtained when performing AVO gradient analysis on the twelve modelled scenarios in the project work. The lower picture shows the gradient analysis performed on the real seismic gather in this thesis.

When the modelled curves for the interbedded sand-shale scenarios were made the density used was an average for a lithology containing both sand and shale and not a lithology with separate sand and shale layering. This means that the upper part of the reservoir can consist of unconsolidated interbedded sand-shale but the exact location where the gradient analysis was performed may be a separate layer of unconsolidated massive sandstone. This means that the results obtained in this thesis are for an oil filled unconsolidated massive sandstone when the top reservoir is being analysed, but that it can still be said that the upper part of the reservoir consists of unconsolidated interbedded sand-shale.

Discussion

This master's thesis is written as a continuation of the project work finished in January 2012 (Eggen 2012). While the project work focused on performing AVO analyses on modelled data extracted from the available wells using rock physics modelling and classifying the different scenarios known to maybe be present in a turbidite reservoir, the work done in the master's thesis has been focused on performing AVO analyses on real seismic data from the Alvheim field. In this thesis two sets of seismic data were used in addition to one of the wells that were used in the project work. When performing the analyses on the modelled data, exact answers were obtained for the different modelled scenarios where the lithologies were assumed to be constant and the fluid content was varied to see how it affected the AVO signatures. When performing the analyses on real seismic data, no exact answers could be expected. The lithologies in the reservoirs will virtually never be constant, and even the smallest changes may affect the results. This means that even if the content of the reservoir is known, it is not possible to be certain about the result obtained by performing AVO analyses.

Due to the many uncertainties related to the complexity of the reservoir, several analyses may be performed to increase the certainty of the answers obtained from the analyses. In this thesis, different AVO attributes, such as crossplots and gradient analyses have been used to help classifying the reservoir. The results from the analyses are largely influenced by the data quality and what assumptions that have been made. Having both seismic data and information from drilled wells does not always mean that there is enough information available to perform the preferred analyses and therefore assumptions have to be made to fill the gaps. In many cases, making the correct assumptions can be decisive to get a good result. A lot of the results obtained in this thesis have already been discussed in the preceding chapter, but there are still some assumptions that need further explanation.

The RPT plot in chapter 5.1.1 was created by using the calculated Acoustic Impedance (AI) and Vp/Vs ratio logs. These logs are calculated from the logs taken from the well penetrating the reservoir and the values should therefore give a good reflection of the reservoir. When creating the RPT plot in Figure 5. 3, an assumption concerning the lithologies was made. To get the templates for the oil-gas boundary and water-gas boundary to place correctly in the plot, they had to be constructed for the correct lithologies. It was already known that the upper part of the reservoir consisted of interbedded sand-shale and since the templates only could be created for constant lithologies, a choice had to be made whether to create them for clean sandstone, clean shale or a mixture of sand and shale. In the end it was chosen to use a mixture consisting of 60% sandstone and 40% shale. Even if the reservoir consisted of separate sand and shale layers it was thought that this would give the

answers closest to the truth. The points that plotted in between the two bounding templates should now have the AI and Vp/Vs values representative for an oil filled reservoir with a sand-shale mixed lithology. The red polygon was drawn around the points which matched the reservoir depth and was located between the two boundaries. Transferring the plotted points over to the logs, shown in Figure 5. 4, it looks like the coloured area matches the already defined reservoir interval very well. Changing the lithology used when creating the templates could improve the colouring to match the real reservoir interval even better and maybe avoiding some of the coloured areas which do not belong to the reservoir interval. However, the result from the shown polygon gave a satisfying answer, and the irrelevant coloured areas can be explained for. They may be caused by wrongful measurements or that there actually are areas in the well, outside the reservoir interval, where the same AI and Vp/Vs ratio values can be found even if there is no oil present. This can be caused by changes in velocity and density since they influence both the AI and the Vp/Vs ratio.

The third template shown on the RPT plot is the shale line. The shale properties used when creating this template were taken from the well report. The same shale values were used when performing the lithology substitution in the project work. The polygon for the sealing shale was chosen based on the known depth of the shale functioning as the cap rock. Since most of the points plot in a large cluster more points than just the ones representing the sealing shale were chosen, and this could be seen on the logs in Figure 5. 4 where there are quite large areas coloured blue. What also can be seen is that the polygon showing the cap rock points is not located along the shale template, but rather beneath the lower end of it. This can be because the template was created using the shale properties from the well report. It is not known where the shales with these properties are located. But since the same properties were used when performing the fluid substitution it gives reason to believe that these properties may match the shales located in between the sandstones in the reservoir interval. The shales working as a cap rock do not necessarily have the same properties as the shales in the reservoir interval, and this may cause this uncertainty. But it was nevertheless chosen to use these shale values since it is possible to be certain that these shales are present in the well.

Another instance where a choice had to be made was when creating the synthetic seismic gather. The choice was between using the wavelet extracted from the well and using a normal Ricker wavelet. It was chosen to use the Ricker wavelet since this resulted in the synthetic seismic with less noise, and the extracted wavelet looked so similar to a Ricker wavelet that it was presumed that it would not make a great difference regarding the main events. What could be seen in Chapter 5.3.1, where the synthetic seismic was compared with the real seismic and the well logs, was that it looked like the upper discussed reflectors, the ones representing the top Balder Formation and the top Tuff Zone, are shifted to somewhat shallower grounds on the synthetic seismic. It is possible to see the same reflectors on the real and synthetic seismic, however not at the same depth. A check shot correction has been

performed to get the well to match the seismic as good as possible. There is a small possibility that this shift is related to the choice made in which wavelet to use, but it may also be caused by the velocities used when creating the synthetic seismic. When a well tie is made it is often centered on the interesting part of the well, the reservoir interval. The reflectors that are shifted on the synthetic seismic are located somewhat over the interesting reservoir interval. In many cases this part of the well will not be seen as that interesting and it is therefore not so important that everything fits perfectly. And since there is real seismic available in this area and not only the synthetic seismic, this does not affect the interpretations that have been made since the reflectors on the real seismic match the log curves. There is also the possibility that the shifting of the reflectors is a result of some wrong measurements performed in the well.

Since there were two sets of seismic data available, it could be performed AVO analyses on both of them. But since the two data sets were of different character, it was only the AVO crossplot that could be created for both data sets and that could show a comparison of the results. It has been concluded that the analyses performed on the data in this thesis show the same answer; that the top reservoir at the well location plot as a class III AVO anomaly. However, when comparing the AVO crossplot created from the post-stack data with the crossplot created from the pre-stack data it could be seen that even if they show the same answer, the one plot is much better than the other one. The crossplot created from the post-stack data where the area around the Kneler oil discovery is picked by hand show a good deviation from the background trend. But the crossplot created from the pre-stack data which only covers a small area around the Kneler discovery, does not show the same clear deviation. Several explanations for this were mentioned in chapter 5.3.1 where these two plots were compared. It could be caused by the large amount of noise in the pre-stack data or the lack of data points from the reservoir interval. There is also the possibility that the plot showing the data from the post-stack data is more robust and will therefore give a better classification. However, even if the pre-stack data do not show the same clear deviation, it is possible to see that there is a deviation there and that when comparing it with the other crossplot it may be possible to classify the anomaly the same way.

There were several analyses that could be performed on the pre-stack data since the seismic gathers can give information that a stacked section cannot give. One feature that was visible on both the seismic gathers and the stacked section was the hard event located beneath the reflector showing the AVO effect (Figure 5. 20). On both the gather and on the stacked section it looks like this event consists of two separate events and it can be interpreted to represent both the diagenesis contact and the OWC. When comparing this seismic wthl the well log data it was found that these two contacts are located at approximately the same depth. There are some small indications from the well logs that the diagenesis contact is located slightly shallower

than the OWC and that the lower part of the reservoir consists of oil-filled cemented massive sandstones. The well report from well 25/4-7 does also conclude with this.

The same hard event was analysed on the super gathers created to interpret the changes in the subsurface when moving away from the well location. These super gathers are created by stacking five and five gathers together to increase the signal to noise ratio. Observing the hard event on these gathers, shown in Figure 5. 21 and Figure 5. 23, it here looks like this event only consists of one separate event. This can be because of the stacking of the gathers. If this event changed a lot over the few gathers closest to the well the weak responses may have cancelled each other out. In these two figures the super gathers are only observed along one inline, the one going through the well location. It is not known how the gathers change along the crossline going through the well location. Knowing this could have given some answers to why this event now only looks like it consists of one separate event.

In chapter 5.3.2 the AVO effect was followed away from the well location and it was found which gather that may represent the outer edge of the sand lobe. At some distance away from the well location the reflector showing the AVO effect had changed so much that it looked like it could be classified as a class II AVO anomaly and not a class III AVO anomaly any more. This was explained by assuming that this gather was located more towards the edge of the sand lobe, where it may dip down a little, and that the top reservoir now was located beneath the diagenesis contact. The top reservoir would then be located in cemented massive sandstones. Assuming that this is the case this would also affect the hard event located beneath the soft reflector representing the top reservoir. If the diagenesis contact were located over the top reservoir that had to mean that the hard event now only had to represent the fluid contact. When observing the hard event from the well location and towards the outer edge of the sand lobe there are no large changes that can indicate this. This does not have to mean that the assumptions made are incorrect, only that there are many possibilities and that not everything is necessarily observable on seismic.

It is not only the content of the reservoir that can change when moving laterally away from the well location. There are also a lot of possibilities of changes within the lithologies. The amount of shale in the area can be a subject to discuss when working with a turbidite reservoir. There are normally small lateral changes related to the shale content, but they may occur. This can actually be an explanation for the changes in the AVO effect previously discussed. Just a small increase in the amount of shale in the reservoir rock can have a great influence on the results obtained from the seismic data. Focusing on the direction away from the well that has already been discussed it can be assumed that there is a chance that the shale content will increase towards higher numbered crosslines. This can be assumed on the basis of the contour map shown in Figure 5. 24 where this is the direction that first leads out of the sand lobe. However, moving in the opposite direction, without observing the super gathers in that direction, it can be assumed that it could be expected to find

more clean channel sands in that direction. This is also stated on the basis of the contour map where this would be the direction leading towards the centre of the sand lobe. Since the contour map shows such a nice sand lobe it is likely to presume that the reservoir sand will continue to be fairly clean for some distance before once more moving towards the other edge of the sand lobe. Here again it can be presumed that the content of more dirty levee deposits will increase towards the edge.

This last discussion on the lateral changes in the reservoir is based on assumptions and is not related to interpretation of any data except for the contour map showing the top reservoir. A map like this will not give any clear results, but it may help by showing what is possible to expect from the data. Many of the possible answers discussed here are based on assumptions, and since this is a fairly complex reservoir due to the turbiditic depositions there should be performed more thorough examination of the data before drawing hasty conclusions. A turbidite reservoir can contain both sinister traps and hidden potential that require detailed interpretations to be discovered.

Conclusion

In this thesis it has been performed analyses on two sets of seismic data from the Kneler oil discovery in the Alvheim field. An AVO effect was found on the pre-stack data and this is where the analyses for this reservoir were made. This AVO effect was interpreted to be the top oil sand and the results from the performed analyses turned out match the expected AVO signatures very well. It has to be taken into consideration that the real seismic data can include both a great deal of noise and tuning effects which may cause the AVO effect to show up slightly different than what was modelled in advance. There may also be some uncertainties with the modelling that has been performed, and this may cause the results from the analyses of the real data and the modelled data to deviate somewhat from each other.

Analyses performed on both the pre-stack and post-stack data resulted in classifying the top oil sand as a class III AVO anomaly. Before performing these analyses it was known that the upper part of the reservoir consisted of unconsolidated interbedded sand-shale. Comparing the result with the modelled scenarios it could be seen that it was the modelled unconsolidated sandstone that showed a class III AVO anomaly and not the interbedded sand-shale. The explanation for this can be that the reservoir consists of separate layers of sand and shale that are placed interchangeably and not of one layer with a mixed sand-shale lithology, which it was assumed when performing the modelling. This means that the analyses performed on the real data actually were performed on a layer of unconsolidated massive sandstone. This shows how important it is to perform a combined fluid and lithology substitution and not to only assume a constant lithology and performing fluid substitution for that lithology.

The analyses were performed on the seismic data where also well log data was available. Due to this information it was already known what type of results that could be expected. However, since the Alvheim reservoir is a turbidite reservoir there are many uncertainties when moving away from the well since there are so many factors inside a turbidite reservoir that can change over a short distance due to the complexity concerning the lithologies. The complex deposition can cause both large lateral and vertical changes. In addition, beginning chemical compaction at the reservoirs depth causes diagenetic changes that make the interpretation of the reservoir even more difficult. When interpreting the seismic away from the well, super gathers were used to enhance the seismic signal and minimize the noise. The AVO effect was followed on seismic gathers towards higher numbered crosslines to see how it would change when moving towards the edge of the sand lobe functioning as the reservoir. It was seen that the AVO effect had faded some distance from the well, when the super gathers were created by stacking 5 gathers together. This was interpreted as an indication that the outer edge of the reservoir was reached and that there were dirtier levee deposits present than there was in the more central parts of the reservoir.

References

Ahmadi, Ziad, et al. "Paleocene." In *The Millennium Atlas: petroleum geology of the central and northern North Sea*, edited by Andrew Armour, Paul Bathurst, Dan Evans, Jon Gammage and Cathy Hickey, 235-259. London: The Geological Society of London, 2003.

AVO Analysis. http://www.fugro-jason.com/software/JGW/modules/avoanalysis.htm (accessed November 29., 2011).

Avseth, Per. *Handed figures* (December 2011).

Avseth, Per. *Interview* (15 May 2012).

Avseth, Per, Anders Dræge, Aart-Jan van Wijngaarden, Tor Arne Johansen, and Arild Jørstad. “Shale rock physics and implications for AVO analysis: A North Sea demonstration.” *The Leading Edge*, June 2008: 788-797.

Avseth, Per, Arild Jørstad, Aart-Jan van Wijngaarden, and Gary Mavko. “Rock physics estimation of cement volume, sorting, and net-to-gross in North Sea sandstones.” *The Leading Edge*, January 2009: 98-108.

Avseth, Per, Tapan Mukerji, and Gary Mavko. *Quantitative Seismic Interpretation.* Cambridge University Press, 2005.

Balder Formation. http://nhm2.uio.no/norges/openarea/balder.php (accessed April 26, 2012).

Eggen, Katharina B. “Lithology and fluid prediction in a North Sea turbidite system.” Project work, Trondheim, 2012.

FactPages - Norwegian Petroleum Directorate. http://factpages.npd.no/factpages/Default.aspx?culture=no (accessed April 26, 2012).

Hudson, Paul F. “Deltas.” 2005.

MATLAB; The Language of Technical Computing. 1994-2012. http://www.mathworks.se/products/matlab/ (accessed April 18, 2012).

Norway: Lundin Petroleum commences oil production from the Volund field, offshore Norway. http://www.energy-pedia.com/news/norway/lundin-petroleum-commences-oil-production-from-the-volund-field--offshore-norway (accessed May 16, 2012).

Petroleumsverksemnd, Norsk. *Fakta.* Oslo: Olje- og energidepartementet, 2011.

Rimstad, Kjartan, Per Avseth, and Henning Omre. “Hierarchical Bayesian lithology/fluid prediction: A North Sea case study.” *Geophysics*, B69-B85 March-April 2012.

Schlumberger Oilfield Glossary. http://www.glossary.oilfield.slb.com/Display.cfm?Term=tuning%20effect (accessed May 1, 2012).

Sele Formation. http://nhm2.uio.no/norges/openarea/sele.php (accessed April 26, 2012).

Simm, Rob. *Well 25/4-7 (Kneler Structure) Studies in Rock Physics Log Conditioning, Modelling and Well Tie Analysis.* Well description, Norway: Marathon Petroleum Company, 2005.

Simm, Rob, Roy White, and Richard Uden. “The anatomy of AVO crossplots.” *The Leading Edge*, February 2000: 150-155.

Appendix

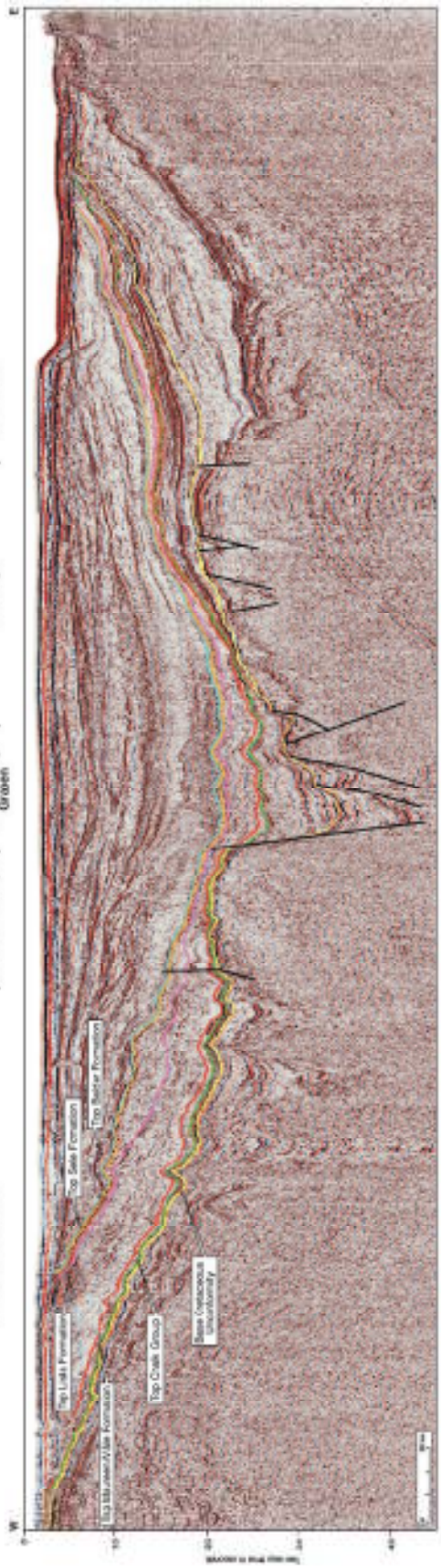

Figure A: Regional seismic line showing the Paleocene interval.

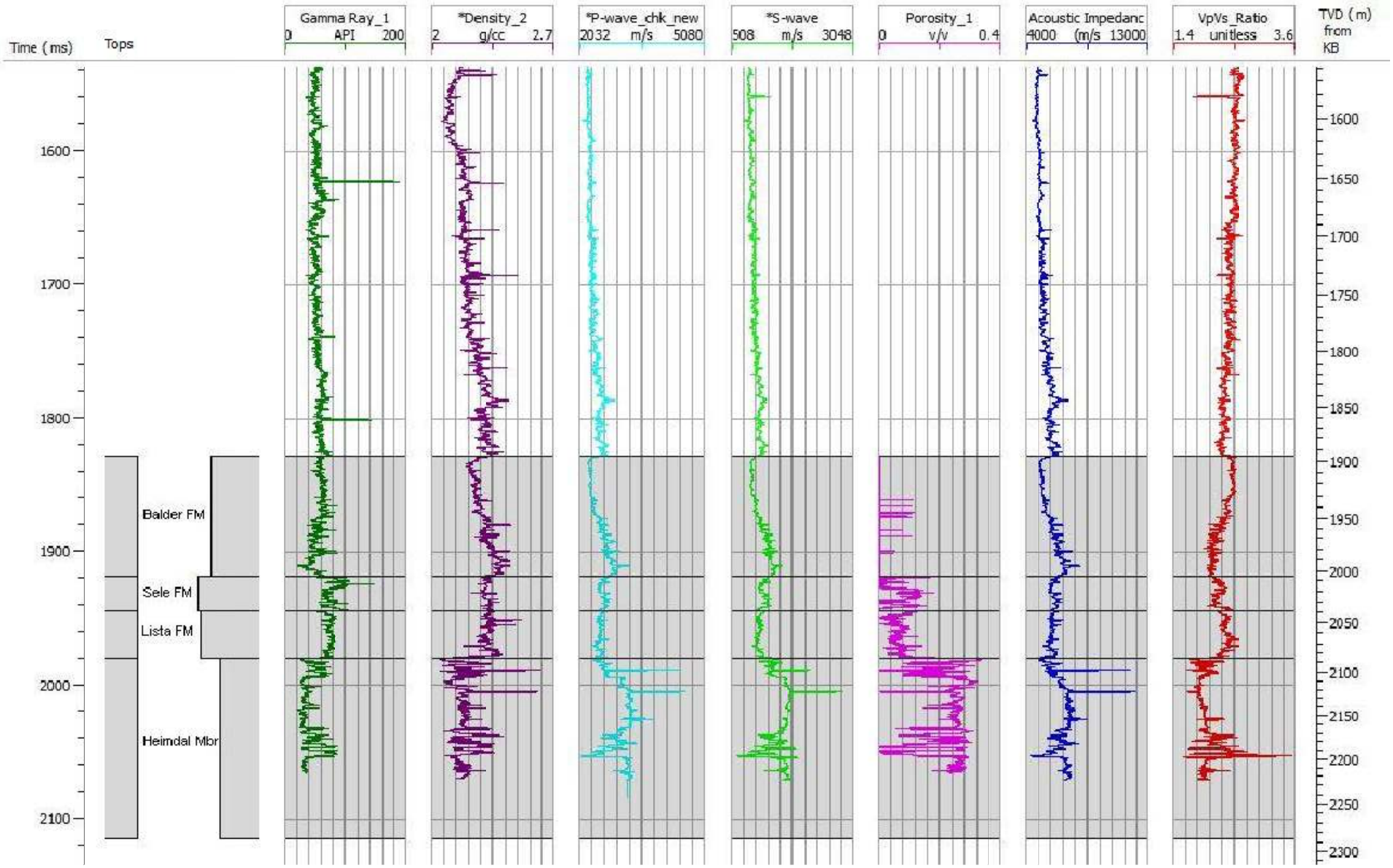

Figure B: Logs from well 25/4-7.

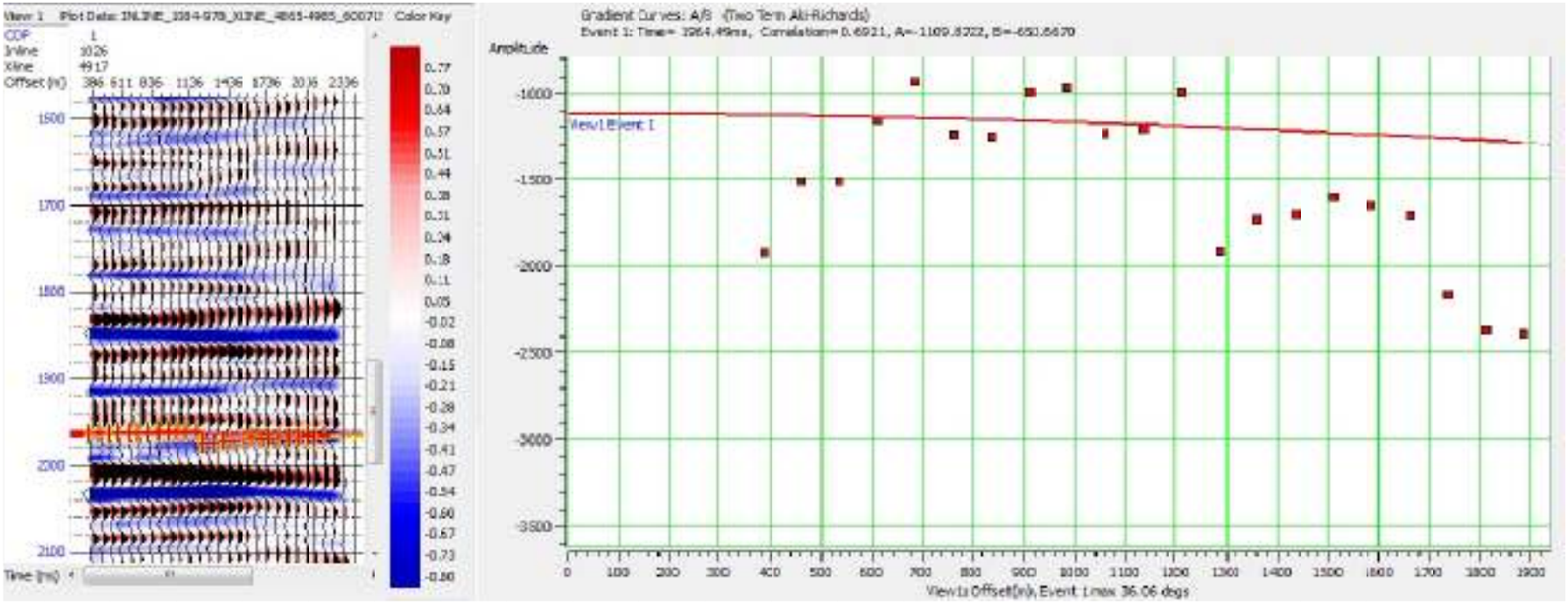

Figure C: AVO gradient analysis performed on real seismic data.

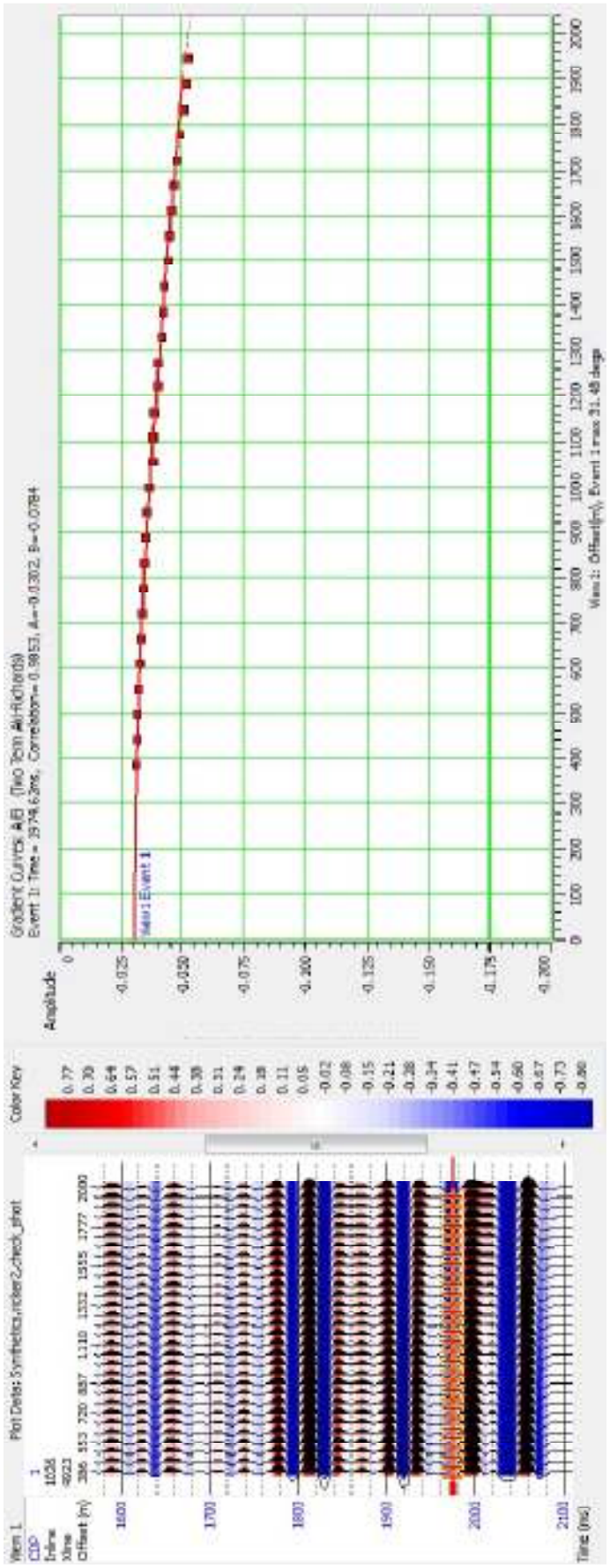

Figure D: AVO gradient analysis performed on synthetic seismic data.

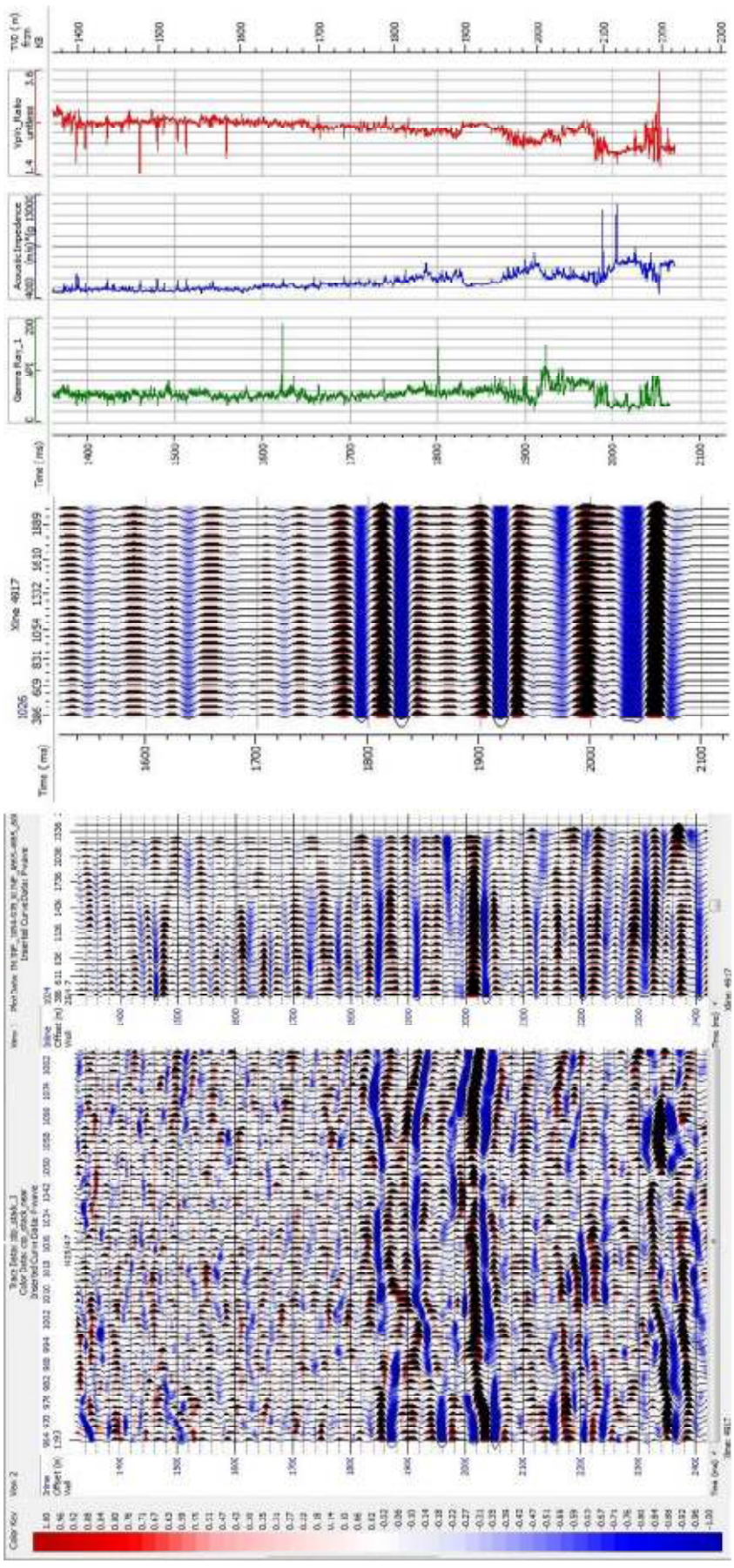

Figure E: Comparison of real data, synthetic data and well logs.